that are short-lived. Although short-lived and cannot be detected easily by conventional experimental techniques, the dissociation and association of such complexes can influence chemical processes, especially reactivity and mechanisms in biochemical reactions. Therefore, progress is being made in our laboratory to apply similar theoretical approaches to investigate short-lived phenomena in some biological systems.

Acknowledgements

The authors would like to acknowledge the financial supports from the Thailand Research Fund (TRF): the Royal Golden Jubilee (RGJ) Ph.D. Program, Grant No. PHD/0071/2547 to Sermsiri Chaiwongwattana and Prof. Kritsana Sagarik: the Advanced Research Scholarship, Grant No. BRG-4880008 to Prof. Kritsana Sagarik. Linux clusters provided by the following organizations are also gratefully acknowledged: School of Mathematics and School of Chemistry, SUT; National Electronics and Computer Technology Center (NECTEC) and National Nanotechnology Center (NANOTEC), National Science and Technology Development Agency (NSTDA); the Thai National Grid Center (THAIGRID), Ministry of Information and Communication Technology.

LIST OF ABBREVIATIONS AND SYMBOLS

T-model = The test-particle model.

π-H-bond = π-hydrogen bond.

PD map = Probability distribution map.

π-PD maps = Solvent probability distribution map.

$< P^{\pi-PD} >_{max}$ = Highest probability at the labeled contour on the π-PD maps.

$MD\text{-}[(PhOH)_n]^{frozen}_{Benz}$ = MD simulations with the structure of $(PhOH)_n$ frozen at the T-model equilibrium geometries.

$MD\text{-}[(PhOH)_n]^{free}_{Benz}$ = MD simulations with all molecules allowed to move, starting from the equilibrated configurations of $MD\text{-}[(PhOH)_n]^{frozen}_{Benz}$.

$< E^{solu-solu}_{Benz} >$ = Average solute-solute interaction energy.

$< E^{solu-solv}_{Benz} >$ = Average solute-solvent interaction energy.

$< E^{pot}_{Benz} >$ = Average potential energies of $[(PhOH)_n]_{Benz}$.

$< E^{L}_{Benz} >$ = The average potential energy barriers to the solvent exchange within, as well as between, the first solvation shells.

$< E^{T}_{Benz} >$ = The average potential energy barriers to the solvent exchange between Benz molecules in the first solvation shell and the outside.

g(R) = Atom-atom pair correlation functions.

n(R) = Average running coordination numbers.

FFT = Fast Fourier transformations.

I_a = Associative-interchange scheme.

$\tau^{PhOH-Benz}_{O-H..\pi}$ = Lifetime of the PhOH-Benz 1 : 1 complex.

PB-PD = The average solute-solvent interaction energy PD maps.

BB-PD = The average solvent-solvent interaction energy PD maps.

PB-BB-PD = The average potential energy PD maps.

$< \Delta E^{PB\text{-}PD}_{Benz} >_{min}$ = Lowest-average interaction energies on the PB-PD map

$< \Delta E^{BB\text{-}PD}_{Benz} >_{min}$ = Lowest-average interaction energies on the BB-PD map

$< \Delta E^{PB\text{-}BB\text{-}PD}_{Benz} >_{min}$ = Lowest-average interaction energies on the PB-BB-PD map

References

[1] E.M. Woolley, L.G. Hepler, J. Phys. Chem. 76 (1972) 3058.

[2] S.H. Weidman, L.E. Swearingen, J. Am. Chem. Soc. 35 (1931) 836.

[3] J.N. Spencer, J.C. Andrefsky, A. Grushow, J. Naghdi, L.M. Patti, J.F. Trader, J. Phys. Chem. 91 (1987) 1673.

[4] F.A. Philbrick, J. Am. Chem. Soc. 56 (1934) 2581.

[5] R.M. Badger, R.C. Greenough, J. Phys. Chem. 65 (1961) 2088.

[6] F.T. Wall, J. Am. Chem. Soc. 64 (1942) 472.

[7] F.T. Wall, P.E. Rouse Jr., J. Am. Chem. Soc. 63 (1941) 3002.

[8] A.K.M. Shamsul Huq, S.A.K. Lodhi, J. Phys. Chem. 70 (1966) 1354.

[9] R. Van Duyne, S.A. Taylor, S.D. Christian, H.E. Affsprung, J. Phys. Chem. 71 (1967) 3427.

[10] K.E. Van Holde, W.C. Johnson, P.S. Ho, Principles of Physical Biochemistry, Prentice Hall, New Jersey, 1998.

[11] B. Brutschy, Chem. Rev. 100 (2000) 3891.

[12] J.L. Knee, L.R. Khundkar, A.H. Zewail, J. Chem. Phys. 87 (1987) 115.

[13] M.F. Perutz, Philos. Trans. Roy. Soc. London Ser. A 345 (1993) 105.

[14] E.A. Meyer, R.K. Castellano, F. Diederich, Angew. Chem. Int. Ed. Engl. 42 (2003) 1210.

[15] W. Roth, M. Schmitt, C. Jacoby, D. Spangenberg, C. Janzen, K. Kleinerman, Chem. Phys. 239 (1998) 1.

[16] N. Mikami, Bull. Chem. Soc. Jpn. 68 (1995) 683.

[17] R.J. Lipert, S.D. Colson, J. Chem. Phys. 89 (1988) 4579.

[18] Ch. Jacoby, W. Roth, M. Schmitt, Ch. Janzen, D. Spangenberg, K. Kleinermanns, J. Phys. Chem. A 102 (1998) 4471.

[19] T. Sawamura, A. Fujii, S. Sato, T. Ebata, N. Mikami, J. Phys. Chem. 100 (1996) 8131.

[20] K. Ohashi, Y. Inokuchi, N. Nishi, Chem. Phys. Lett. 257 (1996) 137.

[21] G.V. Hartland, B.F. Henson, V.A. Venturo, P.M. Felker, J. Phys. Chem. 96 (1992) 1164.

[22] D.C. Young, Computational Chemistry: A practical guide for applying techniques to real-world problems, Wiley Interscience, New York, 2001.

[23] M.O. Sinnokrot, C.D. Sherrill, J. Am. Chem. Soc. 126 (2004) 7690.

[24] B.M. Rode, C.F. Schwenk, T.S. Hofer, B.R. Randolf, Coord. Chem. Rev. 249 (2005) 2993.

[25] M. Ricci, P. Bartolini, R. Chelli, G. Cardini, S. Califano, R. Righini, Phys. Chem. Chem. Phys. 3 (2001) 2795.

[26] A. Magro, D. Frezzato, A. Polimeno, G.J. Moro, R. Chelli, R. Righini, J. Chem. Phys. 123 (2005) 124511.

[27] S. Sun, E.R Bernstein, J. Phys. Chem. 100 (1996) 13348.

[28] G.J. Kearley, M.R. Johnson, J. Tomkinson, J. Chem. Phys. 124 (2006) 044514.

[29] R. Chelli, G. Cardini, P. Procacci, R. Righini, S. Califano, A. Albrecht, J. Chem. Phys. 113 (2000) 6851.

[30] L.S Bartell, F.J. Dulles, J. Phys. Chem. 99 (1995) 17107.

[31] J.R. Grover, E.A. Walters, E.T. Hui, J. Phys. Chem. 91 (1987) 3233.

[32] M.O. Sinnokrot, E.F. Valeev, C.D. Sherrill, J. Am. Chem. Soc. 124 (2002) 10887.

[33] K. Sagarik, S. Chaiwongwattana, P. Sisot, Chem. Phys. 306 (2004) 1.

[34] C.A. Hunter, J. Singh, J.M. Thornton, J. Mol. Biol. 218 (1991) 837.

[35] R. Parthasarathi, V. Subramanian, N. Sathyamurthy, J. Phys. Chem. A 109 (2005) 843.

[36] A. Olkawa, H. Abe, N. Mikami, M. Ito, J. Phys. Chem. 87 (1983) 5083.

[37] R.C. Guedes, K. Coutinho, B.J. Costa Cabral, S. Canuto, C.F. Correia, R.M. Borges dos Santos, J.A. Martinho Simões, J. Phys. Chem. A 107 (2003) 9197.

[38] S. Tsuzuki, K. Honda, T. Uchimaru, M. Mikami, K. Tanabe, J. Am. Chem. Soc. 124 (2002) 104.

[39] K. Kwac, C. Lee, Y. Jung, J. Han, K. Kwak, J. Zheng, M.D. Fayer, M. Cho, J. Chem. Phys. 125 (2006) 244508.

[40] K. Endo, Bull. Chem. Soc. Jpn. 1 (1926) 25.

[41] M. Saunders, J.B. Hyne, J. Chem. Phys. 29 (1958) 1319.

[42] E.N. Lassettre, R.G. Dickinson, J. Am. Chem. Soc. 61 (1939) 54.

[43] J. Zheng, K. Kwak, J. Asbury, X. Chen, I.R. Piletic, M.D. Fayer, Science 309 (2005) 1338.

[44] J. Zheng, K. Kwak, M.D. Fayer, Acc. Chem. Res. 40 (2007) 75.

[45] K. Kwak, J. Zheng, H. Cang, M.D. Fayer, J. Phys. Chem. B 110 (2006) 19998.

[46] J. Zheng, K. Kwak, X. Chen, J.B. Asbury, M.D. Fayer, J. Am. Chem. Soc. 128 (2006) 2977.

[47] I.J. Finkelstein, J. Zheng, H. Ishikawa, S. Kim, K. Kwak, M.D. Fayer, Phys. Chem. Chem. Phys. 9 (2007) 1533.

[48] Y.S. Kim, R.M. Hochstrasser, Proc. Natl. Acad. Sci. 102 (2005) 11185.

[49] R.M. Hochstrasser, Proc. Natl. Acad. Sci. 104 (2007) 14190.

[50] K. Sagarik, P. Asawakun, Chem. Phys. 219 (1997) 173.

[51] K. Sagarik, B.M. Rode, Chem. Phys. 260 (2000) 159.

[52] K. Sagarik, S. Chaiyapongs, Biophys. Chem. 117 (2005) 18.

[53] K. Sagarik, S. Dokmaisrijan, J. Mol. Struct. (THEOCHEM) 718 (2005) 31.

[54] N. Deeying, K. Sagarik, Biophys. Chem. 125 (2006) 14.

[55] M. Orozco, F.J. Luque, Chem. Rev. 100 (2000) 4187.

[56] B.J. Costa Cabral, R.G. Bakker Fonseca, J.A. Martinho Simões, Chem. Phys. Lett. 258 (1996) 436.

[57] H.J, Böhm, R.J. Ahlrichs, J. Chem. Phys. 77 (1982) 2028.

[58] J.H, Dymond, E.B. Smith, The Virial Coefficients of Pure Gases and Mixtures, Clarendon Press, Oxford, 1980.

[59] H.B. Schlegel, J. Comput. Chem. 3 (1982) 214.

[60] Selected Values of Physical and Thermodynamics Properties of Hydrocarbons and Related Compounds, American Petroleum Institute Research Project 44, Carnegie Press, Pittsburg, 1953.

[61] SURFER for Window, V. 6.04, Golden Software Inc., USA, 1997.

[62] G.J. Borse, Numerical Methods with MATLAB: A resources for scientists and engineers, PWS Publishing, Boston, 1997.

[63] J.D. Gezelter, E. Rabani, B.J. Berne, J. Chem. Phys. 107 (1997) 4618.

[64] S. Chaiwongwattana, K. Sagarik, in preparation.

[65] H.G. Hertz, in: F. Franks (Ed). Water, A Comprehensive Treatise, V. 3, Plenum Press, New York, 1973.

[66] R.W. Impey, P.A. Madden, I.R. McDonald, J. Phys. Chem. 87 (1983) 5071.

[67] F. Brugé, E. Parisi, S.L. Fornili, Chem. Phys. Lett. 250 (1996) 443.

[68] C.H. Langford, H.B. Gray, Ligand Substitution Processes, W.A. Benjain, New York, 1966.

[69] E. Rabani, J.D. Gezelter, B.J. Berne, J. Chem. Phys. 107 (1997) 6867.

[70] J.D. Gezelter, E. Rabani, B.J. Berne, J. Chem. Phys. 110 (1999) 3444.

Figure 1 Equilibrium structures and interaction energies of the PhOH-Benz 1 : 1 complexes in the gas phase, computed from the T-model potentials.

Figure 2 Equilibrium structures and interaction energies of the PhOH-Benz 1 : 2 complexes in the gas phase, computed from the T-model potentials.

Figure 3 Structural and energetic results obtained from MD-$[PhOH]^{frozen}_{Benz}$.
X-, Y- and Z-axes are in Å, energies in kJ/mol.
a) – b) The π-PD, PB-PD and PB-BB-PD maps.
c) – d) Average potential energy landscapes and the cross section plots computed from longitudinal and transverse profile lines.
_____ PB-BB-PD cross section plot.
- - - - - PB-PD cross section plot.
- - - - - BB-PD cross section plot.

Note: π-PD contour: min = 0.0 : max = 0.13: interval = 0.01.
PB-PD contour: min = -18.0 : max = -3.0: interval = 2.5.
PB-BB-PD contour: min = -96.0 : max = -75.0: interval = 7.0.

Figure 4 Structural and dynamic results obtained from MD-$[PhOH]^{free}_{Benz}$.
a) – b) g(R); characteristic distances given with n(R) in parentheses.
c) Example of H-bond exchange diagram.
d) Fourier transformations of the O-H.. π H-bond and π_{ph}..π distances.

Note: $\tau^{PhOH-Benz}_{O-H..\pi}$ = the lifetime of the PhOH-Benz complex computed from FFT of the O-H.. π H-bond distance.
$\tau^{PhOH-Benz}_{\pi_{Ph}..\pi}$ = the lifetime of the PhOH-Benz complex computed from FFT of the π_{ph}.. π distance.

Figure 5 Structural and energetic results obtained from MD-$[(PhOH)_2]^{frozen}_{Benz}$.
X-, Y- and Z-axes are in Å, energies in kJ/mol.
a) – c) The π-PD, PB-PD and PB-BB-PD maps.
d) – e) Average potential energy landscapes and the cross section plots computed from longitudinal and transverse profile lines.
_____ PB-BB-PD cross section plot.
- - - - - PB-PD cross section plot.
- - - - - BB-PD cross section plot.

Note: π-PD contour: min = 0.0 : max = 0.13: interval = 0.01.
PB-PD contour: min = -30.0 : max = -1.0: interval = 4.5.
PB-BB-PD contour: min = -99.0 : max = -70.0: interval = 7.2.

Figure 6 Structural and dynamic results obtained from MD-$[(PhOH)_2]^{free}_{Benz}$.
a) – c) g(R); characteristic distances given with n(R) in parentheses.
d) Snapshots of the PhOH-Benz clusters in $[(PhOH)_2]_{Benz}$.
e) – f) Example of H-bond exchange diagram.

Figure 7 g(R) obtained from MD-$[(PhOH)_3]^{free}_{Benz}$, together with characteristic distances.

Figure-1

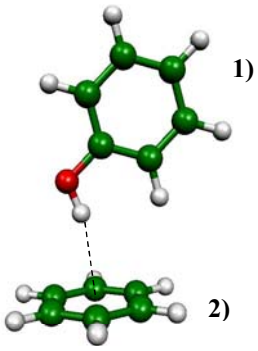

a) $\Delta E_{T\text{-model}}$ = -19.5 kJ/mol

O-H..π (1-2) = 3.4 Å
H..π (1-2) = 2.5 Å
π_{Ph}..π (1-2) = 5.4 Å

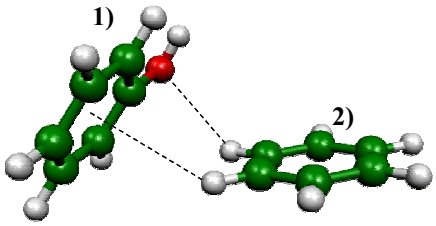

b) $\Delta E_{T\text{-model}}$ = -13.5 kJ/mol

C-H..O (2-1) = 3.4 Å
H..O (2-1) = 2.6 Å
C-H..π_{Ph} (2-1) = 4.0 Å
H..π_{Ph} (2-1) = 3.2 Å
π..π_{Ph} (2-1) = 5.1 Å

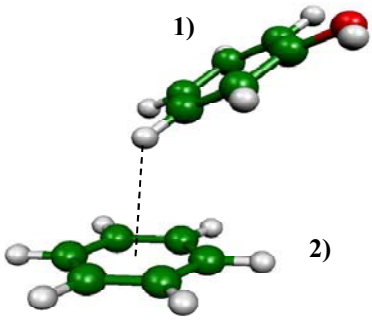

c) $\Delta E_{T\text{-model}}$ = -9.3 kJ/mol

C-H..π (1-2) = 3.8 Å
H..π (1-2) = 3.0 Å
π_{Ph}..π (1-2) = 4.9 Å

Fig. 1

Figure-2

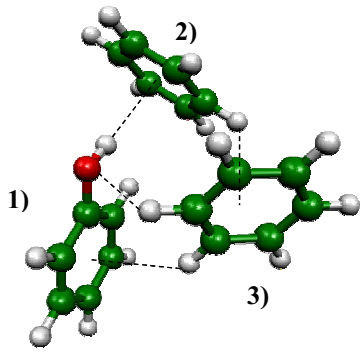

a) $\Delta E_{T\text{-model}}$ = -41.6 kJ/mol

O-H..π (1-2) = 3.4 Å
H..π (1-2) = 2.5 Å
π_{Ph}..π (1-2) = 5.2 Å

C-H..π (2-3) = 3.8 Å
H..π (2-3) = 3.0 Å
π..π (2-3) = 4.9 Å

C-H..O (3-1) = 3.3 Å
H..O (3-1) = 2.7 Å
C-H..π_{Ph} (3-1) = 4.0 Å
H..π_{Ph} (3-1) = 3.2 Å
π..π_{Ph} (3-1) = 5.0 Å

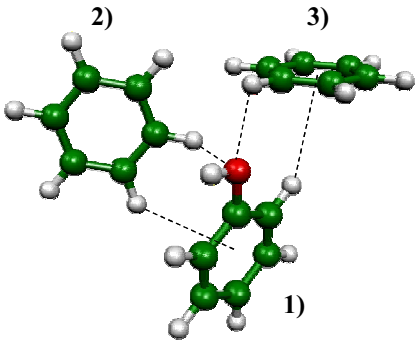

b) $\Delta E_{T\text{-model}}$ = -30.6 kJ/mol

C-H..π (1-3) = 4.4 Å
H..π (1-3) = 3.4 Å

C-H..O (3-1) = 3.3 Å
H..O (3-1) = 2.6 Å

C-H..O (2-1) = 3.3 Å
H..O (2-1) = 2.8 Å
C-H..π_{Ph} (2-1) = 4.0 Å
H..π_{Ph} (2-1) = 3.2 Å
π..π_{Ph} (2-1) = 5.0 Å

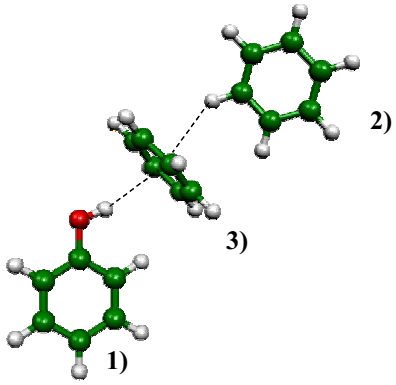

c) $\Delta E_{T\text{-model}}$ = -28.8 kJ/mol

O-H..π (1-3) = 3.4 Å
H..π (1-3) = 2.5 Å
π_{Ph}..π (1-3) = 5.4 Å

C-H..π (2-3) = 3.8 Å
H..π (2-3) = 2.9 Å
π..π (2-3) = 5.0 Å

Fig. 2

Figure-3

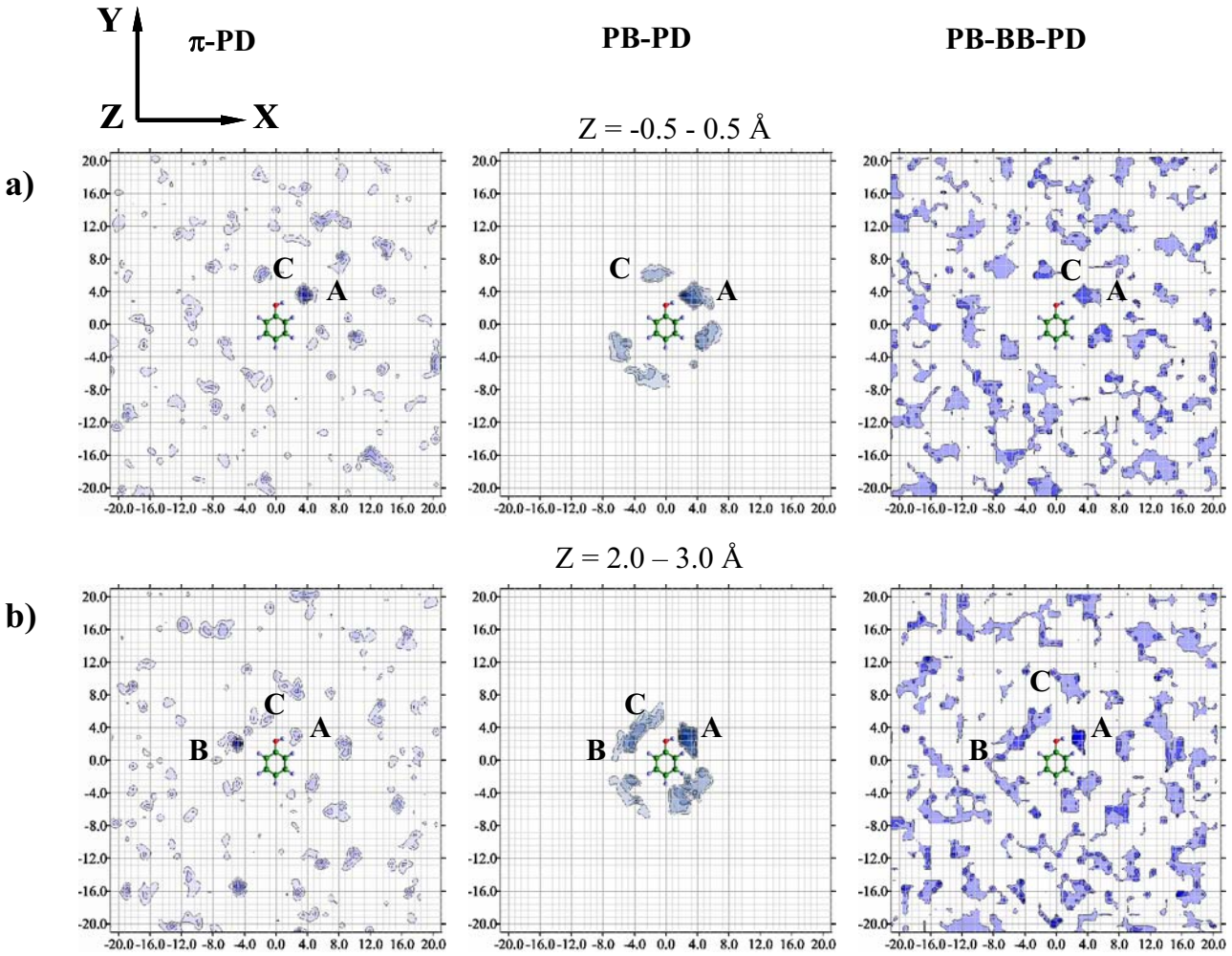

Fig. 3

c) Z = -0.5 – 0.5 Å

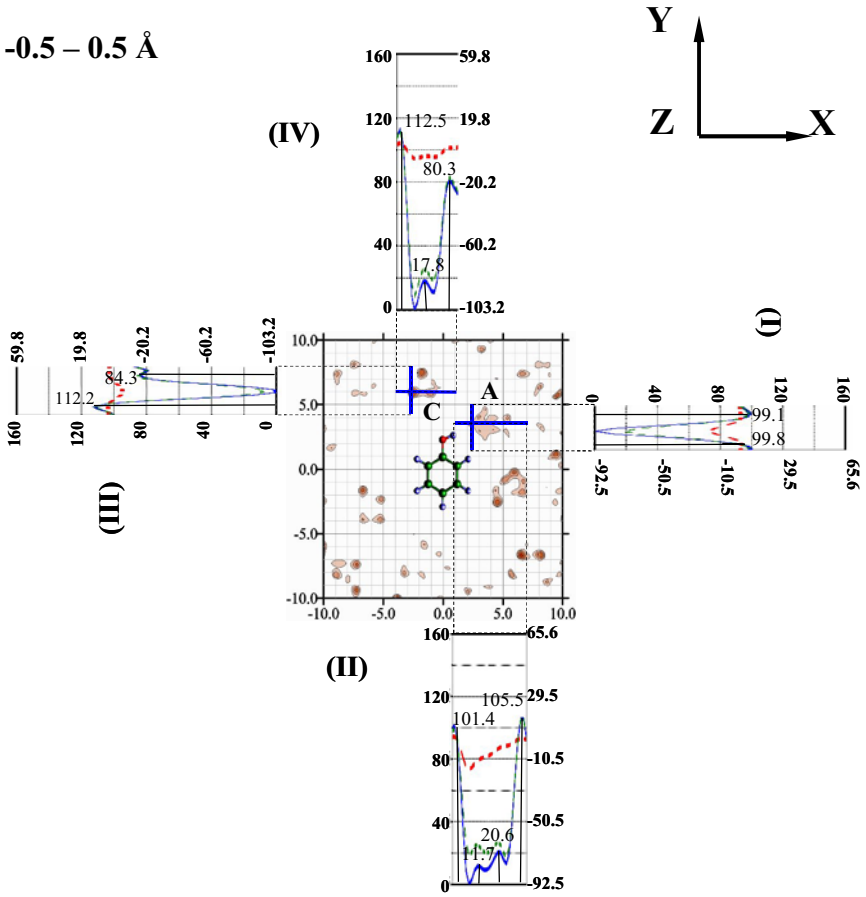

d) Z = 2.0 – 3.0 Å

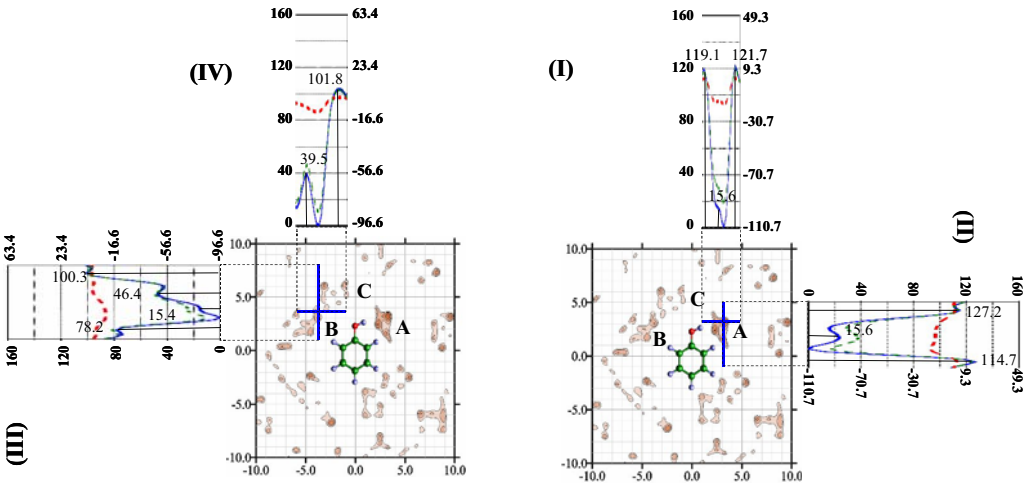

Fig. 3 (continued)

Figure-4

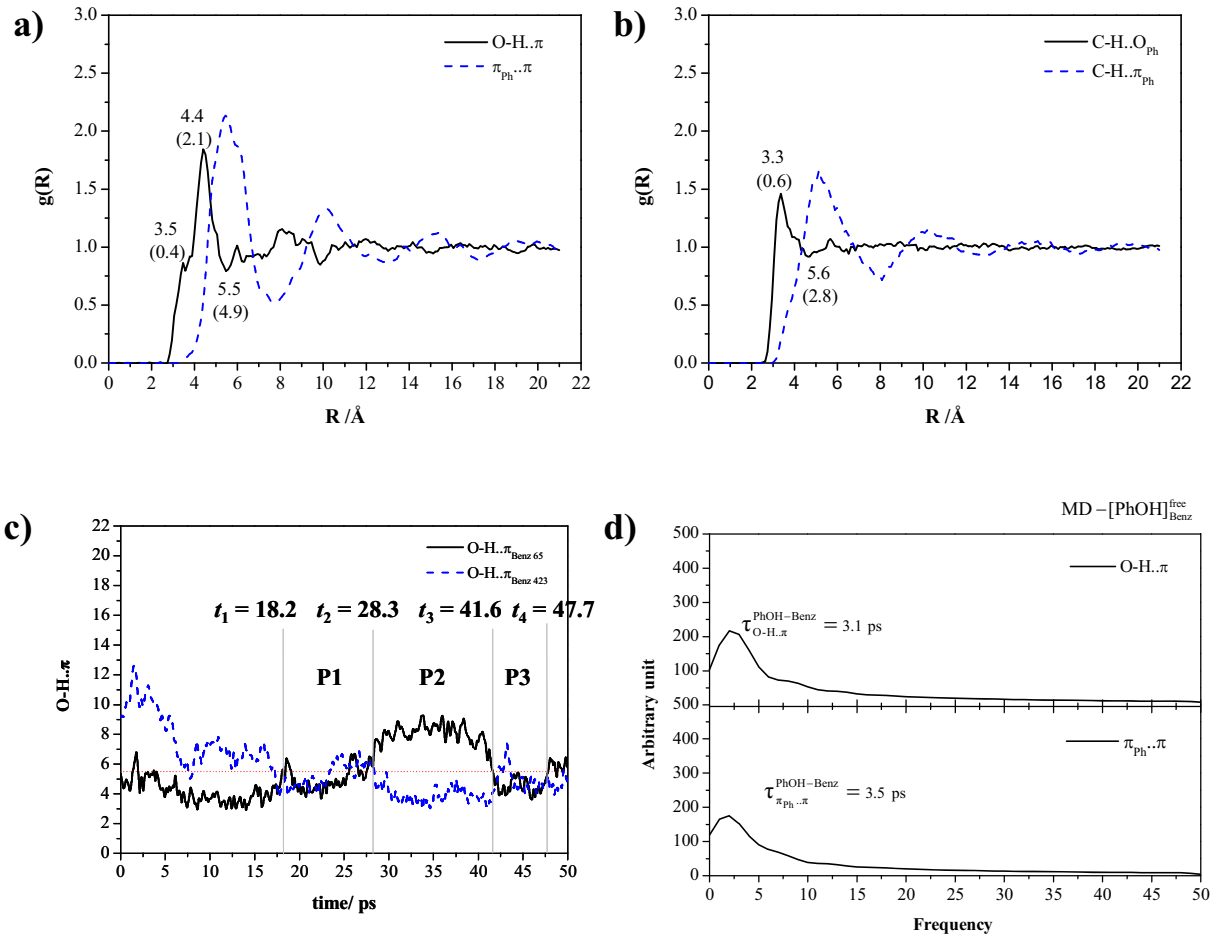

Fig. 4

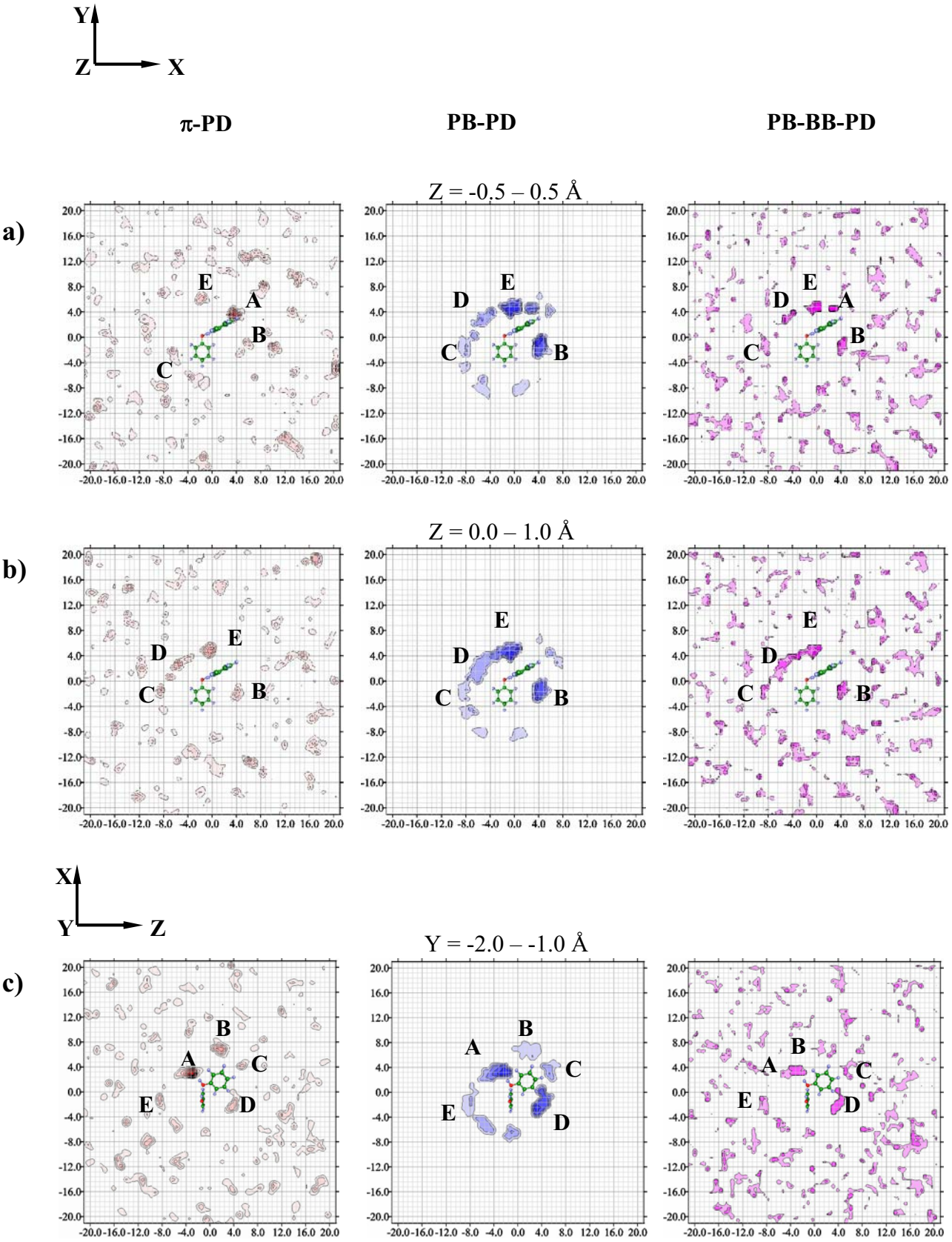

Fig. 5

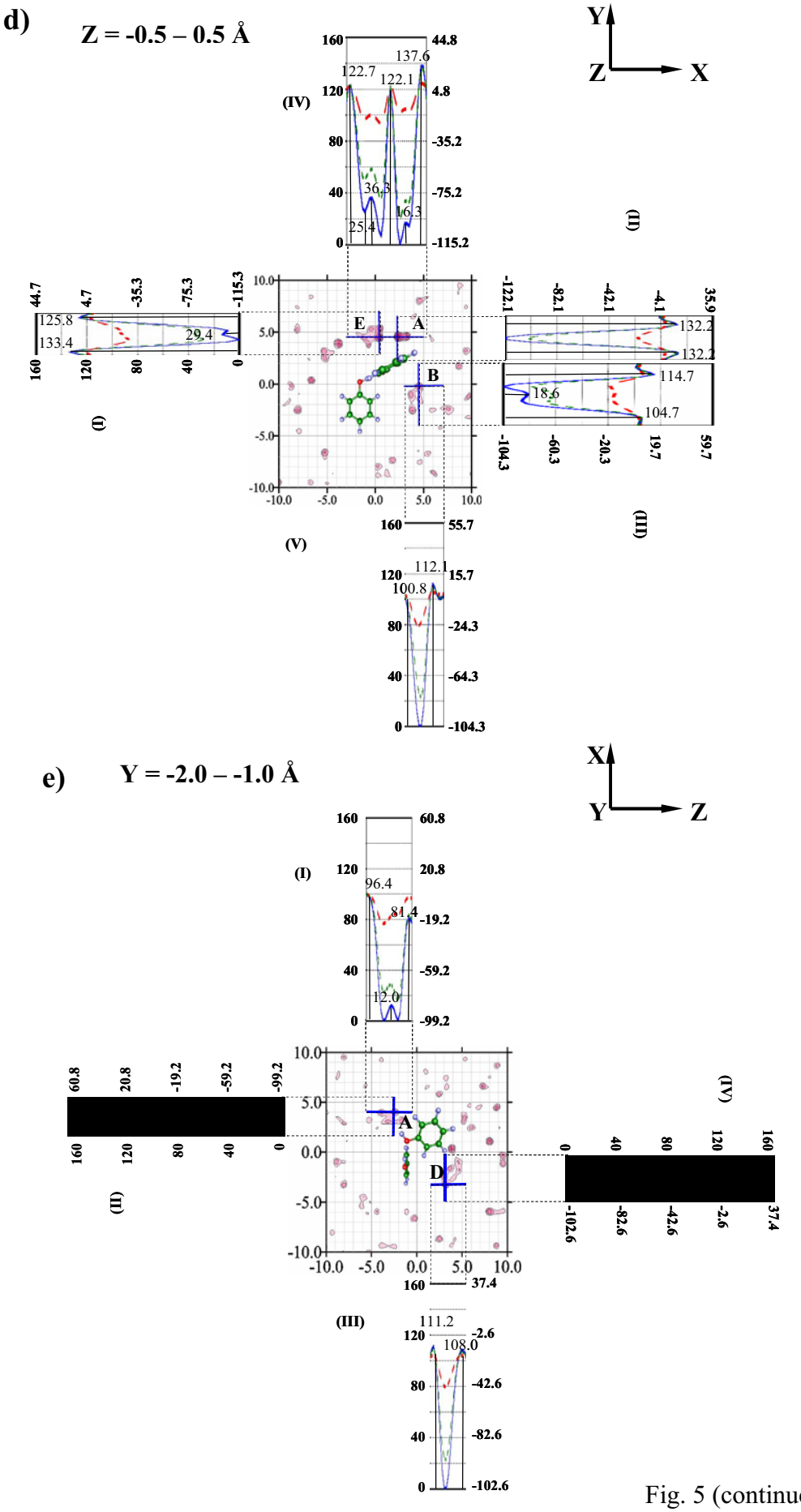

Fig. 5 (continued)

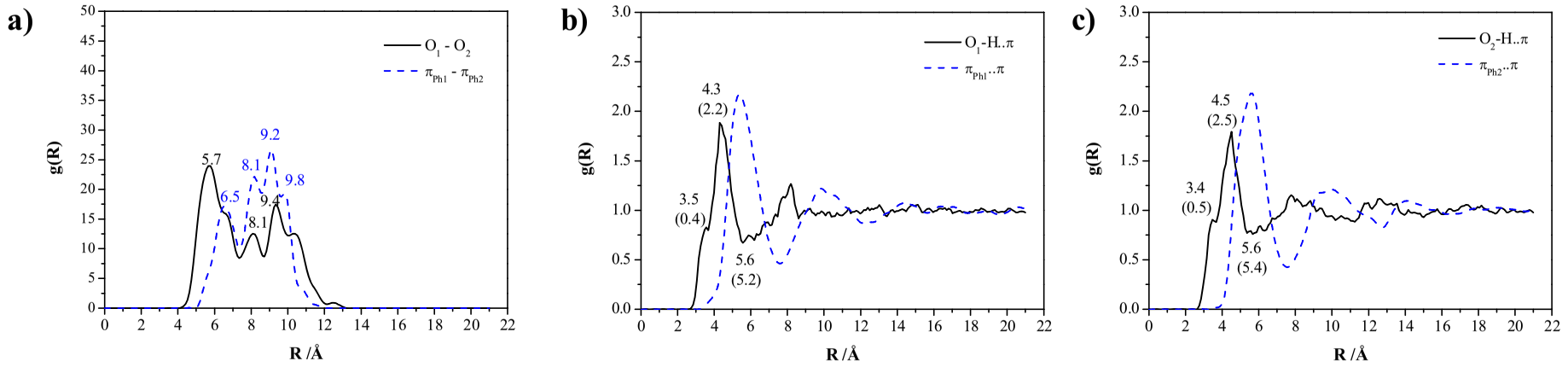

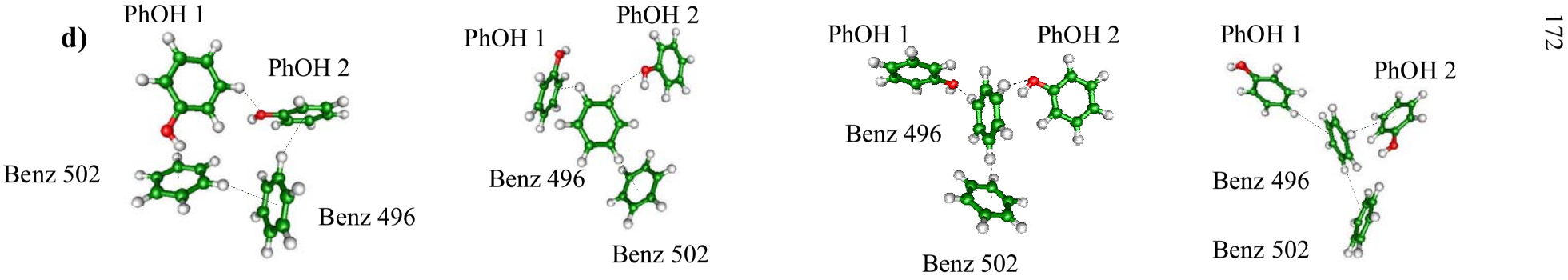

(I) $R_{\pi_{Ph1-Ph2}} = 6.7$ Å

(II) $R_{\pi_{Ph1-Ph2}} = 8.1$ Å

(III) $R_{\pi_{Ph1-Ph2}} = 9.0$ Å

(IV) $R_{\pi_{Ph1-Ph2}} = 9.7$ Å

Fig. 6

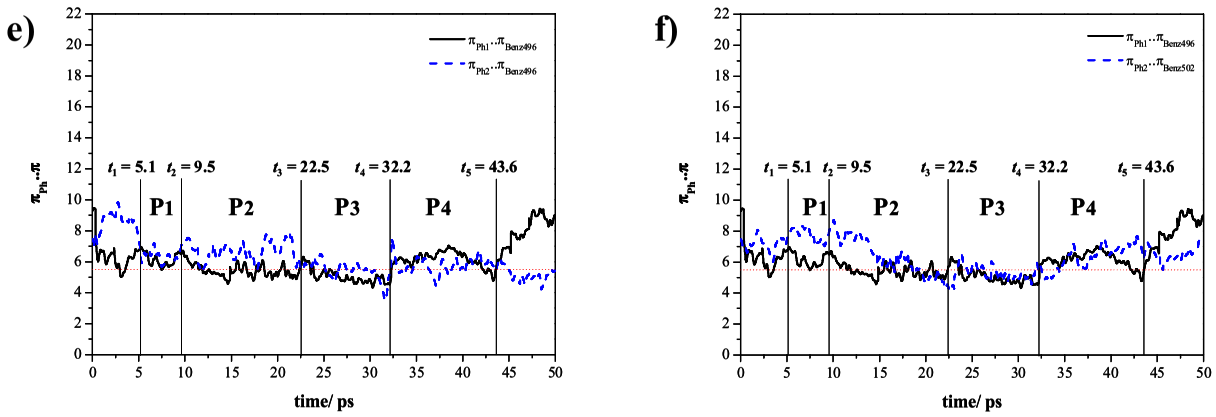

Fig. 6 (continued)

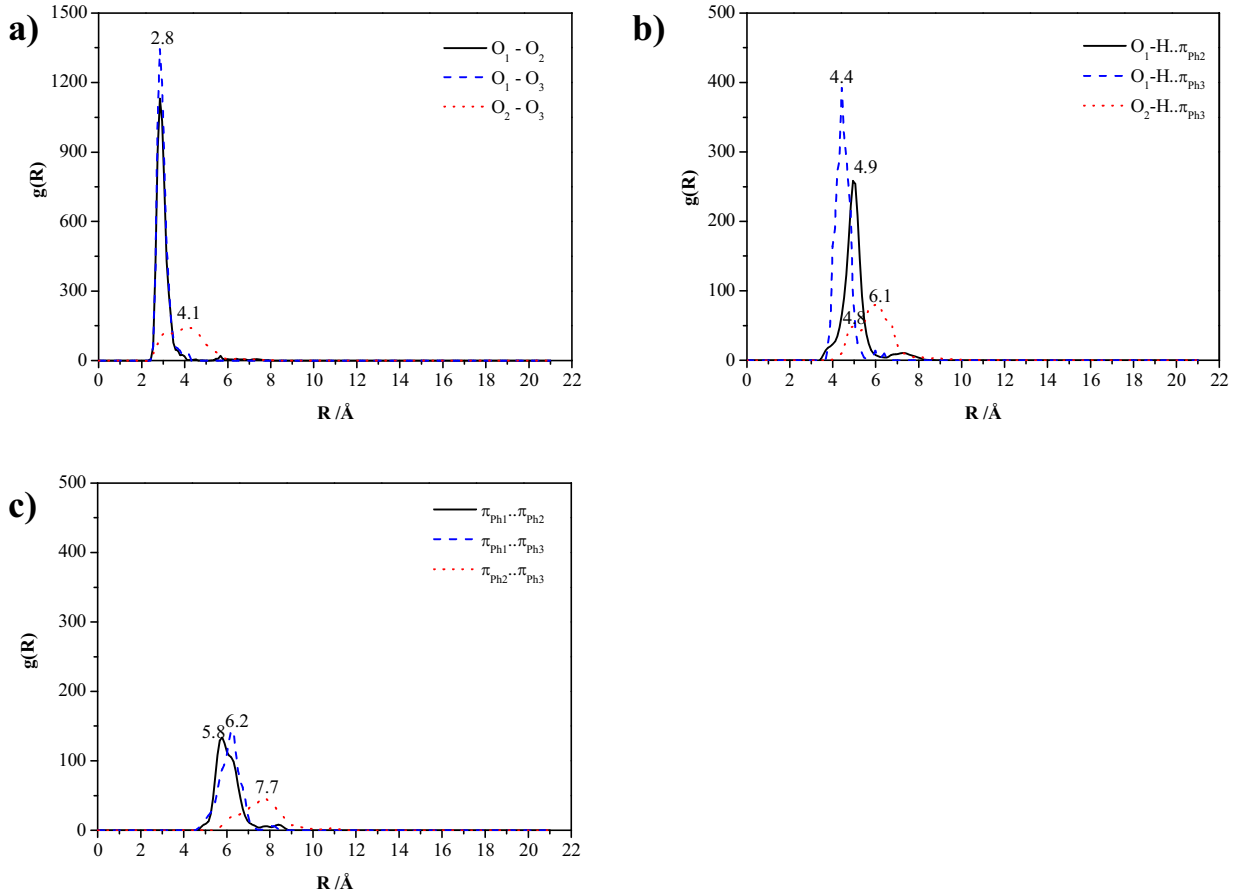
a)
2.8
4.1
O_1 - O_2
O_1 - O_3
O_2 - O_3
g(R)
R /Å
b)
4.4
4.9
6.1
4.8
O_1-H..π_{Ph2}
O_1-H..π_{Ph3}
O_2-H..π_{Ph3}
g(R)
R /Å
c)
5.8
6.2
7.7
π_{Ph1}..π_{Ph2}
π_{Ph1}..π_{Ph3}
π_{Ph2}..π_{Ph3}
g(R)
R /Å

Fig. 7

Table-1

Table 1 Energetic results obtained from MD-$[(PhOH)_n]^{frozen}_{Benz}$ and MD-$[(PhOH)_n]^{free}_{Benz}$, n = 1 – 3. Energies are in kJ/mol.

	$< E^{pot}_{Benz} >$	$< E^{solu-solu}_{Benz} >$	$< E^{solu-solv}_{Benz} >$
MD-$[PhOH]^{frozen}_{Benz}$	-35.4	-	-106.0
MD-$[PhOH]^{free}_{Benz}$	-35.3	-	-58.1
MD-$[(PhOH)_2]^{frozen}_{Benz}$	-35.5	-	-101.0
MD-$[(PhOH)_2]^{free}_{Benz}$	-35.5	-2.3	-123.4
MD-$[(PhOH)_3]^{free}_{Benz}$	-35.4	-51.8	-98.0

$< E^{pot}_{Benz} >$ = average potential energy.

$< E^{solu-solu}_{Benz} >$ = average solute-solute interaction energy.

$< E^{solu-solv}_{Benz} >$ = average solute-solvent interaction energy.

Table-2

Table 2 The highest probabilities at the labeled contours on the π-PD maps ($<P^{\pi\text{-PD}}>_{max}$) in Fig. 3, together with the corresponding lowest average interaction energies ($< \Delta E^{X}_{Benz} >_{min}$) obtained from MD-$[PhOH]^{frozen}_{Benz}$. Energies are in kJ/mol and X = PB-PD, BB-PD or PB-BB-PD.

	$<P^{\pi\text{-PD}}>_{max}$	$< \Delta E^{PB\text{-}PD}_{Benz} >_{min}$	$< \Delta E^{BB\text{-}PD}_{Benz} >_{min}$	$< \Delta E^{PB\text{-}BB\text{-}PD}_{Benz} >_{min}$
Z = -0.5 – 0.5 Å				
A	0.104	-17.28	-74.23	-83.65
C	0.042	-7.29	-79.74	-81.41
Z = 0.0 – 1.0 Å				
A	0.080	-16.10	-78.33	-94.43
C	0.034	-7.53	-77.17	-82.12
Z = 1.0 – 2.0 Å				
A	0.033	-16.10	-72.97	-83.14
B	0.031	-10.84	-72.94	-82.91
C	0.024	-7.91	-76.35	-88.18
Z = 2.0 – 3.0 Å				
A	0.036	-9.48	-76.87	-91.47
B	0.114	-11.71	-75.00	-86.06
C	0.027	-9.78	-74.77	-82.46

Table 3 The highest probabilities at the labeled contours on the π-PD maps ($<P^{\pi\text{-PD}}>_{max}$) in Fig. 5, together with the corresponding lowest average interaction energies ($<\Delta E^{X}_{Benz}>_{min}$) obtained from MD-$[(PhOH)_2]^{frozen}_{Benz}$. Energies are in kJ/mol and X = PB-PD, BB-PD or PB-BB-PD.

	$<P^{\pi\text{-PD}}>_{max}$	$<\Delta E^{PB\text{-}PD}_{Benz}>_{min}$	$<\Delta E^{BB\text{-}PD}_{Benz}>_{min}$	$<\Delta E^{PB\text{-}BB\text{-}PD}_{Benz}>_{min}$
Z = -0.5 – 0.5 Å				
A	0.083	-15.11	-79.86	-94.14
B	0.048	-23.67	-65.44	-79.34
C	0.054	-11.66	-76.19	-79.58
E	0.023	-23.89	-71.31	-93.26
Z = 0.0 – 1.0 Å				
B	0.038	-20.32	-70.17	-89.78
C	0.047	-9.06	-79.95	-82.23
D	0.053	-11.79	-73.16	-84.73
E	0.062	-23.91	-71.35	-91.18
Y = -2.0 – -1.0 Å				
A	0.133	-22.14	-73.05	-86.50
B	0.056	-7.10	-74.90	-80.76
C	0.035	-10.94	-81.60	-81.30
D	0.037	-20.85	-70.79	-86.51
E	0.039	-8.33	-80.29	-84.28
X = -1.0 – 0.0 Å				
A	0.047	-13.68	-74.05	-85.53
B	0.043	-18.03	-74.05	-92.08
C	0.106	-9.08	-75.12	-79.62
D	0.091	-26.68	-67.89	-87.73
E	0.040	-15.16	-78.05	-91.64

ผลผลิต

Publications

1. *Proton transfer reactions and dynamics in the CH_3OH-H_3O^+-H_2O Complexes*,
   K. Sagarik*, S. Chaiwongwattana and V. Vchirawongkwin,
   Phys. Chem. Chem. Phys., **12**, 918-929 (2010). (JIF = 4.12)
2. *Proton transfer reactions and dynamics in protonated water clusters*,
   K. Sagarik*, C. Lao-ngam, P. Asawakun and S. Wannarat, *submitted*.
3. *Proton transfer reactions and dynamics at sulfonic acid group of Nafion®,*
   M. Phonyiem and K. Sagarik, *submitted.*
4. *Structures and Dynamics of Phenol Clusters in Benzene Solutions*,
   S. Chaiwongwattana and **K. Sagarik**, *Chem. Phys*., **355**, 103-117 (2009). (JIF = 2.28)
   (Paper acknowledged BRG 5180022)

Presentations

1. *Structures and Dynamics of Proton Transfer at Sulfonate Group of Nafion®,*
   K. Sagarik, 7th International Conference of Computational Methods
   in Sciences and Engineering 2009 (ICCMSE 2009), Rhodes, Greece 2009.
2. *Proton transfer reactions and dynamics at hydrophilic group of Nafion®:*
   Born-Oppenheimer MD simulations on model systems,
   K. Sagarik, 43rd IUPAC world polymer congress, The Royal Society
   of Chemistry (RSC), Glasgow, United Kingdom 2010.

บทความสำหรับเผยแพร่

ปฏิกิริยาการถ่ายโอนโปรตอนและพลวัตในแนฟิออน

กฤษณะ สาคริก
สาขาวิชาเคมี สำนักวิชาวิทยาศาสตร์
มหาวิทยาลัยเทคโนโลยีสุรนารี นครราสีมา 30000

ปฏิกิริยาการถ่ายโอนโปรตอน (proton transfer reaction) ในสารละลายที่เป็นน้ำ ของเหลว และของแข็ง เป็นปฏิกิริยาสำคัญในวิชาเคมีไฟฟ้า โดยเฉพาะอย่างยิ่ง ที่เกี่ยวข้องกับการพัฒนาพลังงานทดแทน เช่น เซลล์เชื้อเพลิง (fuel cell) เซลล์เชื้อเพลิงที่ใช้เมมเบรนแลกเปลี่ยนโปรตอน (proton exchange membrane fuel cell, PEMFC) ส่วนใหญ่มีน้ำเป็นตัวกลาง โดยแปลงพลังงานเคมีที่เกิดขึ้นจากปฏิกิริยาระหว่างแก๊สไฮโดรเจนและออกซิเจนไปเป็นพลังงานไฟฟ้า เมมเบรนแลกเปลี่ยนโปรตอนที่นิยมใช้ในปัจจุบัน ได้แก่ Nafion® ซึ่งเป็นพอลิเมอร์ประเภท perfluorinated Nafion® มีความคงทนค่อนข้างสูง เนื่องจากการทำงานพื้นฐานของเซลล์เชื้อเพลิงขึ้นอยู่กับความสามารถในการถ่ายโอนโปรตอน (H^+) จากขั้วไฟฟ้าแอโนด (anode) ผ่านเมมเบรนแลกเปลี่ยนโปรตอนไปยังแคโทด (cathode) การพัฒนาประสิทธิภาพของเซลล์เชื้อเพลิงจึงต้องศึกษาปฏิกิริยามูลฐาน (elementary reaction) และพลวัต (dynamics) ของโปรตอนในตัวกลางต่างๆ ในรายละเอียด ถึงแม้ว่าที่ผ่านมาจะมีรายงานผลการศึกษาปฏิกิริยาการถ่ายโอนโปรตอนทั้งทางทฤษฎีและการทดลองมากพอควร ปรากฏว่าในปัจจุบันยังไม่มีข้อสรุปที่ชัดเจนและเป็นที่ยอมรับ

งานวิจัยเรื่องนี้ศึกษาปฏิกิริยามูลฐาน กลไกปฏิกิริยา และพลวัตของปฏิกิริยาการถ่ายโอนโปรตอนในแบบจำลอง protonated water clusters สารเชิงซ้อน CH_3OH-H_3O^+-H_2O และ CF_3SO_3H-H_3O^+-H_2O โดยใช้วิธีเคมีควอนตัมและ Born-Oppenheimer Molecular Dynamics (BOMD) simulations ที่ 350 K การศึกษาเริ่มจากการคำนวณโครงสร้างของสารเชิงซ้อนในสภาวะสมดุลโดยวิธี density functional theory (DFT method) ที่ระดับ B3LYP/TZVP โดยเน้นโครงสร้างพันธะไฮโดรเจนที่สามารถเกิดการถ่ายโอนโปรตอนได้ง่าย ผลการวิเคราะห์ IR spectra แสดง asymmetric O-H stretching frequency ของโปรตอนที่มีศักยภาพในการถ่ายโอนที่ $\nu^{OH} \approx 1000$ cm^{-1} โดยมีความถี่ขีดเริ่มเปลี่ยน (threshold frequency) (ν^{OH*}) ในช่วง 1700 ถึง 2200 cm^{-1} ทั้งนี้ ขึ้นกับชนิดและสภาพแวดล้อมของพันธะไฮโดรเจนที่นำมาศึกษา BOMD simulations แสดง ν^{OH} เพิ่มเติมที่ความถี่สูงขึ้น โดยแถบ IR ที่ความถี่ต่ำสัมพันธ์กับ oscillatory shuttling motion และที่ความถี่สูงสัมพันธ์กับ structural diffusion motion ความถี่ทั้งสองนี้ถือเป็นอัตลักษณ์สำคัญสำหรับโปรตอนที่มีศักยภาพในการถ่ายโอนโปรตอนสูง ผลการศึกษายังแสดงด้วยว่า การที่ในพันธะไฮโดรเจนมีการสั่นหลายประเภทคู่ควบกัน (coupling) ทำให้ไม่สามารถศึกษาปฏิกิริยาการถ่ายโอนโปรตอนโดยใช้ static proton transfer potential และแบบจำลองการคำนวณที่นำมาใช้ต้องพิจารณาการกระเพื่อมของพลังงานความร้อน (thermal energy fluctuation) และพลวัตในพันธะไฮโดรเจนด้วย

งานวิจัยเรื่องนี้ทำให้ทราบพฤติกรรมการสั่นของโปรตอนที่กำลังถ่ายโอนในรายละเอียด โดยได้เสนอทฤษฎีและแนวทางในการเปรียบเทียบความสามารถในการถ่ายโอนโปรตอนในพันธะไฮโดรเจนเมื่ออยู่ในสภาพแวดล้อมต่าง ๆ ตลอดจนเสนอเกณฑ์และวิธีการใช้ IR spectroscopy ในการติดตามปฏิกิริยาการถ่ายโอนโปรตอนที่ซับซ้อนขึ้น เช่น ในการทดลอง ทั้งนี้ ผลการวิจัยสามารถนำไปเป็นแนวทางในการประยุกต์ เพื่อการปรับปรุงประสิทธิภาพการถ่ายโอนโปรตอนในเมมเบรนแลกเปลี่ยนโปรตอนได้ในอนาคต

Proton transfer reactions and dynamics in Nafion®

Kritsana Sagarik
School of Chemistry, Institute of Science, Suranaree University of Technology
Nakhon Ratchasima 30000, THAILAND

Proton transfer reaction in condensed phase represents one of the most important problems in electrochemistry, especially in connection with the development of alternative energy sources such as fuel cells (FC). Since the basic operations in fuel cells depend upon the transportation of protons (H^+) generated at anode across proton exchange membrane (PEM) to cathode, it is vital to understand elementary reactions and dynamics of proton transfer processes in liquid, solid and aqueous solution. Although some theoretical and experimental information has been accumulated, precise mechanisms of proton transfer in PEMFC, especially in hydrogen bond (H-bond) complexes, are not completely known. In the present work, elementary reactions, energetic and dynamics of proton transfer were studied using three model systems namely, protonated water clusters, CH_3OH-H_3O^+-H_2O and CF_3SO_3H-H_3O^+-H_2O complexes. The H-bond complexes were investigated using quantum chemical methods and Born-Oppenheimer Molecular Dynamics (BOMD) simulations. The investigations began with searching for equilibrium structures at low hydration levels using the DFT method at the B3LYP/TZVP level, from which the H-bonds susceptible to proton transfer were characterized and analyzed. The analyses of IR spectra showed characteristic asymmetric O-H stretching frequencies of the transferring proton at $\nu^{OH} \approx 1000$ cm^{-1} and the threshold frequencies for proton transfer (ν^{OH*}) in the range of 1700 and 2200 cm^{-1}. However, these cannot be definitive, due to the neglect of the thermal energy fluctuation and dynamics in B3LYP/TZVP calculations. BOMD simulations at 350 K revealed an additional ν^{OH} at a higher frequency. The low- and high-frequency bands can be associated with the oscillatory shuttling and structural diffusion motions of the transferring proton in H-bond, respectively. The present results concluded that, due to coupling among various modes of vibrations, the discussions on proton transfer reactions cannot be made based on static proton transfer potentials. In order to study proton transfer reactions, thermal energy fluctuations and dynamics must be included in the model calculations, as in the case of BOMD simulations. The present work provided insights into vibrational behaviors of the transferring protons, as well as suggested theoretical methods and criteria to monitor and improve the efficiency of proton transfer in more complex systems.

กิตติกรรมประกาศ

The authors would like to acknowledge the financial supports from the Thailand Research Fund (TRF); the Advanced Research Scholarship (BRG-5180022) for Prof. Kritsana Sagarik; the Royal Golden Jubilee (RGJ) Ph.D. Program, Grant No. PHD/0110/2548 for Prof. Kritsana Sagarik and Mayuree Phonyiem; RGJ-Ph.D. Program, Grant No. PHD/0121/2549 for Prof. Kritsana Sagarik and Chareonsak Lao-Ngam. High- performance computer facilities provided by the following organizations are gratefully acknowledged: School of Mathematics and School of Chemistry, SUT; National Electronics and Computer Technology Center (NECTEC) and National Nanotechnology Center (NANOTEC), National Science and Technology Development Agency (NSTDA); the Thai National Grid Center (THAIGRID), Ministry of Information and Communication Technology (MICT).

ภาคผนวก

Proton transfer reactions and dynamics in CH_3OH–H_3O^+–H_2O complexes

Kritsana Sagarik,*[a] Sermsiri Chaiwongwattana,[a] Viwat Vchirawongkwin[b] and Supakit Prueksaaroon[c]

Received 7th July 2009, Accepted 26th October 2009
First published as an Advance Article on the web 4th December 2009
DOI: 10.1039/b913385b

Proton transfer reactions and dynamics in hydrated complexes formed from CH_3OH, H_3O^+ and H_2O were studied using theoretical methods. The investigations began with searching for equilibrium structures at low hydration levels using the DFT method, from which active H-bonds in the gas phase and continuum aqueous solution were characterized and analyzed. Based on the asymmetric stretching coordinates (Δd_{DA}), four H-bond complexes were identified as potential transition states, in which the most active unit is represented by an excess proton nearly equally shared between CH_3OH and H_2O. These cannot be definitive due to the lack of asymmetric O–H stretching frequencies (ν^{OH}) which are spectral signatures of transferring protons. Born–Oppenheimer molecular dynamics (BOMD) simulations revealed that, when the thermal energy fluctuations and dynamics were included in the model calculations, the spectral signatures at $\nu^{OH} \approx 1000\ cm^{-1}$ appeared. In continuum aqueous solution, the H-bond complex with incomplete water coordination at charged species turned out to be the only active transition state. Based on the assumption that the thermal energy fluctuations and dynamics could temporarily break the H-bonds linking the transition state complex and water molecules in the second hydration shell, elementary reactions of proton transfer were proposed. The present study showed that, due to the coupling among various vibrational modes, the discussions on proton transfer reactions cannot be made based solely on static proton transfer potentials. Inclusion of thermal energy fluctuations and dynamics in the model calculations, as in the case of BOMD simulations, together with systematic IR spectral analyses, have been proved to be the most appropriate theoretical approaches.

Introduction

Proton transport in condensed phases represents one of the most important problems in electrochemistry, especially in connection with the development of alternative energy sources such as fuel cells (FC).[1,2] Since the basic operations in fuel cells depend upon the transportation of protons (H^+) generated at the anode across a proton exchange membrane (PEM)—often made from Nafion®—to the cathode, where they react with oxygen to produce water,[1] it is vital to understand elementary reactions and dynamics of proton transfer processes in liquids, solid and aqueous solutions. Although some theoretical and experimental information has been accumulated,[3–6] precise mechanisms of proton transfer in PEMFC, especially for those employing methanol (CH_3OH) as a direct fuel, are not completely known. Since some basic chemistry of proton transfer reactions has been discussed in details in many review articles,[4–6] only the theoretical and experimental information relevant to the present study will be briefly summarized here.

CH_3OH has been frequently selected as a model compound for the investigation of proton transport in hydrogen bonds (H-bonds).[7–20] The abnormally high mobility of an excess proton in liquid methanol ($[CH_3OH]_{liq}$) has been extensively studied using *ab initio* molecular dynamics (MD) simulations, from which a structural diffusion mechanism of cationic defects was proposed.[16] Having both hydrophobic (CH_3) and hydrophilic (OH) groups in the same molecule makes the H-bond structures in $[CH_3OH]_{liq}$ different from $[H_2O]_{liq}$; one-dimensional linear H-bond chains with occasional branches seem to be the predominant species from 153 K to room temperature.[19] Due to significant roles played by the methyloxonium ion ($CH_3OH_2^+$) in direct methanol fuel cells (DMFC),[17] delocalization of proton in the H-bond complexes formed from H_3O^+, CH_3OH and H_2O has been extensively studied.[13–16] In the presence of an excess proton, two H-bond structures dominate in the CH_3OH–H_2O clusters, namely the fully solvated and open chain structures.[13] The excess proton is preferentially taken by CH_3OH in the open chain structure.[13] A structural analogue of the Zundel complex ($C_2H_9O_2^+$) and $CH_3OH_2^+$ were suggested by density functional theory (DFT) calculations at the B3LYP/6-31 + G(d) level and

[a] *School of Chemistry, Institute of Science, Suranaree University of Technology, Nakhon Ratchasima 30000, Thailand. E-mail: kritsana@sut.ac.th; Fax: (6644) 224635; Tel: (6644) 224635*
[b] *Department of Chemistry, Faculty of Science, Chulalongkorn University, Bangkok 10500, Thailand*
[c] *National Electronics and Computer Technology Center (NECTEC), Pathumthani 12120, Thailand*

vibrational predissociation spectroscopy to play important roles in proton transfer in the mixed H-bond clusters.[15]

Proton affinities in the CH_3OH–H_3O^+–H_2O $1:1:n$ complexes, $1 \leqslant n \leqslant 5$, were investigated in the gas phase using DFT calculations and IR spectroscopy at 170 K.[20] DFT calculations at the B3LYP/6-31G + (d) level revealed that the excess proton can be either localized close to CH_3OH or H_2O, forming $CH_3OH_2^+$ or H_3O^+, respectively. The position of the excess proton is sensitive to the number of water molecules, as well as the geometry of the H-bond complexes. The IR spectral signatures determined from the free O–H stretching frequencies in the range of 2700 and 3900 cm^{-1} indicated that $CH_3OH_2^+$ and H_3O^+ possess comparable stability and could be concurrently detected in the gas phase.[20] Moreover, in the CH_3OH–H_3O^+–H_2O $1:1:n$ complexes, the excess proton could be preferentially captured by CH_3OH when $n = 1$ and equally shared by CH_3OH and H_2O when $n = 3$. The excess proton could gradually move away from CH_3OH when $n \geq 3$. The results in ref. 20 led to the conclusion that the protonated ions in acidic $[CH_3OH]_{aq}$ are quite flexible and can fluctuate rapidly over $CH_3OH_2^+$, H_3O^+ and $CH_9O_3^+$.

Vibrational spectroscopy has been one of the most powerful techniques in H-bond research.[21] This is due to the fact that the most evident effects of the A–H$\cdots$B H-bond formation are the red shifts of the A–H stretching mode, accompanied by its intensity increase and band broadening.[13,18] Analyses of the A–H stretching frequencies could also lead to valuable information on proton transfer reactions in H-bonds.[17] As an example, IR experiments,[22] quantum-dynamical calculations[23–25] and Born–Oppenheimer MD (BOMD) simulations[26] suggested that the vibrational spectra of the Zundel complex ($H_5O_2^+$) in aqueous solutions can be divided into three distinct regions. The vibrational frequencies above 3000 cm^{-1} correspond to the symmetric and asymmetric stretching modes of individual water molecules, whereas those between 1000 and 2000 cm^{-1} are associated with the characteristic vibrational frequencies of the transferring protons.[25] The correlation between the O–H stretching frequency and the probability of proton transfer in H-bond was investigated and discussed in detail in ref. 13 and 17. Although the assignments of all the features of the individual spectra were not made due to the coupling and overlapping of various vibrational modes, as well as the detection limit of the IR equipment,[20,21] the probability of proton transfer could be associated with the degree of the red shift, by comparison with the corresponding "free" or "non-H-bonded" O–H stretching frequency.[13]

In our previous work,[27] elementary reactions of proton transfer processes at a sulfonic acid group (–SO_3H) of Nafion® were studied using the H-bond complexes formed from triflic acid (CF_3SO_3H), H_3O^+ and H_2O as model systems. BOMD simulations at 298 K revealed that a quasi-dynamic equilibrium could establish between the Eigen ($H_9O_4^+$) and Zundel complexes, and is considered to be one of the most important elementary reactions. It was demonstrated that proton transfer reactions at –SO_3H are not concerted due to the thermal energy fluctuations, leading to quasi-dynamic equilibriums among precursors, transition state complexes and products. Most importantly, –SO_3H could directly and indirectly mediate proton transfer reactions through the formation of proton defects, as well as the –SO_3^- and –$SO_3H_2^+$ transition states.

In order to obtain information for the investigations of DMFC, elementary reactions and dynamics of proton transfer in hydrated complexes formed from CH_3OH, H_3O^+ and H_2O were studied in the present work. The H-bond complexes were systematically investigated using quantum chemical methods and BOMD simulations, both in the gas phase and continuum aqueous solution. Since proton transfer reactions could be characterized by vibrational motions of the active protons, vibrational frequencies in H-bonds were computed, categorized and analyzed. Based on the information from quantum chemical calculations and BOMD simulations, elementary reactions and dynamics of proton transfer in the model systems were discussed in comparison with available theoretical and experimental data of the same and similar systems.

Computational methods

Since proton transfer reactions are complicated, care must be exercised in selecting appropriate model systems and theoretical methods. Our experience[27] showed that elementary reactions and dynamics of proton transfer in H-bonds could be studied reasonably well by taking the following three basic steps: (1) searching for all potential precursors and transition state complexes in proton transfer pathways using pair potentials; (2) refinements of the computed structures using an accurate quantum chemical method; (3) BOMD simulations starting from the refined structures. These three steps were also applied in the present work.

Our experience also showed that the inclusion of too many water molecules in the model systems could lead to difficulties in the analyses of proton transfer reactions.[27] Therefore, it was the strategy of the present work to restrict the number of water molecules in the model systems. Since the $CH_3OH_2^+$–CH_3OH complex contributes only 5% to the proton transfer events[14] and the excess proton starts to move away from $CH_3OH_2^+$ when $n = 3$,[20] the CH_3OH–H_3O^+–H_2O $1:1:n$ complexes, $1 \leq n \leq 3$, were chosen in the present study. Some basic structural and dynamic properties of the CH_3OH–H_2O and CH_3OH–H_3O^+ complexes were also investigated.

In order to characterize IR spectra of the transferring proton, as well as their correlations with the probability of proton transfer,[28] O–H stretching frequencies in H-bonds were computed and analyzed, using a quantum chemical method and BOMD simulations. Since the electric field introduced by the polar solvent could determine the potential energy surface on which the active proton moves, a continuum solvent model had to be included in the model calculations. In the present work, the conductor-like screening model (COSMO), with a dielectric constant (ε) of 78, was employed to account for the effects of the extended H-bond networks of water, which were not explicitly included in the model systems. A literature survey showed that COSMO has been applied successfully in various H-bond systems.[29]

Searching for potential precursors and transition state complexes

All the H-bond complexes which could serve as precursors and transition state complexes in proton transfer pathways were

searched, characterized and analyzed. In order to effectively scan the intermolecular potential energy surfaces, test-particle model (T-model) potentials[30–39] were constructed and employed in the calculations of the equilibrium structures and interaction energies of the hydrated complexes. Since the applicability of the T-model had been discussed in details in our previous studies,[30–39] only some important aspects relevant to the geometry optimizations will be briefly summarized using the CH_3OH–H_3O^+–H_2O 1 : 1 : 1 complex as an example.

Experimental geometries of CH_3OH, H_3O^+ and H_2O were employed[40] and kept constant in the geometry optimizations. For the CH_3OH–H_3O^+–H_2O 1 : 1 : 1 complex, a rigid CH_3OH was placed at the origin of the Cartesian coordinate system. The coordinates of H_3O^+ and H_2O were randomly generated in the vicinities of CH_3OH. Based on the T-model potentials, equilibrium structures of the complex were searched using a minimization technique. One hundred starting configurations were generated and employed as starting configurations in the geometry optimizations. The same procedures were applied in the calculations of equilibrium structures and interaction energies of the hydrated complexes considered here.

Structural refinements and vibrational spectra

Since the T-model potentials are based on rigid molecules, in which cooperative effects are not taken into account, structural refinements with full geometry optimizations had to be made using an appropriate quantum chemical method. A literature survey showed that DFT methods have been frequently chosen due to their ability to predict the effects of electron correlations with a reasonable degree of accuracy, especially for similar H-bond systems.[41–46] Since, in the present investigations, the calculations of vibrational spectra and lengthy BOMD simulations had to be performed, it was necessary to compromise between the accuracy of the theoretical method and available computer resources. In order to achieve all the objectives, DFT calculations were performed using the B3LYP hybrid functional[47] and the triple-zeta valence basis sets augmented by polarization functions (TZVP).[48] The performance of B3LYP in the calculations of vibrational spectra of similar systems was examined and discussed in detail in ref. 49 and 50. It was shown that B3LYP/TZVP calculations are sufficient for the systems with and without occupied d-states, and could be applied reasonably well in the calculations of equilibrium structures and interaction energies, as well as vibrational spectra, of such systems.[49]

The absolute and local minimum energy geometries of the H-bond complexes computed from the T-model potentials were employed as starting configurations in B3LYP/TZVP geometry optimizations. In order to ensure that the optimized geometries are at the stationary points of the potential energy surfaces, a tight SCF (self consistent field) energy convergence criterion (less than 10^{-8} au) with a maximum norm of Cartesian gradients of less than 10^{-4} au were adopted in B3LYP/TZVP geometry optimizations. In the present work, B3LYP/TZVP calculations were made using the TURBOMOLE 6.0 software package.[51]

The experiment in ref. 17 showed that the H-bond distance ($R_{O\cdots O}$) in concentrated HCl solutions could be divided into three groups, namely the internal, external and solvation groups. The H-bonds linking directly to proton belong to the internal group, with $R_{O\cdots O}$ in the range of 2.45–2.57 Å, whereas $R_{O\cdots O}$ in the external and solvation groups are in the ranges of 2.60–2.70 Å and longer than 2.70 Å, respectively. The H-bond protons in the internal group are considered to be active in proton transfer. In the present work, an attempt was made to use similar criteria[17] to discuss the tendency of proton transfer in H-bonds. A concept of the "most active" H-bond[52] was tentatively applied to describe the Grothuss mechanism.[53] Within the framework of the most active H-bond, the asymmetric stretching coordinate of a donor (D)–acceptor (A) pair is defined by $\Delta d_{DA} = |d_{A\cdots H} - d_{B\cdots H}|$;[14] $d_{A\cdots H}$ and $d_{B\cdots H}$ are the A–H and B$\cdots$H distances, respectively. A H-bond is considered to be "active" with respect to proton transfer when $\Delta d_{DA} < 0.1$ Å, and "inactive" when $\Delta d_{DA} > 0.4$ Å.[14] Therefore, according to Δd_{DA}, the H-bond in $H_5O_2^+$ is the most active ($\Delta d_{DA} = 0$); the H-bond proton is equally shared by the two water molecules. In the present work, the internal and external H-bonds were classified using plots between Δd_{DA} and $R_{O\cdots O}$; appropriate functions were chosen by the least squares method to represent the relationships in the internal and external groups.

Assuming no coupling between degrees of freedom, harmonic vibrational frequencies were computed in the present work from numerical second derivatives, from which the analyses of normal modes in terms of internal coordinates were made, using NUMFORCE and AOFORCE programs,[51] respectively. Being associated with the dynamics of proton transfer in H-bonds,[54] asymmetric O–H stretching frequencies (ν^{OH}) were of primary interest. It should be noted that vibrational frequencies derived from quantum chemical calculations are generally overestimated compared to experimental values, and a scaling factor which partially accounts for anharmonicities and systematic errors is required. Although the exact O–H stretching frequencies were not the main objective, a scaling factor was applied in the present study; the scaling factor of 0.9614 was proved to be appropriate for B3LYP calculations.[55]

In order to measure the activity of H-bond protons in terms of ν^{OH}, classical interpretations of IR stretching frequencies for concentrated acid solutions[56] were employed as criteria; IR stretching frequencies of H-bond protons were divided into three groups, namely the internal (1300–2200 cm^{-1}), external (2500–3200 cm^{-1}) and outer layer groups (3300–3400 cm^{-1}). In order to correlate the concept of the most active H-bond with the classical interpretations of IR stretching frequencies,[56] the H-bonds in the internal and external groups were distinguished based on the relationship between ν^{OH} and $R_{O\cdots O}$; ν^{OH} and $R_{O\cdots O}$ were plotted and appropriate functions were chosen using the least squares method.

Quantum MD simulations

Dynamics of rapid covalent bond formation and cleavage could be studied reasonably well using quantum MD simulations,[57] among which DFT-MD simulations have been widely used in recent years.[58,59] In the present work, proton transfers in the CH_3OH–H_3O^+ and CH_3OH–H_3O^+–H_2O complexes were investigated using BOMD simulations[60,61]

with canonical ensemble (NVT) at 350 K. Within the framework of BOMD simulations, classical equations of motion of nuclei on the BO (Born–Oppenheimer) surfaces are integrated, whereas forces on nuclei are calculated in each MD step from quantum energy gradients, with the molecular orbitals (MOs) updated by solving Schrödinger equations. BOMD simulations are therefore more accurate, as well as considerably CPU time consuming, compared to conventional classical MD simulations, in which forces on nuclei are determined from predefined empirical or quantum pair potentials. Although the high mobility of protons was initially attributed to quantum mechanical (QM) tunneling,[62,63] the results of BOMD simulations[25] and conductivity measurements[64] showed that mechanisms of proton transfer could be explained reasonably well without assuming proton tunneling to be the important pathways.

In order to ensure that all important dynamics of proton transfer processes in the CH_3OH–H_3O^+–H_2O complexes were taken into account, the equilibrium structures computed in the previous section were used as starting configurations in BOMD simulations. Since proton transfer in aqueous solutions involves dynamic processes with different timescales,[65–67] the complexity of proton transfer reactions could be reduced using various approaches. The observation that the actual proton transfer occurs on a femtosecond (fs) timescale,[67] which is, in general, faster than solvent structure reorganization,[66] made it possible to perform BOMD simulations by focusing on short-lived phenomena taking place before H-bond structure reorganizations. Since, in aqueous solutions, the rapid interconversion between the Zundel and Eigen complexes happens within 100 fs (10^{-13} s),[65] the timestep used in solving dynamic equations was set to about 1 fs (0.968 fs = 40 au). In each BOMD simulations, 4000 timesteps were devoted to equilibration and 10 000 timesteps to property calculations, corresponding to about 10 ps. In order to ensure that, in the course of the BOMD simulations, the active proton is not trapped in a minimum, appropriate temperature fluctuations must be selected, as suggested in ref. 68. This was accomplished in TURBOMOLE 6.0[51] by applying the Nose-Hoover thermostat at every 30 BOMD steps.

In order to search for spectral signatures of transferring protons, IR spectra of H-bonds were computed from Fourier transformations of the velocity autocorrelation function (VACF);[69] the approach is appropriate as it allows various vibrational modes to be computed separately. Since only the H-bond protons involved in structural diffusion were of interest and the reorientation of water molecules takes about 1–2 ps,[70,71] IR spectra were calculated within a short time limit of 1 ps. This choice can be justified by the observation that the average lifetime of the H-bond in CH_3OH–H_2O solutions is approximately 1.2 ps.[14] Only symmetric and asymmetric O–H stretching frequencies (ν^{OH}) of the H-bond protons, as well as the O–O vibrations, were of interest.

The diffusion coefficient (D) of the active proton could be computed from BOMD simulations. The Einstein equation[72–74] was employed in the present work, by which the diffusion coefficient is determined from the slope of the mean square displacement (MSD). Since the calculations of the diffusion coefficient of a single particle (H^+) confined in a short H-bond distance are not straightforward,[73,74] care must be exercised, especially in selecting the time interval over which MSDs were computed; the time interval cannot be too large due to the limitation of the allowed displacement.[74] After several test calculations, linear relationships between MSD and simulation time could be obtained when the time intervals are not larger than 0.5 ps.

Results and discussions

Equilibrium structures and vibrational frequencies

Fig. 1 shows the refined equilibrium structures and interaction energies (ΔE) of the H-bond complexes in the gas phase and continuum aqueous solution, together with characteristic H-bond distances and asymmetric stretching coordinates (Δd_{DA}). Asymmetric O–H stretching frequencies (ν^{OH}) of H-bond protons are given in Fig. 2, together with the frequency shifts ($\Delta\nu^{OH}$) due to the continuum aqueous solvent. The red shifts are designated by negative values of $\Delta\nu^{OH}$. It appeared that the equilibrium structures in the gas phase and continuum aqueous solution are the same and agree well with the theoretical results in ref. 20. Therefore, only Δd_{DA}, ν^{OH} and $\Delta\nu^{OH}$, which could be related to the tendencies of proton transfer in H-bonds, are discussed in details. In order to simplify the discussion, the H-bonds in Fig. 1 and 2 are labeled with numbers in parentheses.

For the CH_3OH–H_2O complex in the gas phase, B3LYP/TZVP calculations predicted the structure, in which a water molecule acts as a proton donor, to be about 1.8 kJ mol^{-1} more stable than the one as proton acceptor (structures (a) and (b) in Fig. 1, respectively). The results are in excellent agreement with microwave[75] and IR measurements.[76] The stabilities of structures (a) and (b) are considerably increased in continuum aqueous solution, with $\Delta E = -73.4$ and -72.8 kJ mol^{-1}, respectively. Δd_{DA} and ν^{OH} do not show a tendency of proton transfer in structures (a) and (b), both in the gas phase and continuum aqueous solution.

Interesting results were obtained for the CH_3OH–H_3O^+ complex (structure (c) in Fig. 1). B3LYP/TZVP calculations revealed that the H-bond proton tends to protonate at CH_3OH, forming $CH_3OH_2^+$. This is in accordance with the observation that CH_3OH in acid solution possesses a higher proton affinity than water.[75] Δd_{DA} shows a slightly higher tendency of proton transfer in the continuum aqueous solution compared to the gas phase (0.24 and 0.32 Å, respectively). The trends of Δd_{DA} are supported by the asymmetric O–H stretching frequencies in Fig. 2. The strong IR absorption peaks at $\nu^{OH} = 2086$ and 1690 cm^{-1} appeared to be the characteristics of the H-bond proton in the CH_3OH–H_3O^+ complex in the gas phase and continuum aqueous solution, respectively, with $\Delta\nu^{OH} = -369$ cm^{-1}. It was reported in ref. 20 that the asymmetric O–H stretching frequencies cannot be measured easily in experiments since the energy provided by a single IR photon is much lower than the minimum energy required to dissociate this complex *via* one-photon excitation processes.

Structures (d) and (e) in Fig. 1 are the two minimum energy geometries of the CH_3OH–H_3O^+–H_2O 1 : 1 : 1 complex. For structure (d), the H-bond between CH_3OH and H_3O^+

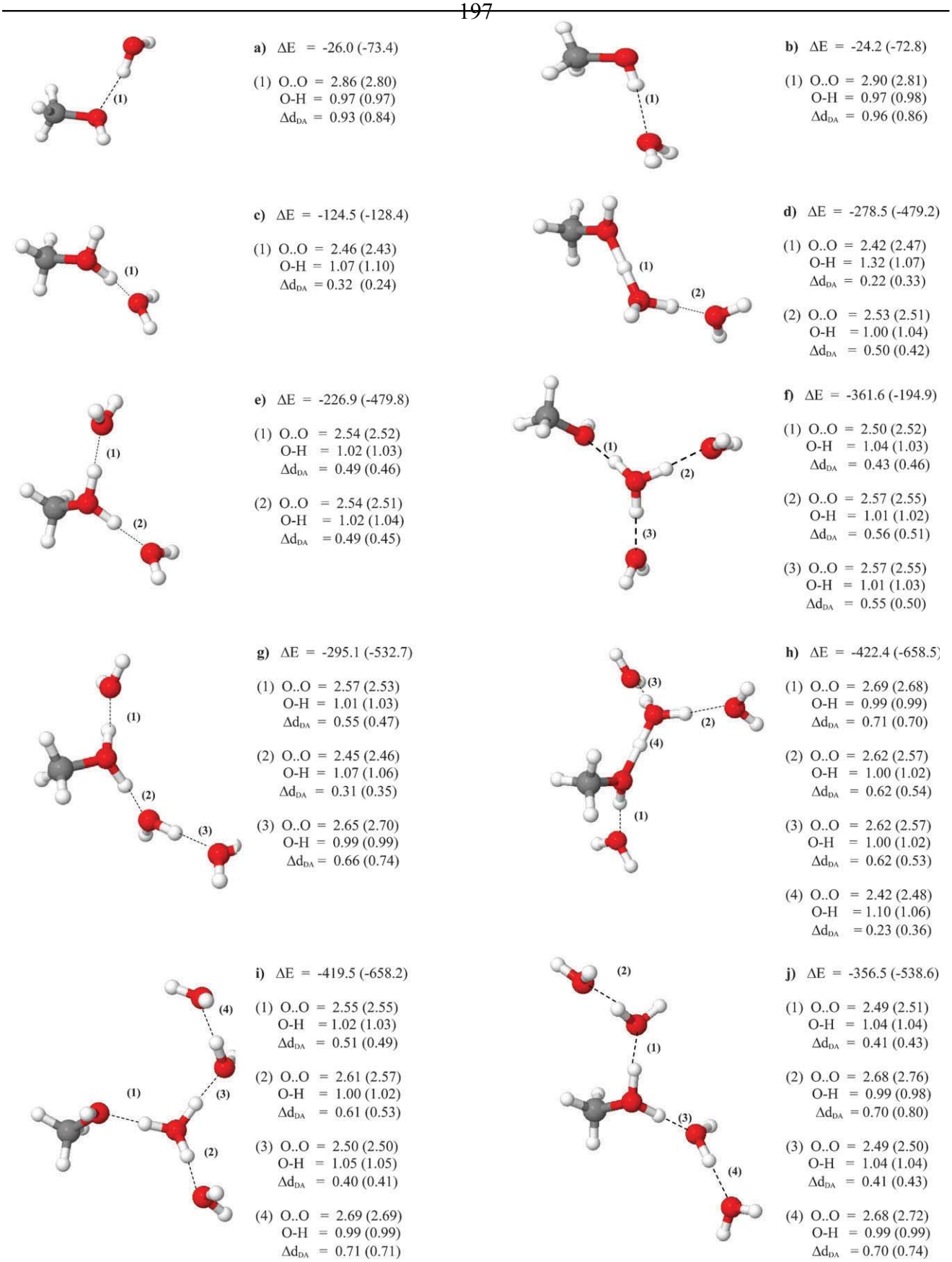

Fig. 1 Refined equilibrium structures, interaction energies (ΔE) and asymmetric stretching coordinates (Δd_{DA}) of the CH_3OH–H_2O, CH_3OH–H_3O^+ and CH_3OH–H_3O^+–H_2O complexes, obtained from B3LYP/TZVP geometry optimizations. H-bond distances are in Å and energies in kJ mol^{-1}. The values in parentheses are the results in continuum aqueous solution. (a)–(b) CH_3OH–H_2O complexes. (c) CH_3OH–H_3O^+ complex. (d)–(e) CH_3OH–H_3O^+–H_2O 1 : 1 : 1 complexes. (f)–(g) CH_3OH–H_3O^+–H_2O 1 : 1 : 2 complexes. (h)–(j) CH_3OH–H_3O^+–H_2O 1 : 1 : 3 complexes.

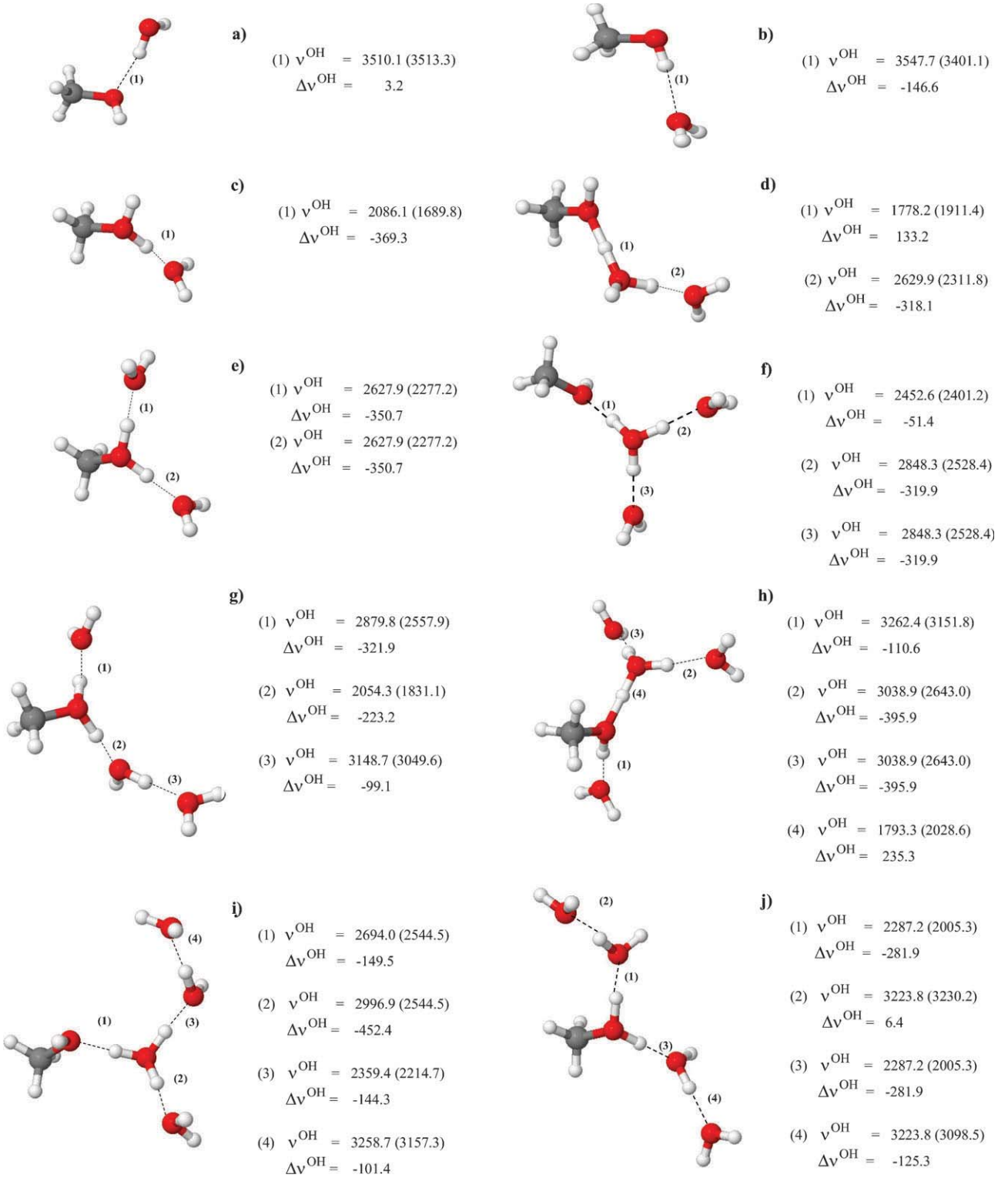

Fig. 2 Asymmetric O–H stretching frequencies (ν^{OH}) of the H-bond protons in the CH_3OH–H_2O, CH_3OH–H_3O^+ and CH_3OH–H_3O^+–H_2O complexes, obtained from B3LYP/TZVP calculations. The values in parentheses are the results in continuum aqueous solution. $\Delta\nu^{OH}$ are the frequency shifts in continuum aqueous solution. ν^{OH} and $\Delta\nu^{OH}$ are in cm^{-1}. (a)–(b) CH_3OH–H_2O complexes. (c) CH_3OH–H_3O^+ complex. (d)–(e) CH_3OH–H_3O^+–H_2O 1 : 1 : 1 complexes. (f)–(g) CH_3OH–H_3O^+–H_2O 1 : 1 : 2 complexes. (h)–(j) CH_3OH–H_3O^+–H_2O 1 : 1 : 3 complexes.

(H-bond (**1**)) shows a higher tendency of proton transfer than H-bond (**2**). In the gas phase and continuum aqueous solution, H-bond (**1**) possesses Δd_{DA} = 0.22 and 0.33 Å, and ν^{OH} = 1778 and 1911 cm^{-1}, respectively. The continuum aqueous solvent leads to a blue shift in H-bond (**1**) and a red shift in H-bond (**2**), with $\Delta\nu^{OH}$ = 133 and −318 cm^{-1},

respectively. The results are different for structure (e), in which $CH_3OH_2^+$ is equally stabilized by two adjacent water molecules, with Δd_{DA} in the gas phase and continuum aqueous solution of 0.49 and 0.46 Å, respectively, and ν^{OH} = 2628 and 2277 cm^{-1}, respectively. These indicated that H-bonds (**1**) and (**2**) in structure (e) are not as active as H-bond (**1**) in structure (d).

Based on the above discussions and the results on the larger hydrated complexes in Fig. 1 and 2, the trends of proton transfer could be anticipated. It appeared that the incomplete water coordination at the charged species, $CH_3OH_2^+$ and H_3O^+ (as in structures (c) and (d), respectively), and the asymmetric H-bond structure at $CH_3OH_2^+$ (as in structures (g) and (h)) could help promote structural diffusion. Therefore, according to Δd_{DA} and the criteria in ref. 14, the H-bond protons in structures (c), (d), (g) and (h) could be active in proton transfer (Δd_{DA} < 0.4 Å), with the tendencies decreasing in the following order:

Gas phase: (d) ≥ (h) > (g) ≥ (c).

Continuum aqueous solution: (c) > (d) ≥ (g) ≥ (h).

Fig. 3a and b show the relationships between the asymmetric stretching coordinate (Δd_{DA}) and the H-bond distance (R_{O-O}), and between ν^{OH} and R_{O-O}, respectively. The trends in Fig. 3a suggest a separation between the internal and external H-bonds at R_{O-O} = 2.55 Å, in good agreement with R_{O-O} = 2.57 Å in ref. 17. The linear relationships for the internal and external H-bonds in the gas phase and continuum aqueous solution could be represented by eqn (1) and (2), respectively.

$$\text{Internal H-bonds: } \Delta d_{DA} = 2.1464R_{O-O} - 4.9559 \quad (1)$$

$$\text{External H-bonds: } \Delta d_{DA} = 1.2936R_{O-O} - 2.7735 \quad (2)$$

Due to the asymptotic behavior at large R_{O-O}, the relationship between ν^{OH} and R_{O-O} in Fig. 3b cannot be approximated by a linear function; at large R_{O-O}, ν^{OH} converges to the asymmetric O–H stretching frequency of a non-H-bonded proton. After several test fittings, an exponential function similar to the integrated rate expression for the first order reaction was found to be the most appropriate. The fitted functions in the gas phase and continuum aqueous solution are shown in eqn (3) and (4), respectively.

$$\text{Gas phase: } \nu^{OH} = -1.17 \times 10^{10}e^{-R_{O-O}/0.1544} + 3526.2 \quad (3)$$

Continuum aqueous solution:

$$\nu^{OH} = -0.71 \times 10^{10}e^{-R_{O-O}/0.1617} + 3583.8 \quad (4)$$

The agreements between ν^{OH} derived from B3LYP/TZVP calculations and the fitted values are included in Fig. 3b.

Based on the results obtained from the static proton transfer potentials (B3LYP/TZVP calculations), one could conclude that, ν^{OH} for the H-bond protons in structures (c), (d), (g) and (h) in the gas phase range from 1778 to 2086 cm^{-1}, and from 1690 to 2029 cm^{-1} in continuum aqueous solution. According to the classical interpretations,[56] the H-bonds in structures (c), (d), (g) and (h) belong to the internal group and could be active in proton transfer reactions. However, these cannot be definitive due to the lack of the IR spectral signatures at ν^{OH} < 1000 cm^{-1}, as in the case of the Zundel complex.[77]

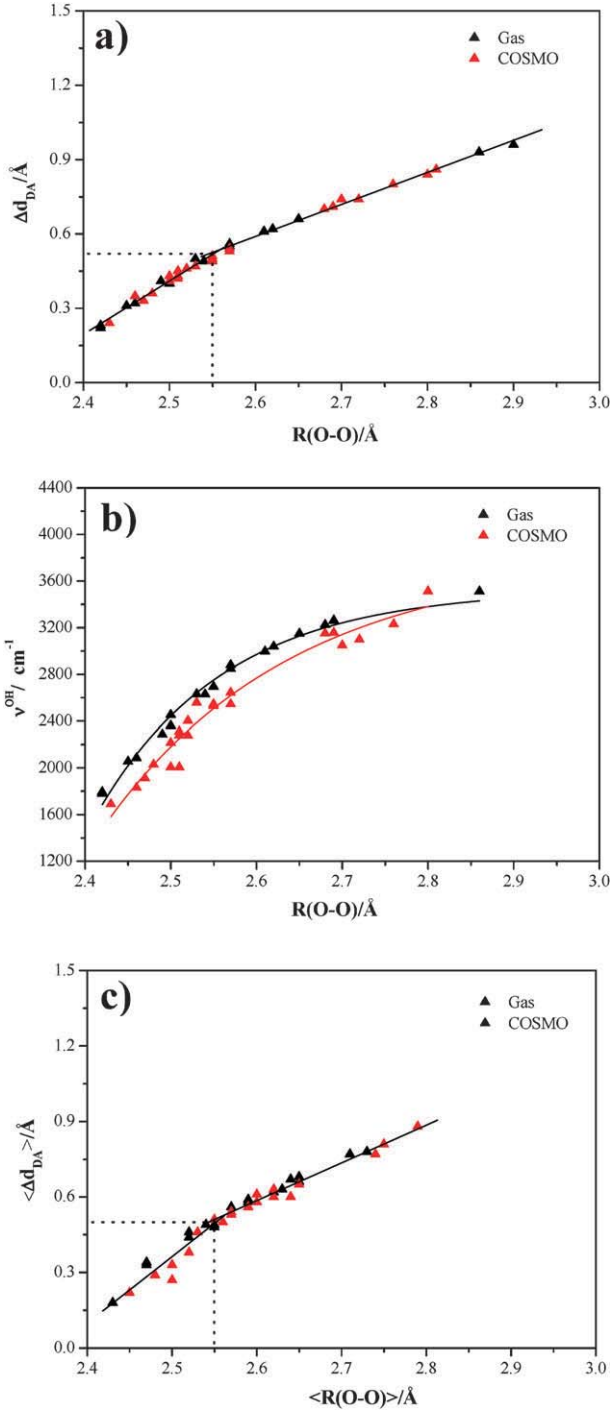

Fig. 3 (a) Plot of asymmetric stretching coordinates (Δd_{DA}) and O–H···O H-bond distances (R_{O-O}), obtained from B3LYP/TZVP calculations. (b) Plot of asymmetric O–H stretching frequencies (ν^{OH}) and O–H···O H-bond distances (R_{O-O}), obtained from B3LYP/TZVP calculations. (c) Plot of average asymmetric stretching coordinates ($\langle\Delta d_{DA}\rangle$) and average O–H···O H-bond distances ($\langle R_{O-O}\rangle$) obtained from BOMD simulations at 350 K.

It should be noted that, using the same approaches, ν^{OH} for the Zundel complex in the gas phase and continuum aqueous solution are 961 and 677 cm^{-1}, respectively.[77] The former is comparable with the theoretical result in ref. 78 of 983 cm^{-1}.

Table 1 Average H-bond distances ($\langle R_{O-O}\rangle$), average asymmetric stretching coordinates ($\langle \Delta d_{DA}\rangle$) and characteristic asymmetric O–H stretching frequencies (ν^{OH}) of the active protons in the transition state complexes. I_A/I_{O-O} are the relative probabilities of proton transfer in the course of the BOMD simulations. Distances and ν^{OH} are in Å and cm^{-1}, respectively

		$\langle R_{O-O}\rangle$	$\langle \Delta d_{DA}\rangle$	ν^{OH} A	ν^{OH} B	I_A/I_{O-O}
c) 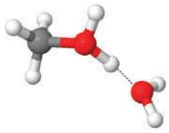	Gas	2.47	0.34	2178.9	2558.8	0.09
	COSMO	2.45	0.22	1138.9	1582.4	0.15
d) 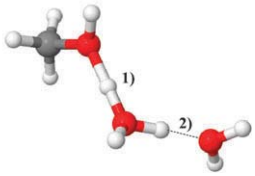	Gas	(1) 2.43	0.18	1115.5	1874.5	0.11
		(2) 2.57	0.54	2305.3	2695.7	0.11
	COSMO	(1) 2.50	0.33	977.7	1716.9	0.41
		(2) 2.57	0.54	2265.7	2680.1	0.13
g) 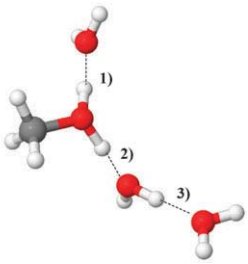	Gas	(1) 2.59	0.59	—	—	—
		(2) 2.47	0.33	1313.5	1613.2	0.03
		(3) 2.71	0.77	—	—	—
	COSMO	(1) 2.60	0.58	—	—	—
		(2) 2.48	0.29	935.0	1590.8	0.08
		(3) 2.75	0.81	—	—	—
h) 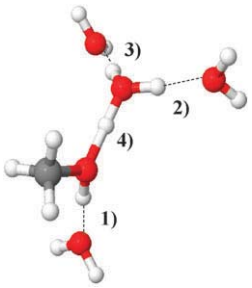	Gas	(1) 2.73	0.78	—	—	—
		(2) 2.65	0.68	—	—	—
		(3) 2.65	0.66	—	—	—
		(4) 2.45	0.22	911.0	1511.3	0.08
	COSMO	(1) 2.74	0.77	—	—	—
		(2) 2.65	0.65	—	—	—
		(3) 2.65	0.65	—	—	—
		(4) 2.50	0.27	979.7	1590.5	0.05

In the gas phase, the experimental O–H stretching frequency of the transferring proton in the Zundel complex was reported to be 1085 cm^{-1}.[79] Therefore, the asymmetric O–H stretching frequencies at $\nu^{OH} \leq 1000\ cm^{-1}$ could be regarded as spectral signatures of proton transfer in H-bonds. In this subsection, one could also conclude that the incomplete water coordination at the central charged species (H_3O^+ and $CH_3OH_2^+$), as well as the electrostatic effects introduced by the continuum aqueous solvent, could directly affect the tendency of proton transfer in H-bonds.

Dynamics and mechanisms of proton transfer reactions

The dynamics and mechanisms of proton transfer reactions in the CH_3OH–H_3O^+ and CH_3OH–H_3O^+–H_2O complexes are discussed in this subsection, with the emphasis on structures (c), (d), (g) and (h). The average H-bond distances ($\langle R_{O-O}\rangle$) and the average asymmetric stretching coordinates ($\langle \Delta d_{DA}\rangle$) obtained from BOMD simulations are listed in Table 1, together with characteristic asymmetric O–H stretching frequencies (ν^{OH}). Similar to the analyses made in the previous subsection, $\langle \Delta d_{DA}\rangle$ and $\langle R_{O-O}\rangle$ were plotted and shown in Fig. 3c. The power spectra of the symmetric and asymmetric O–H stretching modes of the H-bond protons in structures (c) and (d), as well as the O–O stretching modes (ν^{OO}), are given as examples in Fig. 4. The definitions of the three vibrational modes are also included in Fig. 4.

It appeared in Fig. 3c that linear relationships between $\langle \Delta d_{DA}\rangle$ and $\langle R_{O-O}\rangle$ could also be approximated for the internal and external H-bonds, with a separation at $\langle R_{O-O}\rangle$ = 2.55 Å, the same as that from B3LYP/TZVP calculations. The linear functions are shown in eqn (5) and (6), respectively.

$$\text{Internal H-bonds: } \langle \Delta d_{DA}\rangle = 2.6440\langle R_{O-O}\rangle - 6.2468 \quad (5)$$

$$\text{External H-bonds: } \langle \Delta d_{DA}\rangle = 1.4993\langle R_{O-O}\rangle - 3.3128 \quad (6)$$

In order to correlate the probability of proton transfer with ν^{OH} computed from BOMD simulations, the results on the Zundel complex[77] included in Fig. 4 should be discussed. The IR spectra of the H-bond proton in the Zundel complex computed from BOMD simulations at 350 K show two asymmetric O–H stretching bands, labeled **A** and **B** in

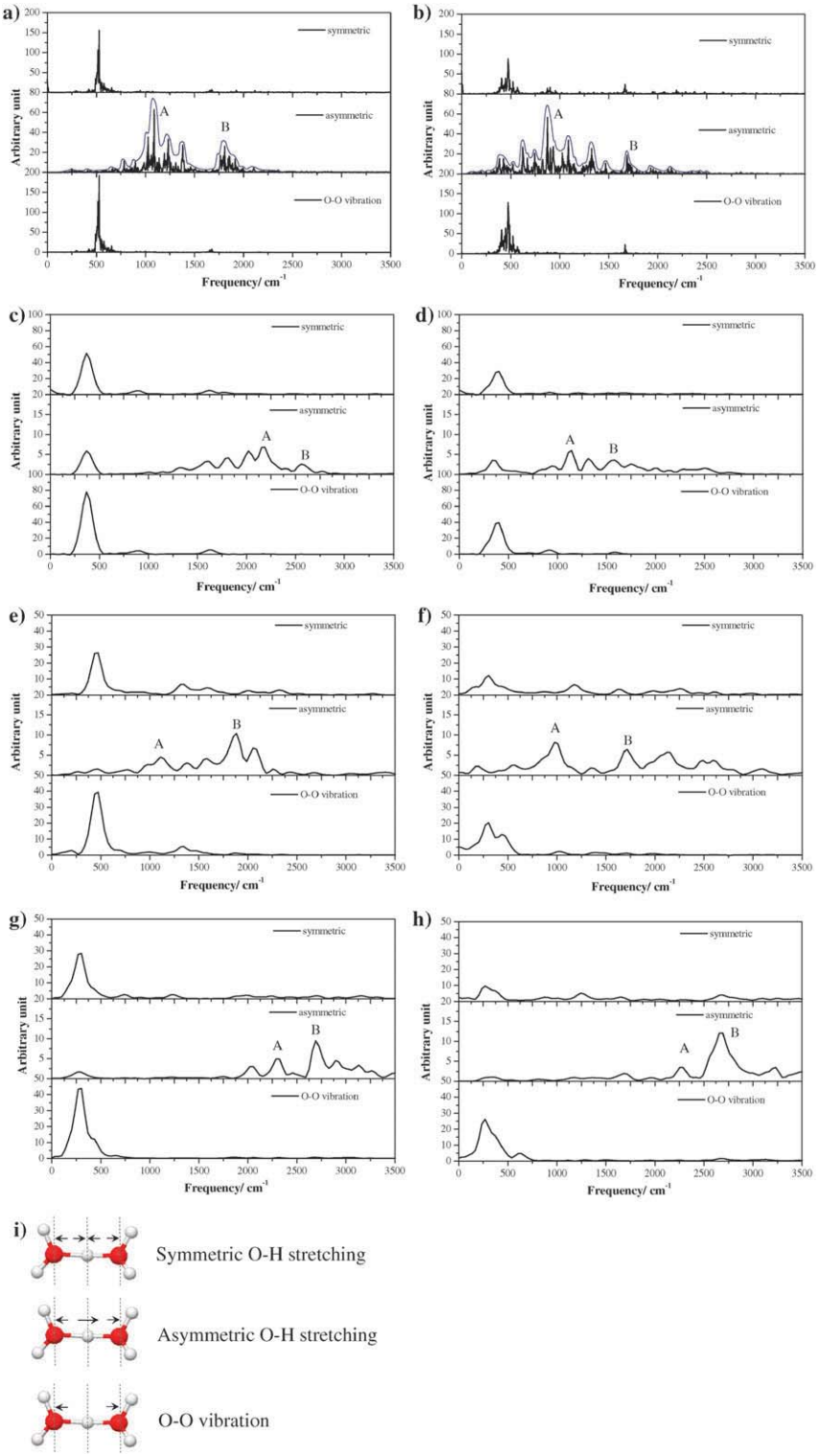

Fig. 4 Symmetric and asymmetric O–H stretching frequencies of the H-bond protons in the $H_5O_2^+$, CH_3OH–H_3O^+ and CH_3OH–H_3O^+–H_2O complexes, together with the O–O stretching frequencies, obtained from BOMD simulations at 350 K. (a) $H_5O_2^+$ in the gas phase. (b) $H_5O_2^+$ in continuum aqueous solution. (c) CH_3OH–H_3O^+ in the gas phase. (d) CH_3OH–H_3O^+ in continuum aqueous solution. (e) CH_3OH–H_3O^+–H_2O 1 : 1 : 1 complex in the gas phase (H-bond (**1**)). (f) CH_3OH–H_3O^+–H_2O 1 : 1 : 1 complex in continuum aqueous solution (H-bond (**1**)). (g) CH_3OH–H_3O^+–H_2O 1 : 1 : 1 complex in the gas phase (H-bond (**2**)). (h) CH_3OH–H_3O^+–H_2O 1 : 1 : 1 complex in continuum aqueous solution (H-bond (**2**)). (i) Definitions of the symmetric and asymmetric O–H stretching modes, as well as the O–O vibration.

Fig. 4a and b; in the gas phase at ν^{OH} = 1090 and 1809 cm^{-1} and in continuum aqueous solution at ν^{OH} = 875 and 1686 cm^{-1}, respectively. The low-frequency bands at **A** are comparable with the characteristic ν^{OH} derived from

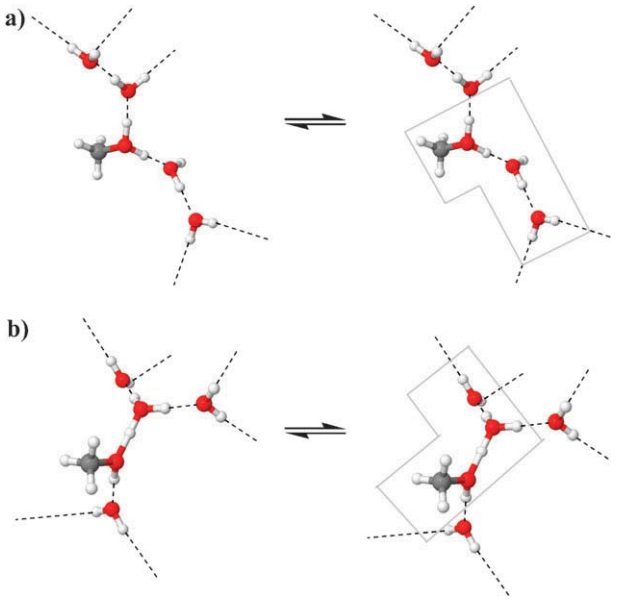

Fig. 5 Elementary reactions consisting of quasi-dynamic equilibriums for the interconversion between the formation and cleavage of the H-bonds linking the transition state complex and water molecules in the second hydration shells. The transition state complex is inside the boundary line. (a) The excess proton transferring in a linear H-bond structure. (b) The excess proton transferring in a fully hydrated transition state complex.

B3LYP/TZVP calculations.[77] They could be associated with the vibration modes, in which a proton shuttles back and forth at the center of the O–H···O H-bond. For the higher-frequency bands at **B**, the centers of vibration are shifted towards an oxygen atom of water. Therefore, ν^{OH} at **A** and **B** could be considered as the IR spectral signatures of the transferring proton in the Zundel complex.

As the proton transfer in the Zundel complex depends strongly on the O–O stretching mode,[27] the relative probability or the extent of proton transfer in BOMD simulations could be estimated from the ratio between the intensity of the asymmetric O–H stretching mode at **A** (I_A) and the intensity of the O–O stretching mode (I_{O-O}); a high I_A/I_{O-O} reflects a high probability of proton transfer in BOMD simulations. For the Zundel complex in the gas phase and continuum aqueous solution at 350 K, I_A/I_{O-O} amounts to 0.33 and 0.44, respectively, indicating a higher probability of proton transfer in continuum aqueous solution. At 298 K, the diffusion coefficient of the transferring proton in the Zundel complex is 5×10^{-5} cm^2 s^{-1},[77] slightly lower than the experimental value of 7×10^{-5} cm^2 s^{-1};[66] the diffusion coefficient of a proton moving across a single water molecule was approximated from the NMR hopping time (τ_p) and the Einstein relation, $D = l^2/6\tau_p$, where l is the hopping length. It should be mentioned that the value of D in ref. 66 was computed by subtracting the water self-diffusion coefficient, 2.3×10^{-5} cm^2 s^{-1}, from the proton diffusion coefficient, 9.3×10^{-5} cm^2 s^{-1}. The discrepancy of about 28% could be partly due to the lack of extensive H-bond networks of water in the model systems. Based on the information on the Zundel complex, one could anticipate proton transfer from the following three spectral evidences: (a) the existence of a threshold frequency at $\nu^{OH} < 1000$ cm^{-1}; (b) the appearance of an additional asymmetric O–H stretching frequency at ν^{OH} between 1600–1800 cm^{-1}; and (c) I_A/I_{O-O} is comparable with the Zundel complex.

For structure (c), the broadening of the asymmetric O–H stretching bands made it difficult to analyze IR spectra. In the gas phase, the appearance of the low- and high-frequency bands at 2179 and 2559 cm^{-1}, respectively, rules out structure (c) from being an active transition state. Similarly, in continuum aqueous solution, $I_A/I_{O-O} = 0.15$ indicates a restricted number of proton transfer events in BOMD simulations. Spectral evidences of proton transfer are clearly seen for structure (d), especially in continuum aqueous solution. Fig. 4f reveals that, H-bond (**1**) possesses an asymmetric O–H stretching frequencies of $\nu^{OH} = 978$ and 1717 cm^{-1}, with $I_A/I_{O-O} = 0.41$; I_A/I_{O-O} is slightly smaller than the Zundel complex.[77] The IR spectra of the active protons in structures (g) and (h) (not shown here) are similar to structure (d), but with I_A/I_{O-O} smaller than 0.1, indicating a small number of proton transfer events in BOMD simulations. Thus, one could conclude that, for the CH_3OH–H_3O^+–H_2O complex, structure (d) is the most active transition state in proton transfer pathways, with a proton diffusion coefficient (D) of 1.95×10^{-5} cm^2 s^{-1}. Since the time interval used in the calculations of MSD was short, the diffusion coefficient could be considered as a pure structural diffusion constant. *Ab initio* MD simulations were employed in the study of proton transfer in CH_3OH–H_2O mixtures at 300 K.[14] It was reported that the diffusion coefficient of an excess proton in the mixture, with a CH_3OH mole fraction of 0.5 (16 H_2O and 16 CH_3OH), is 4.2×10^{-5} cm^2 s^{-1}. Based on the approximation in ref. 66 and the report that the self-diffusion coefficients of $[CH_3OH]_{liq}$ at 298 and 340 K are 2.4×10^{-5} and 4.9×10^{-5} cm^2 s^{-1}, respectively,[80] the proton diffusion coefficient in the present system could be approximated as 4.35×10^{-5} and 6.85×10^{-5} cm^2 s^{-1}, respectively. The values agree well with the theoretical results in ref. 80.

The conclusion that structure (d) is the most active transition state complex is supported by the theoretical results in ref. 14, which showed that the nearest neighbors of the defect oxygen, the oxygen atom attached to an excess proton, consist of two water molecules, independent of whether the defect oxygen is in water or methanol. This corresponds to structure (d) in the present work. Based on the assumption that the thermal energy fluctuations could temporarily break the H-bonds connecting the transition state complex and water molecules in the second hydration shell, two potential elementary reactions of proton transfer could be proposed in Fig. 5: Fig. 5a assumes that the excess proton is transferred in a linear H-bond structure, whereas Fig. 5b assumes a fully hydrated transition state complex. The former was suggested to be more preferential.[13] Finally, as in the case of the Zundel and Eigen complexes,[27] one could further anticipate that the rate-determining steps could be determined from the lifetimes of the quasi-dynamic equilibriums for the interconversion between the formation and cleavage of the H-bonds linking the first and second hydration shells, with structure (d) as the only active transition state complex.

Conclusions

The dynamics and mechanisms of proton transfer in hydrated complexes formed from CH_3OH, H_3O^+ and H_2O were studied using theoretical methods. The investigations began with a search for equilibrium structures at low hydration levels using DFT calculations at the B3LYP/TZVP level. Based on asymmetric stretching coordinates (Δd_{DA}) and asymmetric O–H stretching frequencies (ν^{OH}), four H-bond complexes were identified as transition states, in which the most active unit is represented by an excess proton nearly equally shared between CH_3OH and H_2O. Linear relationships between Δd_{DA} and the H-bond distance (R_{O-O}) could be approximated for both internal and external H-bonds, with a separation at 2.55 Å, whereas the relationship between ν^{OH} and R_{O-O} could be represented by an exponential function similar to the integral rate expression for the first-order reaction. Based on the static proton transfer potentials (B3LYP/TZVP calculations), ν^{OH} for the H-bond protons in the transition state complexes in the gas phase range from 1778 to 2086 cm^{-1}, and from 1690 to 2029 cm^{-1} in continuum aqueous solution. According to the classical interpretations, all the H-bonds in the transition state complexes belong to the internal group, and could be active in proton transfer. These, however, cannot be definitive due to the lack of the IR spectral signatures at $\nu^{OH} \approx 1000$ cm^{-1}; using the same theoretical methods, the Zundel complex possesses $\nu^{OH} = 961$ and 677 cm^{-1}, in the gas phase and continuum aqueous solution, respectively. Therefore, $\nu^{OH} \approx 1000$ cm^{-1} or lower could be considered as an IR spectral signature of the transferring proton in H-bonds.

More definitive results were obtained from BOMD simulations. Based on the three spectral evidences obtained from the Zundel complex, the H-bond structure (structure (d)) with incomplete water coordination at $CH_3OH_2^+$ and H_3O^+ appeared to be the most active transition state in continuum aqueous solution, with a characteristic ν^{OH} of 978 cm^{-1}. This is in accordance with the observation that the excess proton is preferentially taken by CH_3OH in the open chain structures, not the fully hydrated structures. Based on the assumption that the thermal energy fluctuations could temporarily separate or break the H-bonds connecting the transition state complex and the water molecules in the second hydration shell, and the observation that the incomplete water coordination at the charged species could help promote structural diffusion, as in the case of the Zundel and Eigen complex, two elementary reactions of proton transfer were proposed, with structure (d) as the only transition state complex.

The present theoretical results suggested that, due to the coupling among various vibrational modes, the discussions on proton transfer reactions cannot be made based solely on static proton transfer potentials. In order to study proton transfer reactions, thermal energy fluctuations and dynamics must be included in the model calculations. Although the asymmetric O–H stretching frequencies of the transferring protons cannot be measured easily in experiment, due to the limitations of the IR equipment and the difficulties in the assignment of absorption bands, the present theoretical results could provide insights into the vibrational behavior of transferring protons, as well as suggest theoretical methods and criteria to monitor proton transfer reactions in more complex environments. Together with systematic analyses of IR spectra, it has been shown that BOMD simulations are the most appropriate theoretical methods for the investigations of proton transfer reactions.

Acknowledgements

The authors would like to acknowledge the financial supports from the Thailand Research Fund (TRF): the Advanced Research Scholarship, Grant No. BRG5180022 to Prof. Kritsana Sagarik; the Royal Golden Jubilee (RGJ) PhD Program, Grant No. PHD/0071/2547 to Sermsiri Chaiwongwattana and Prof. Kritsana Sagarik. Linux clusters provided by the following organizations are also gratefully acknowledged: School of Mathematics and School of Chemistry, SUT; National Electronics and Computer Technology Center (NECTEC), National Science and Technology Development Agency (NSTDA); the Thai National Grid Center (THAIGRID), Ministry of Information and Communication Technology.

References

1 J. Larminie and A. Dicks, *Fuel Cell Systems Explained*, John Wiley & Sons Ltd, Chichester, 2001.
2 C. A. Vincent and B. Scrosati, *Modern Batteries: An introduction to electrochemical power sources*, John Wiley & Sons Ltd, New York, 1997.
3 M. Cappadonia, J. W. Erning, S. M. S. Niaki and U. Stimming, *Solid State Ionics*, 1995, **77**, 65.
4 J. A. Elliott and S. J. Paddison, *Phys. Chem. Chem. Phys.*, 2007, **9**, 2602.
5 K. D. Kreuer, *Chem. Mater.*, 1996, **8**, 610.
6 K. D. Kreuer, S. J. Paddison, E. Spohr and M. Schuster, *Chem. Rev.*, 2004, **104**, 4637.
7 M. Hachiya, Y. Matsuda, K. Suhara, N. Mikami and A. Fujii, *J. Chem. Phys.*, 2008, **129**, 094306.
8 F. Huisken, S. Mohammad-Pooran and O. Werhahn, *Chem. Phys.*, 1998, **239**, 11.
9 E. E. Fileti, M. A. Castro and S. Canuto, *Chem. Phys. Lett.*, 2008, **452**, 54.
10 S. Urata, J. Irisawa, A. Takada and S. Tsuzuki, *J. Fluorine Chem.*, 2005, **126**, 1312.
11 A. Vishnyakov and A. V. Neimark, *J. Phys. Chem. B*, 2001, **105**, 7830.
12 J. C. Jiang, C. Chaudhuri, Y. T. Lee and H.-C. Chang, *J. Phys. Chem. A*, 2002, **106**, 10937.
13 C.- C. Wu, C. Chaudhuri, J. C. Jiang, Y. T. Lee and H.- C. Chang, *J. Phys. Chem. A*, 2004, **108**, 2859.
14 J. A. Morrone, K. E. Haslinger and M. E. Tuckerman, *J. Phys. Chem. B*, 2006, **110**, 3712.
15 H.-C. Chang, J.-C. Jiang, S. H. Lin, Y. T. Lee and H.-C. Chang, *J. Phys. Chem. A*, 1999, **103**, 2941.
16 J. A. Morrone and M. E. Tuckerman, *J. Chem. Phys.*, 2002, **117**, 4403.
17 R. Buzzoni, S. Bordiga, G. Ricchiardi, G. Spoto and A. Zecchina, *J. Phys. Chem.*, 1995, **99**, 11937.
18 J. B. Asbury, T. Steinel and M. D. Fayer, *J. Lumin.*, 2004, **107**, 271.
19 T. Kabeya, Y. Tamai and H. Tanaka, *J. Phys. Chem. B*, 1998, **102**, 899.
20 C.-C. Wu, J. C. Jiang, D. W. Boo, S. H. Lin, Y. T. Lee and H.-C. Chang, *J. Chem. Phys.*, 2000, **112**, 176.
21 M. Okumura, L. I. Yeh, J. D. Myers and Y. T. Lee, *J. Phys. Chem.*, 1990, **94**, 3416.
22 I. Natkaniec, K. Holderna-Natkaniec, I. Majerz and K. Parlinski, *Chem. Phys.*, 2005, **317**, 171.
23 O. Vendrell, F. Gatti and H.-D. Meyer, *J. Chem. Phys.*, 2007, **127**, 184303.

24 R. Vuilleumier and D. Borgis, *J. Chem. Phys.*, 1999, **111**, 4251.
25 U. W. Schmitt and G. A. Voth, *J. Chem. Phys.*, 1999, **111**, 9361.
26 H.-P. Cheng and J. L. Krause, *J. Chem. Phys.*, 1997, **107**, 8461.
27 K. Sagarik, M. Phonyiem, C. Lao-ngam and S. Chaiwongwattana, *Phys. Chem. Chem.Phys.*, 2008, **10**, 2098.
28 N. Rekik, B. Oujia and M. J. Wójcik, *Chem. Phys.*, 2008, **352**, 65.
29 J. Rejnek, M. Hanus, M. Kabeláč, F. Ryjáček and P. Hobza, *Phys. Chem. Chem. Phys.*, 2005, **7**, 2006.
30 K. P. Sagarik and B. M. Rode, *Chem. Phys.*, 2000, **260**, 159.
31 K. P. Sagarik, S. Chaiwongwattana and P. Sisot, *Chem. Phys.*, 2004, **306**, 1.
32 K. P. Sagarik and S. Dokmaisrijan, *THEOCHEM*, 2005, **718**, 31.
33 K. Sagarik and S. Chaiyapongs, *Biophys. Chem.*, 2005, **117**, 18.
34 N. Deeying and K. Sagarik, *Biophys. Chem.*, 2007, **125**, 72.
35 K. P. Sagarik and R. Ahlrichs, *J. Chem. Phys.*, 1987, **86**, 5117.
36 K. P. Sagarik, V. Pongpituk, S. Chaiyapongs and P. Sisot, *Chem. Phys.*, 1991, **156**, 439.
37 K. P. Sagarik, *THEOCHEM*, 1999, **465**, 141.
38 K. P. Sagarik and E. Spohr, *Chem. Phys.*, 1995, **119**, 73.
39 K. P. Sagarik and P. Asawakun, *Chem. Phys.*, 1997, **219**, 173.
40 *CRC Handbook of Chemistry & Physics, 89th Edition,* CRC Press, 2008–2009, 1476–3508; David W. H. Rankin, *Crystallogr. Rev.*, 2009, **15**(3), 223–224.
41 S. J. Paddison, *Annu. Rev. Mater. Res.*, 2003, **33**, 289.
42 S. J. Paddison and T. Zawodzinski Jr., *Solid State Ionics*, 1998, **113–115**, 333.
43 S. J. Paddison, L. R. Pratt and T. A. Zawodzinski Jr., *J. New Mater. Electrochem. Syst.*, 1999, **2**, 183.
44 S. J. Paddison, L. R. Pratt and T. Zawodzinski Jr., *J. Phys. Chem. A*, 2001, **105**, 6266.
45 S. J. Paddison, *J. New Mater. Electrochem. Syst.*, 2001, **4**, 197.
46 S. J. Paddison and J. A. Elliott, *J. Phys. Chem. A*, 2005, **109**, 7583.
47 R. Dreizler and E. Gross, *Density Functional Theory*, Plenum Press, New York, 1995.
48 A. Schäfer, C. Huber and R. Ahlrichs, *J. Chem. Phys.*, 1994, **100**, 5829.
49 G. Santambrogio, M. Brümmer, L. Wöste, J. Döbler, M. Sierka, J. Sauer, G. Meijer and K. R. Asmis, *Phys. Chem. Chem. Phys.*, 2008, **10**, 3992.
50 R. W. Larsen, P. Zielke and M. A. Suhm, *J. Chem. Phys.*, 2007, **126**, 194307.
51 TURBOMOLE V6.0 2009, a development of University of Karlsruhe and Forschungszentrum Karlsruhe GmbH, 1989–2007, TURBOMOLE GmbH, since 2007; available from http://www.turbomole.com.
52 D. Marx, M. E. Tuckerman, J. Hutter and M. Parrinello, *Nature*, 1999, **397**, 601.
53 C. J. D. von Grotthuss, *Annu. Chim.*, 1806, **58**, 54.
54 N. B. Librovich, V. P. Sakun and N. D. Sokolov, *Chem. Phys.*, 1979, **39**, 351.
55 D. Xenides, B. R. Randolf and B. M. Rode, *J. Chem. Phys.*, 2005, **122**, 174506.
56 G. C. Pimentel and A. L. McClellan, *The Hydrogen Bond*, W. H. Freeman, San Francisco, 1960.
57 P. B. Balbuena and J. M. Seminario, *Theoretical and Computational Chemistry 7, Molecular Dynamics; From Classical to Quantum Methods*, Elsevier, Amsterdam, 1999.
58 C. J. Cramer, *Essentials of Computational Chemistry: Theory and Models*, John Wiley & Sons Ltd, New York, 2002.
59 D. C. Young, *Computational Chemistry: A Practical Guide for Applying Techniques to Real World Problems*, Wiley Interscience, New York, 2001.
60 R. N. Barnett and U. Landman, *Phys. Rev. B: Condens. Matter*, 1993, **48**, 2081.
61 X. Jing, N. Troullier, D. Dean, N. Binggeli, J. R. Chelikowsky, K. Wu and Y. Saad, *Phys. Rev. B: Condens. Matter*, 1994, **50**, 12234.
62 A. R. Leach, *Molecular Modelling: Principles and Applications*, Longman, Edinburgh, 1996.
63 F. Fillaux, A. Cousson and M. Gutmann, *Pure Appl. Chem.*, 2007, **79**, 1023.
64 B. E. Conway, J. O. M. Bockris and H. Linton, *J. Chem. Phys.*, 1956, **24**, 834.
65 K. D. Kreuer, *Solid State Ionics*, 2000, **136–137**, 149.
66 N. Agmon, *Chem. Phys. Lett.*, 1995, **244**, 456.
67 P. A. Giguere, *J. Chem. Educ.*, 1979, **56**, 571.
68 R. R. Sadeghi and H.-P. Cheng, *J. Chem. Phys.*, 1999, **111**, 2086.
69 P. Bopp, *Chem. Phys.*, 1986, **106**, 205.
70 C. J. Montrose, J. A. Bucaro, J. Marshall-Coakley and T. A. Litovitz, *J. Chem. Phys.*, 1974, **60**, 5025.
71 M.-C. Bellissent-Funel and J. Teixeira, *J. Mol. Struct.*, 1991, **250**, 213.
72 M. P. Allen and D. J. Tildesley, *Computer Simulation of Liquids*, Oxford University Press, New York, 1987.
73 J. M. Haile, *Molecular Dynamics Simulations*, John Wiley & Sons Ltd, New York, 1997.
74 D. C. Rapaport, *The Art of Molecular Dynamics Simulation*, Cambridge University Press, London, 1995.
75 A. J. Stace and G. A. Shukla, *J. Am. Chem. Soc.*, 1982, **104**, 5314.
76 J. Crooks, A. J. Stace and B. J. Whitaker, *J. Phys. Chem.*, 1988, **92**, 3554.
77 K. Sagarik and C. Lao-ngam, submitted.
78 L. Ojamäe, I. Shavitt and J. Singer, *Int. J. Quantum Chem.*, 1995, **56**, 657.
79 J. M. Headrick, E. G. Diken, R. S. Walters, N. I. Hammer, R. A. Christie, J. Cui, V. M. Myshakin, M. A. Johnson and K. D. Jordan, *Science*, 2005, **308**, 1765.
80 G. Guevara-Carrion, C. Nieto-Draghi, J. Vrabec and H. Hasse, *J. Phys. Chem. B*, 2008, **112**, 16664.

Chemical Physics 355 (2009) 103–117

Contents lists available at ScienceDirect

Chemical Physics

journal homepage: www.elsevier.com/locate/chemphys

Structures and dynamics of phenol clusters in benzene solutions

Sermsiri Chaiwongwattana, Kritsana Sagarik *

School of Chemistry, Institute of Science, Suranaree University of Technology, 111 University Avenue, Nakhon-Ratchasima 30000, Thailand
National Nanotechnology Center (NANOTEC), National Science and Technology Development Agency (NSTDA), Pathumthani 12120, Thailand

ARTICLE INFO

Article history:
Received 25 December 2007
Accepted 18 November 2008
Available online 27 November 2008

Keywords:
Phenol clusters
Benzene solutions
T-model
Molecular dynamics

ABSTRACT

Structures and dynamics of phenol clusters ($(PhOH)_n$, $n = 1–3$) in benzene (Benz) solutions ($[(PhOH)_n]_{Benz}$) at 298 K were studied using intermolecular potentials derived from the Test-particle model (T-model) and molecular dynamics (MD) simulations. Although Benz molecules interact weakly among themselves and with PhOH, the average three-dimensional structures and interaction energy distributions obtained from MD simulations showed that, they could form well-defined solvent cages in $[(PhOH)_n]_{Benz}$. At infinite dilution, some solvent-separated structures, in which a Benz molecule linked between two PhOH molecules, were observed in $[(PhOH)_2]_{Benz}$, whereas hydrogen bond (H-bond) structures dominated in $[(PhOH)_3]_{Benz}$. Based on the observation that, under thermal equilibrium conditions and at short time, the exchange dynamics between the associated and dissociated forms involved periodic motions of the O–H$\cdots\pi$ H-bond, the lifetimes of the PhOH–Benz 1:1 complex were estimated and in reasonable agreement with 2D-IR vibrational echo experiment. Due to high potential energy barriers on the average potential energy landscapes, solvent exchanges in $[(PhOH)_n]_{Benz}$ could take place through large-amplitude intermolecular vibrations of molecules in the first solvation shell. In order to provide insights into structures and dynamics in $[(PhOH)_n]_{Benz}$, it was shown that, explicit solvent molecules have to be included in the theoretical models.

1. Introduction

Structures and stability of clusters of aromatic compounds in aqueous and non-aqueous solutions are examples of classical problems in the area of molecular associations [1–9]. Molecular clusters formed from aromatic compounds have been of interest, since they represent interactions between π-systems, which are found in DNA and side chains of proteins [10]. Therefore, various experimental and theoretical investigations have been performed in the past two decades to obtain basic information concerning with the driving forces responsible for interactions in aromatic systems, especially among biomolecules [11]. For example, the so-called "π–hydrogen bond" (π–H-bond) has been put forward due to its importance in biological systems, *e.g.* the ability to stabilize α-helix in proteins [12–14].

The presence of π-electrons enables clusters of aromatic compounds, generated in continuous or pulsed supersonic beams, to be examined effectively using modern spectroscopic techniques, such as resonance two photon ionization [15–17], disperse fluorescence [18], cluster ion dip spectroscopy [19,20] and ionization-detected stimulated Raman spectroscopy [21]. Significant advancement in computational chemistry software packages and parallel computer technology [22] has also allowed *ab initio* calculations that include the effects of electron correlations to study large clusters of aromatic compounds with higher accuracy [23]. It has, therefore, become a general practice to apply structural models obtained from *ab initio* calculations for the fitting of spectroscopic observations [24]. Since a large number of review articles on molecular associations have been published, only some important information relevant to the present work will be briefly summarized.

Clusters of benzene ($(Benz)_n$) are considered as prototypes for the $\pi\cdots\pi$ and C–H$\cdots\pi$ interactions. They have been extensively studied by theoretical and experimental methods [25–31]. Theoretical methods [23,32] predicted at least four equilibrium structures of $(Benz)_2$ in the gas phase namely, parallel displaced, T-shaped, parallel staggered and herringbone structures. The parallel displaced structure is stabilized solely by the $\pi\cdots\pi$ interaction, whereas the T-shaped structure mainly by the C–H$\cdots\pi$ interaction. The former was suggested by *ab initio* calculations at the highest level of accuracy [32] to possess the lowest interaction energy and in good agreement with experiment [31], whereas the latter was pointed out to represent a low-energy saddle point for the interconversion between parallel displaced structures.

Fast dynamics of single Benz molecule in the liquid phase ($[Benz]_{liquid}$) was studied in femtosecond heterodyne detected optical Kerr effect (HD-OKE) experiments in a wide temperature range [25]. The results at short times were interpreted by assuming that the basic microscopic system consists of a Benz molecule

* Corresponding author. Tel./fax: +66 44 224635.
E-mail address: kritsana@sut.ac.th (K. Sagarik).

0301-0104/$ - see front matter © 2008 Elsevier B.V. All rights reserved.
doi:10.1016/j.chemphys.2008.11.018

Nomenclature

T-model the Test-particle model
π–H-bond π–hydrogen bond
PD map probability distribution map
π-PD maps solvent probability distribution map
$\langle P^{\pi\text{-PD}}\rangle_{max}$ highest probability at the labeled contour on the π-PD maps
MD-$[(PhOH)_n]^{frozen}_{Benz}$ MD simulations with the structure of $(PhOH)_n$ frozen at the T-model equilibrium geometries
MD-$[(PhOH)_n]^{free}_{Benz}$ MD simulations with all molecules allowed to move, starting from the equilibrated configurations of MD-$[(PhOH)_n]^{frozen}_{Benz}$
$\langle E^{solu-solu}_{Benz}\rangle$ average solute–solute interaction energy
$\langle E^{solu-solv}_{Benz}\rangle$ average solute–solvent interaction energy
$\langle E^{pot}_{Benz}\rangle$ average potential energies of $[(PhOH)_n]_{Benz}$
$\langle E^{T}_{Benz}\rangle$ the average potential energy barriers to the solvent exchange within, as well as between, the first solvation shells
$\langle E^{T}_{Benz}\rangle$ the average potential energy barriers to the solvent exchange between Benz molecules in the first solvation shell and the outside
$g(R)$ atom–atom pair correlation functions
$n(R)$ average running coordination numbers
FFT fast Fourier transformations
I_a associative-interchange scheme
$\tau^{PhOH-Benz}_{O-H\pi}$ lifetime of the PhOH–Benz 1:1 complex
PB-PD the average solute–solvent interaction energy PD maps
BB-PD the average solvent–solvent interaction energy PD maps
PB-BB-PD the average potential energy PD maps
$\langle \Delta E^{PB-PD}_{Benz}\rangle_{min}$ lowest-average interaction energies on the PB-PD map
$\langle \Delta E^{BB-PD}_{Benz}\rangle_{min}$ lowest-average interaction energies on the BB-PD map
$\langle \Delta E^{PB-BB-PD}_{Benz}\rangle_{min}$ lowest-average interaction energies on the PB-BB-PD map

librating and oscillating in a local confinement or solvent "cage". The instantaneous cage structures and dynamics in $[Benz]_{liquid}$ and $[Benz]_{crystal}$ were studied in details by spectroscopic measurements [26], as well as molecular dynamics (MD) [29] and lattice dynamics simulations [28]. It was reported in Ref. [29] that, a reminiscence of crystalline structure was evident in $[Benz]_{liquid}$, although no preferential orientation was observed in the first coordination shell. Moreover, the cages in $[Benz]_{liquid}$ are similar in composition to those in $[Benz]_{crystal}$, and the majority of the cages in $[Benz]_{liquid}$ could live several hundred femtoseconds (fs) or picoseconds (ps), depending upon the radius used to define the cage [29]. Similar solvent cages were observed in our previous theoretical studies [33] to accommodate benzoic acid dimer ($(BA)_2$), as well as BA–H_2O *m*:*n* complexes, *m* and *n* = 1–2, in Benz solutions.

As the simplest aromatic compound which can form O–H···π and O–H···O H-bonds, and a prototype for structurally related subunits in larger biomolecules, such as tyrosine (Tyr) residue in proteins, phenol (PhOH) has been frequently selected as a model molecule in both experimental and theoretical investigations [23,34]. For example, theoretical methods at MP2/6-31G(d) and B3LYP/6-31G(d) levels were employed in the study of structures and stabilities of the O–H···O H-bond in $(PhOH)_n$ and $(H_2O)_n$, n = 1–4, as well as the PhOH–H_2O *m*:*n* complexes, m and n = 1–3, and $m + n \leqslant 4$ [35]. MP2/6-31G(d) results showed that $(PhOH)_n$ and $(H_2O)_n$ possess similar H-bond patterns, and $(PhOH)_n$ are slightly more stable due to the effects of electron correlations. Moreover, it was shown that, the H-bonds in the PhOH–H_2O *m*:*n* complexes are similar to $(H_2O)_n$.

The interplay between electrostatic and dispersion interactions has been frequently studied through the weak interaction between the O–H group in PhOH and the polarizable π-electron clouds in Benz [36,37]. For example, in the gas phase, B3LYP/6-31G(d,p) calculations revealed that, the PhOH–Benz 1:1 complex is stabilized mainly by the O–H···π H-bond, whereas in the 1: 2 complex, the O–H group of PhOH acts simultaneously as proton donor and acceptor towards Benz molecules [37]. It should be noted that, although the density functional theory (DFT) and MP2 have been frequently employed in the calculations of molecular clusters, there have been examples in which both methods could not describe accurately the long-range electron correlation effects; $(Benz)_2$ was predicted to be unstable by almost all standard DFT functionals [32,38], whereas the interaction energy of the PhOH–Benz 1:1 complex was pointed out to be overestimated at the MP2 level [39].

Molecular associations of PhOH in Benz solutions were examined in classical partition experiments, in which distributions of PhOH between Benz and water were studied at 298 K [40]. The measurements of partition coefficients revealed that, in Benz, equilibrium could establish between PhOH and $(PhOH)_3$, whereas in water, PhOH is monomolecular up to at least 0.15 M. It was emphasized in Ref. [40] that, PhOH associates itself in triple molecules and not in double molecules. The existence of the monomer–trimer equilibrium was also suggested from NMR experiment [41], in which the equilibrium constant was determined in CCl_4 by measuring the hydroxyl NMR frequencies as functions of concentrations. However, Philbrick [4] proposed the existence of $(PhOH)_2$ in Benz solutions, by measuring the partition coefficients of PhOH between Benz and water at the concentrations in the water layer below 0.1 M. The results were confirmed by isopiestic experiments in anhydrous solutions [42].

Two-dimensional IR (2D-IR) vibrational echo spectroscopy [39,43–49], an ultrafast vibrational analog of two-dimensional NMR [45], has been developed to study fast chemical exchange in the ground electronic state under thermal equilibrium conditions. For small H-bonded systems, Hochstrasser et al. [48] investigated the H-bond exchange between CH_3OH and the CN of CH_3CN, using 2D-IR heterodyne echo spectroscopy. The activation energy for the exchange from the H-bonded state to the free state was reported to be 6.2 kJ/mol. With the enthalpy of formation of about 17 kJ/mol [12], the association and dissociation of the PhOH–Benz complex in solutions seem too rapid to measure using conventional spectroscopic methods. In Ref. [43], equilibrium dynamics in the PhOH–Benz complex was studied in a mixed solvent of Benz, by measuring in real time the appearance of off-diagonal peaks in the 2D-IR vibrational echo spectra of the PhOH hydroxyl stretching. The high-frequency hydroxyl stretching was assigned to the free PhOH, whereas the low-frequency to the PhOH–Benz complex. According to the analysis of the 2D-IR spectra, the dissociation time of the PhOH–Benz 1:1 complex was estimated to be about 8 ps.

In our previous work, $[PhOH]_{aq}$ [50], $[BA]_{aq}$ and $[(BA)_2]_{aq}$ [51], as well as $[(BA)_2]_{Benz}$ and small microhydrates of BA in Benz [33], were studied using intermolecular potentials derived from the Test-particle model (T-model) and MD simulations at 298 K. It was shown that, in the gas phase and dilute aqueous solutions, the strong cyclic H-bonds in $(BA)_2$ could be disrupted by H-bonding with water. Whereas in Benz, some microhydrates, not particularly associated in the gas phase and dilute aqueous solutions, become quite stable in the course of MD simulations. This reflects

the impact of weak but complicated C–H···π, O–H···π and π···π interactions on structures and stability of H-bond clusters.

In the present study, the effects of weak C–H···π, O–H···π and π···π interactions on structures, energetic and dynamics of H-bond clusters in non-aqueous environment were further examined using $[(PhOH)_n]_{Benz}$, n = 1–3 as model systems. In order to acquire some basic information, equilibrium structures and interaction energies of the PhOH–Benz m:n complexes, m and n = 1–2, in the gas phase, were investigated using the T-model potentials. Then, NVE-MD simulations were performed on $[(PhOH)_n]_{Benz}$ at 298 K. The average three-dimensional structures and interaction energy distributions in $[(PhOH)_n]_{Benz}$ were visualized and analyzed based on solvent probability distribution (PD) maps and average solute–solvent and solvent–solvent interaction energy PD maps, respectively [52–54]. The dynamics in the first solvation shell of $[(PhOH)_n]_{Benz}$ was analyzed and discussed using the average interaction energy PD maps and their cross section plots [52–54], as well as the H-bond and solvent exchange diagrams. The results were discussed in comparison with available theoretical and experimental results of the same and similar systems.

2. Theoretical methods

The theoretical methods employed in the studies of solutions fall into two categories [55]. Microscopic methods consider solvent molecules with solute explicitly, whereas macroscopic methods take into account solvent as a continuum medium characterized by a dielectric constant. Although in principle, *ab initio* calculations, such as the self-consistent reaction field (SCRF) method [56], could provide insights into the stability of clusters of molecules in a continuum solvent, it is inappropriate in the present case, since the average three-dimensional structures and dynamics of solvent molecules were of primary interest.

2.1. The T-model potentials

Intermolecular potentials employed in the present work were constructed based on the T-model. Since the T-model has been explained in details in our previous investigations [33,50–53], only some important aspects will be briefly summarized here. Within the framework of the T-model, the interaction energy ($\Delta E_{T\text{-model}}$) between molecules A and B is written as a sum of the first-order SCF interaction energy (ΔE^1_{SCF}) and a higher-order energy (ΔE^r) [57]

$$\Delta E_{T\text{-model}} = \Delta E^1_{SCF} + \Delta E^r. \quad (1)$$

ΔE^1_{SCF} accounts for the exchange repulsion and electrostatic energies, and takes the following form:

$$\Delta E^1_{SCF} = \sum_{i\in A}\sum_{j\in B}\left[\exp\left[\frac{-R_{ij}+\sigma_i+\sigma_j}{\rho_i+\rho_j}\right]+\frac{q_iq_j}{R_{ij}}\right]. \quad (2)$$

i and j in Eq. (2) label the sites of molecules A and B, respectively. σ_i, ρ_i and q_i are the site parameters. R_{ij} is the site–site distance. The exponential term in Eq. (2) takes into account the sizes and shapes of the interacting molecules A and B. The point charges q_i and q_j are determined to reproduce the electrostatic potentials of the molecules. The higher-order energy, ΔE^r in Eq. (1), represents the dispersion and polarization contributions of the T-model potential. ΔE^r could be determined from both theoretical and experimental data, and takes the following form:

$$\Delta E^r = -\sum_{i\in A}\sum_{j\in B} C^6_{ij}F_{ij}(R_{ij})R^{-6}_{ij}, \quad (3)$$

where

$$F_{ij}(R_{ij}) = \exp\left[-(1.28R^0_{ij}/R_{ij}-1)^2\right], \quad R_{ij} < 1.28R^0_{ij}$$
$$= 1, \quad \text{elsewhere} \quad (4)$$

and

$$C^6_{ij} = C_6\frac{3}{2}\frac{\alpha_i\alpha_j}{(\alpha_i/N_i)^{1/2}+(\alpha_j/N_j)^{1/2}}. \quad (5)$$

R^0_{ij} in Eq. (4) is the sum of the van der Waals radii of the interacting atoms. Eq. (5) is the Slater–Kirkwood relation; α_i and N_i denote the atomic polarizability and the number of valence electrons of the corresponding atom, respectively. $F_{ij}(R_{ij})$ in Eq. (4) is a damping function, introduced to correct the behavior of R^{-6}_{ij} at short R_{ij} distance. Only C_6 in Eq. (5) is unknown. C_6 could be determined by a fit of the incomplete potential, including ΔE^1_{SCF}, to the experimental second-virial coefficients ($B(T)$) [58]. In the present study, α_i, ρ_i, q_i and C_6 for PhOH and Benz were taken from Refs. [33,50]. They were applied successfully in MD simulations of H-bond and aromatic systems, both in aqueous [50] and non-aqueous solutions [33].

2.2. Equilibrium structures in the gas phase

In this subsection, some important aspects of geometry optimization will be briefly summarized, using the PhOH–Benz 1:1 complex as an example. The geometries of PhOH and Benz were taken from Refs. [33,50], respectively. They were kept constant throughout the calculations. The equilibrium structures and interaction energies of the PhOH–Benz 1:1 complex were computed by placing PhOH at the origin of the Cartesian coordinate system. The coordinates of Benz were randomly generated in the vicinities of PhOH. Based on the T-model potentials [33,50], the absolute and local minimum energy geometries of the PhOH–Benz 1:1 complex were searched using a minimization technique [59]. One hundred starting configurations were employed in each geometry optimization. Similar approaches were applied in the calculations of equilibrium structures and interaction energies of the PhOH–Benz m:n complexes, m and n = 1–2. Some characteristic H-bond distances in the PhOH–Benz complexes were computed and used in the discussion of $[(PhOH)_n]_{Benz}$.

2.3. Molecular dynamics simulations

In order to obtain insights into structures, energetic and dynamics in $[(PhOH)_n]_{Benz}$, n = 1–3, NVE-MD simulations were performed at 298 K. MD-$[(PhOH)_n]^{frozen}_{Benz}$ and MD-$[(PhOH)_n]^{free}_{Benz}$ represent two scenarios in $[(PhOH)_n]_{Benz}$. In MD-$[(PhOH)_n]^{frozen}_{Benz}$, the structures of $(PhOH)_n$ were frozen at the T-model equilibrium geometries [50] and only Benz molecules were allowed to move. MD-$[(PhOH)_n]^{frozen}_{Benz}$ was aimed primarily at the average three-dimensional structures and interaction energy distributions of Benz molecules in $[(PhOH)_n]_{Benz}$. MD-$[(PhOH)_n]^{free}_{Benz}$ represents the situation, in which all PhOH and Benz molecules were free to move, starting from the equilibrium configurations of MD-$[(PhOH)_n]^{frozen}_{Benz}$. MD-$[(PhOH)_n]^{free}_{Benz}$ was aimed at the structures and stabilities of solutes, as well as the dynamics in $[(PhOH)_n]_{Benz}$.

In both MD-$[(PhOH)_n]^{frozen}_{Benz}$ and MD-$[(PhOH)_n]^{free}_{Benz}$, $(PhOH)_n$ and five hundred Benz molecules were put in a cubic box subject to periodic boundary conditions. The center of mass of $(PhOH)_n$ was coincident with the center of the simulation box. The density of $[(PhOH)_n]_{Benz}$ was maintained at the liquid density of 0.87 g cm^{-3} [60], corresponding to the box length of about 42 Å. The cut-off radius was half of the box length. The long-range Coulomb interaction was taken into account by means of the Ewald summations. Fifty thousand MD steps of 0.5 fs were devoted to equilibration and one hundred thousand steps to property calculations. The primary energetic results of interest were the average solute–solute ($\langle E^{solu-solu}_{Benz}\rangle$) and solute–solvent ($\langle E^{solu-solv}_{Benz}\rangle$) interaction energies, as well as the average potential energies of $[(PhOH)_n]_{Benz}$ ($\langle E^{pot}_{Benz}\rangle$). $\langle E^{solu-solu}_{Benz}\rangle$ resulted from the average over the number of

MD steps, whereas $\langle E_{Benz}^{solu-solv} \rangle$ over the number of MD steps and solute molecules.

In order to visualize the average three-dimensional structures of solvent molecules in $[(PhOH)_n]_{Benz}$, solvent probability distribution (π-PD) maps were constructed from MD-$[(PhOH)_n]_{Benz}^{frozen}$; the center of mass of Benz is denoted by π and that of PhOH by π_{Ph}. In the calculations of the π-PD maps, molecular plane of a PhOH molecule was assumed to coincide with the *XY* plane of the simulation box ($Z = 0$ Å). The volumes above and below the plane were divided into layers, with the thickness of 1 Å. In each layer, a π-PD map was constructed from 61×61 grid intersections, by following the trajectories of the center of mass of Benz in the course of MD simulations. The π-PD maps were represented by contour lines, computed and displayed using SURFER program [61]. Therefore, the densities of the contour lines could reflect the probability of finding Benz in $[(PhOH)_n]_{Benz}$. For simplicity, the minimum and maximum values of the contour lines, as well as the contour intervals, were chosen to be the same for all π-PD maps. Since the solvent cages in $[(PhOH)_2]_{Benz}$ and $[(PhOH)_3]_{Benz}$ were rather complicated, additional π-PD maps were constructed with respect to *XZ* and *YZ* planes.

Based on similar approaches, the average solute–solvent and solvent–solvent interaction energy PD maps, denoted by the PB–PD and BB–PD maps, respectively, were constructed from MD-$[(PhOH)_n]_{Benz}^{frozen}$. The PB-PD maps were computed from the interaction energies between Benz at the grid intersections and $(PhOH)_n$, whereas BB-PD maps from the interaction energies between Benz at the grid intersections and all other Benz molecules. The average potential energy landscapes in $[(PhOH)_n]_{Benz}$ were represented by the PB-BB-PD maps, computed by combinations of the PB-PD and BB-PD maps. Because the solvent cages tend to bring about stabilization effects in $[(PhOH)_n]_{Benz}$, only negative-energy contour lines were displayed on the PB-PD, BB-PD and PB-BB-PD maps. It should be noted that, since the solvent–solvent interaction energies dominate in $[(PhOH)_n]_{Benz}$, the minimum and maximum values of the contours, as well as the contour intervals, must be assigned differently for the PB-PD, BB-PD and PB-BB-PD maps.

Since the dynamics of PhOH and Benz in the first solvation shell was one of the main objectives, additional MD analyses had to be made. Our experience in aqueous solutions [52–54] showed that, although not straightforward, the dynamics of specific solvent molecules in the first solvation shell could be anticipated at least qualitatively from the structures of the average potential energy landscapes. Therefore, the PB-PD, BB-PD and PB-BB-PD maps computed from MD-$[(PhOH)_n]_{Benz}^{frozen}$ were further analyzed in details. Several cross section plots were generated by taking vertical slices along the predefined profile lines, through the surfaces of the PB-BB-PD maps, as well as the PB-PD and BB-PD maps, using the methods described in Ref. [53]. The cross section plots derived from the longitudinal profile lines could be associated with the average potential energy barriers to solvent exchanges within, as well as between, the first solvation shells ($\langle \langle E_{Benz}^{L} \rangle \rangle$). Whereas those computed from the transverse profile lines are connected to the average potential energy barriers to the solvent exchanges between Benz molecules in the first solvation shell and the outside ($\langle \langle E_{Benz}^{T} \rangle \rangle$).

Solvation structures, stability and dynamics in $[(PhOH)_n]_{Benz}$ were further analyzed based on MD-$[(PhOH)_n]_{Benz}^{free}$. Some atom–atom pair correlation functions ($g(R)$) and the corresponding average running coordination numbers ($n(R)$) related to the $\pi\cdots\pi$ interactions, the C–H$\cdots\pi$, O–H$\cdots\pi$ and O–H$\cdots$O H-bonds were computed and employed in the discussion. $g(R)$ represents basic one-dimensional views on the structures in solutions. Because large-amplitude intermolecular motions, which could lead to solvent structure reorganization, were pointed out to be one of the main reasons for the non-rigidity in aromatic van der Waals clusters [27], they were also investigated in the present study. Since under thermal equilibrium conditions, the PhOH–Benz complexes are repeatedly dissociating and forming, and the O–H$\cdots\pi$ and O–H$\cdots$O H-bonds, as well as $\pi\cdots\pi$ interactions are responsible for the molecular associations in $[(PhOH)_n]_{Benz}$, their periodic motions at short time could be related to the lifetimes of the complexes. In the present case, fast Fourier transformations (FFT) [62] were performed on the O–H$\cdots\pi$ and $\pi\cdots\pi$ distances, from which the large-amplitude intermolecular vibrational frequencies and the lifetimes of the complexes were approximated. Additionally, in the present case, the H-bond exchange diagrams, showing the distance between the oxygen atom of PhOH and the center of mass of a specific Benz molecule as a function of MD simulation time, were constructed.

3. Results and discussion

3.1. The PhOH–Benz m:n complexes

The absolute and some low-lying minimum energy geometries of the PhOH–Benz complexes, obtained from the T-model potentials, are displayed in Figs. 1 and 2. In Fig. 1, the absolute minimum energy geometry of the PhOH–Benz 1:1 complex is represented by structure **a**, in which the O–H group of PhOH acts as proton donor towards the π-electron cloud of Benz, with the interaction energy ($\Delta E_{T\text{-model}}$) of -19.5 kJ/mol and the O–H$\cdots\pi$ and $\pi_{Ph}\cdots\pi$ distances of 3.4 and 5.4 Å, respectively. The structure and interaction energy of structure **a** are in good agreement with the T-shaped structure obtained from *ab initio* calculations [37,39] and the picosecond photofragment spectroscopy [12]. Structures **b** and **c** are two local minimum energy geometries, with $\Delta E_{T\text{-model}}$ of -13.5 and -9.3 kJ/mol, respectively. Structure **b** shows a possibility for the oxygen atom and the π-electron cloud of PhOH to act as proton acceptor towards the C–H groups of Benz, with the C–H$\cdots$O and C–H$\cdots\pi_{Ph}$ H-bond distances of 3.4 and 4.0 Å, respectively. Structure **c** is sta-

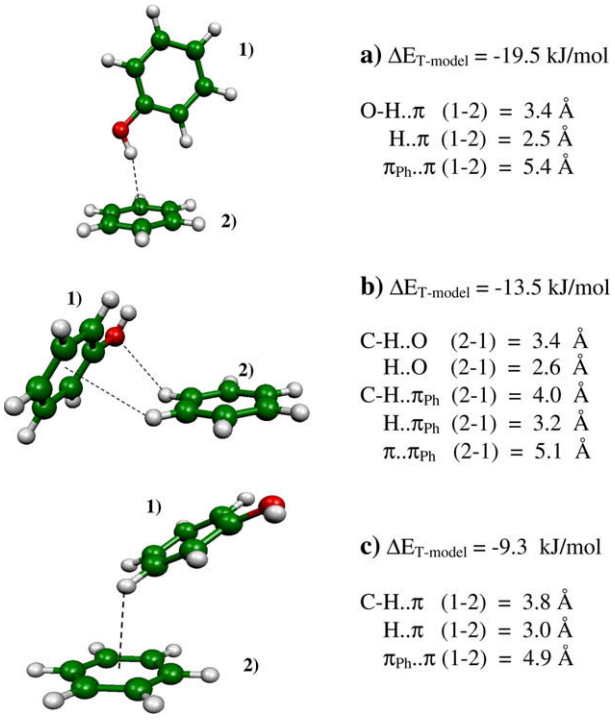

Fig. 1. Equilibrium structures and interaction energies of the PhOH–Benz 1:1 complexes in the gas phase, computed from the T-model potentials.

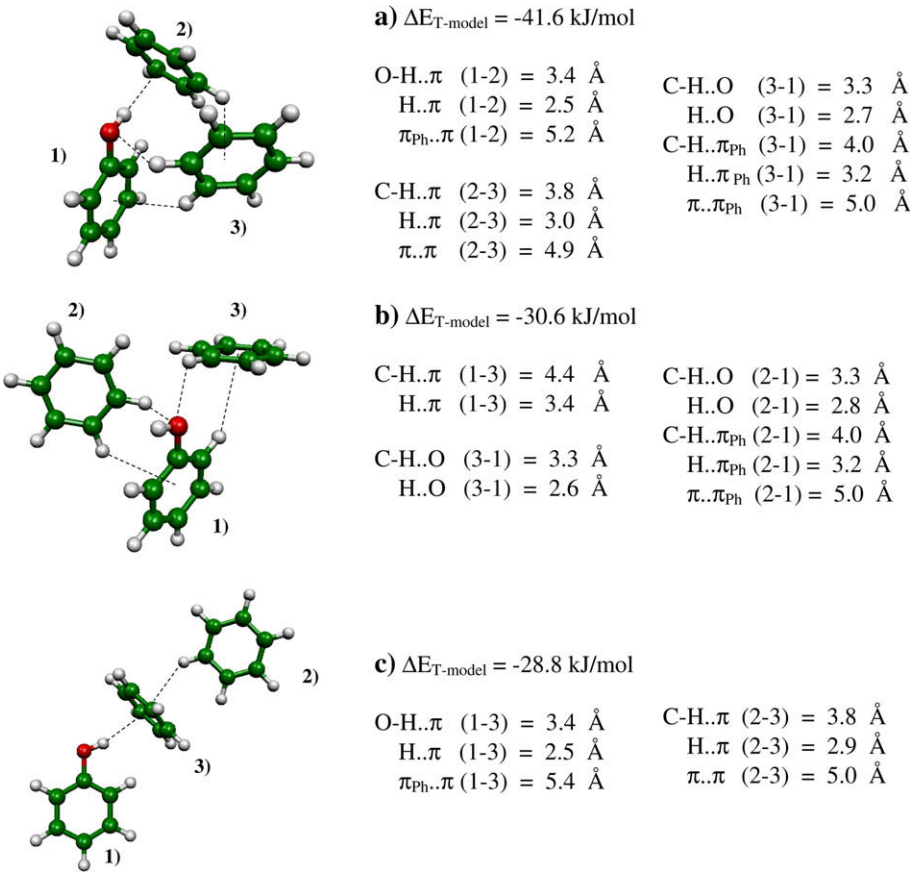

Fig. 2. Equilibrium structures and interaction energies of the PhOH–Benz 1:2 complexes in the gas phase, computed from the T-model potentials.

bilized solely by the C–H···π H-bonds, with the C–H···π and π_{Ph}···π distances of 3.8 and 4.9 Å, respectively.

A compact H-bond cluster formed from the O–H···π, C–H···O, C–H···π and C–H···π_{ph} H-bonds represents the absolute minimum energy geometry of the PhOH–Benz 1:2 complex, structure **a** in Fig. 2. Structure **a** possesses $\Delta E_{T\text{-model}}$ of −41.6 kJ/mol, with the H-bond distances similar to the PhOH–Benz 1:1 complexes. Structure **a** has more C–H···π H-bonds compared to that suggested from supersonic jet spectroscopy [36]. Structure **b** is about 11 kJ/mol less stable than structure **a**. In structure **b**, the oxygen atom of PhOH acts as proton acceptor towards two C–H groups of Benz, with the C–H···O H-bond distances of 3.3 Å. The stability of structure **c** is comparable to structure **b**, with $\Delta E_{T\text{-model}}$ of −28.8 kJ/mol and the O–H···π and C–H···π H-bond distances of 3.4 and 3.8 Å, respectively. The O–H···π H-bond in structure **c** is similar to structure **a** of the PhOH–Benz 1:1 complex, whereas the C–H···π H-bond resembles the T-shaped structure in $(Benz)_2$ [23].

Since H-bonds in the PhOH–Benz 2:1 and 2:2 complexes are not substantially different from the PhOH–Benz 1:1 and 1:2 complexes, in which all characteristic H-bond structures were explained, they are not presented here. Comparison of the results obtained in this subsection with those from experiments [12,36] and *ab initio* calculations [31,45] showed that the T-model potentials [33,50] are accurate enough for further application in MD simulations.

3.2. MD simulations on $[(PhOH)_n]_{Benz}$

The T-model potentials applied in the previous subsection were employed in MD simulations of $[(PhOH)_n]_{Benz}$, n = 1–3, at 298 K. $\langle E^{pot}_{Benz}\rangle$, $\langle E^{solu-solu}_{Benz}\rangle$ and $\langle E^{solu-solv}_{Benz}\rangle$ obtained from MD-$[(PhOH)_n]^{frozen}_{Benz}$ and MD-$[(PhOH)_n]^{free}_{Benz}$ are summarized in Table 1. In order to limit the number of figures, only selected $g(R)$, π-PD, PB-PD and PB-BB-PD maps are displayed. High-density contours on the PD maps are labeled with capital letters.

The average interaction energies in Table 1 show both expected and unexpected trends in $[(PhOH)_n]_{Benz}$. Due to large number of Benz molecules, $\langle E^{pot}_{Benz}\rangle$ are nearly the same for all MD simulations, and since the degree of freedom in MD-$[PhOH]^{free}_{Benz}$ is higher than MD-$[PhOH]^{frozen}_{Benz}$, $\langle E^{solu-solv}_{Benz}\rangle$ is about a factor two higher, −58.1 and −106.0 kJ/mol, respectively. As only one O–H group could act as proton donor towards Benz molecules in both MD-$[(PhOH)_2]^{frozen}_{Benz}$ and MD-$[PhOH]^{frozen}_{Benz}$, $\langle E^{solu-solv}_{Benz}\rangle$ are not substantially different, the former is about 5 kJ/mol higher than the latter. The energetic results seem to be more complicated in MD-$[(PhOH)_2]^{free}_{Benz}$, in which $\langle E^{solu-solv}_{Benz}\rangle$ is about 21 kJ/mol lower than MD-$[(PhOH)_2]^{frozen}_{Benz}$, and $\langle E^{solu-solu}_{Benz}\rangle = -2.3$ kJ/mol. These represent direct evidences for substantial changes in H-bond structures in

Table 1
Energetic results obtained from MD-$[(PhOH)_n]^{frozen}_{Benz}$ and MD-$[(PhOH)_n]^{free}_{Benz}$, n = 1–3. Energies are in kJ/mol.

	$\langle E^{pot}_{Benz}\rangle$	$\langle E^{solu-solu}_{Benz}\rangle$	$\langle E^{solu-solv}_{Benz}\rangle$
MD-$[PhOH]^{frozen}_{Benz}$	−35.4	–	−106.0
MD-$[PhOH]^{free}_{Benz}$	−35.3	–	−58.1
MD-$[(PhOH)_2]^{frozen}_{Benz}$	−35.5	–	−101.0
MD-$[(PhOH)_2]^{free}_{Benz}$	−35.5	−2.3	−123.4
MD-$[(PhOH)_3]^{free}_{Benz}$	−35.4	−51.8	−98.0

$\langle E^{pot}_{Benz}\rangle$ = average potential energy.
$\langle E^{solu-solu}_{Benz}\rangle$ = average solute–solute interaction energy.
$\langle E^{solu-solv}_{Benz}\rangle$ = average solute–solvent interaction energy.

MD-$[(PhOH)_2]^{free}_{Benz}$; an increase in solute–solvent interaction is accompanied by a decrease in solute–solute interaction, leading to some solvent-separated structures. The situations seem to be less complicated in MD-$[(PhOH)_3]^{free}_{Benz}$, in which $\langle E^{solu-solu}_{Benz}\rangle$ is about 64% of $\Delta E_{T\text{-model}}$ of $(PhOH)_3$ in the gas phase [50], and $\langle E^{solu-solv}_{Benz}\rangle = -98.0$ kJ/mol. These indicate that, on average, the three H-bonds in $(PhOH)_3$ did not change substantially in the course of MD-$[(PhOH)_3]^{free}_{Benz}$. The formations of solvent-separated structures in $[(PhOH)_2]_{Benz}$ and close-contact trimers in $[(PhOH)_3]_{Benz}$ will be discussed in detail in the forthcoming sections.

3.2.1. $[PhOH]_{Benz}$

The average three-dimensional structures and interaction energy distributions of solvent molecules obtained from MD-$[PhOH]^{frozen}_{Benz}$ are shown in Fig. 3. The values of the highest probabilities at the labeled contours on the π-PD maps ($\langle P^{\pi\text{-PD}}\rangle_{max}$), together with the corresponding lowest-average interaction energies on the PB-PD, BB-PB and PB-BB-PD maps, denoted by $\langle \Delta E^{PB\text{-}PD}_{Benz}\rangle_{min}$, $\langle \Delta E^{BB\text{-}PD}_{Benz}\rangle_{min}$ and $\langle \Delta E^{PB\text{-}BB\text{-}PD}_{Benz}\rangle_{min}$, respectively, are summarized in Table 2.

The π-PD maps in Fig. 3a and b reveal that, at least three Benz molecules stay in the vicinity the O-H group of PhOH, labeled with **A** (Z = −0.5–0.5 Å), **B** (Z = 2.0–3.0 Å) and **C** (Z = 2.0–3.0 Å). It is obvious that, the π-electron clouds of Benz molecules at **A** and **B** act as proton acceptor towards the O–H and C–H groups of PhOH, respectively, whereas a C–H group of Benz at **C** acts as proton donor towards the oxygen atom of PhOH. Table 2 shows that, Benz molecules at **A**, **B** and **C** possess $\langle \Delta E^{PB\text{-}PD}_{Benz}\rangle_{min}$ of −17.3, −11.7 and −9.8 kJ/mol, respectively. Comparison of $\Delta E_{T\text{-model}}$ in Fig. 1 and $\langle \Delta E^{PB\text{-}PD}_{Benz}\rangle_{min}$ suggests a possibility for a C–H group of Benz at **B** to act as proton donor towards the oxygen atom of PhOH.

The preferential solvation order according to $\langle P^{\pi\text{-}PD}\rangle_{max}$ and the average interaction energy orders based on the absolute values of $\langle \Delta E^{PB\text{-}PD}_{Benz}\rangle_{min}$, $\langle \Delta E^{BB\text{-}PD}_{Benz}\rangle_{min}$ and $\langle \Delta E^{PB\text{-}BB\text{-}PD}_{Benz}\rangle_{min}$ in Table 2 can be written as

$\langle P^{\pi\text{-}PD}\rangle_{max}$: **B** > **A** > **C**
$\langle \Delta E^{PB\text{-}PD}_{Benz}\rangle_{min}$: **A** > **B** > **C**
$\langle \Delta E^{BB\text{-}PD}_{Benz}\rangle_{min}$: **C** > **A** > **B**
$\langle \Delta E^{PB\text{-}BB\text{-}PD}_{Benz}\rangle_{min}$: **A** > **C** > **B**

It should be noted that, the preferential solvation order and the average interaction energy orders in the present case, as well as in many cases [52–54], are different. This is due to the fact that, the π-PD maps show relative probabilities that, a specific "position" in the first solvation shell of PhOH is occupied by Benz molecules, whereas the minima on the average potential energy landscapes, such as $\langle \Delta E^{PB\text{-}BB\text{-}PD}_{Benz}\rangle_{min}$, represent "low-lying interaction energy

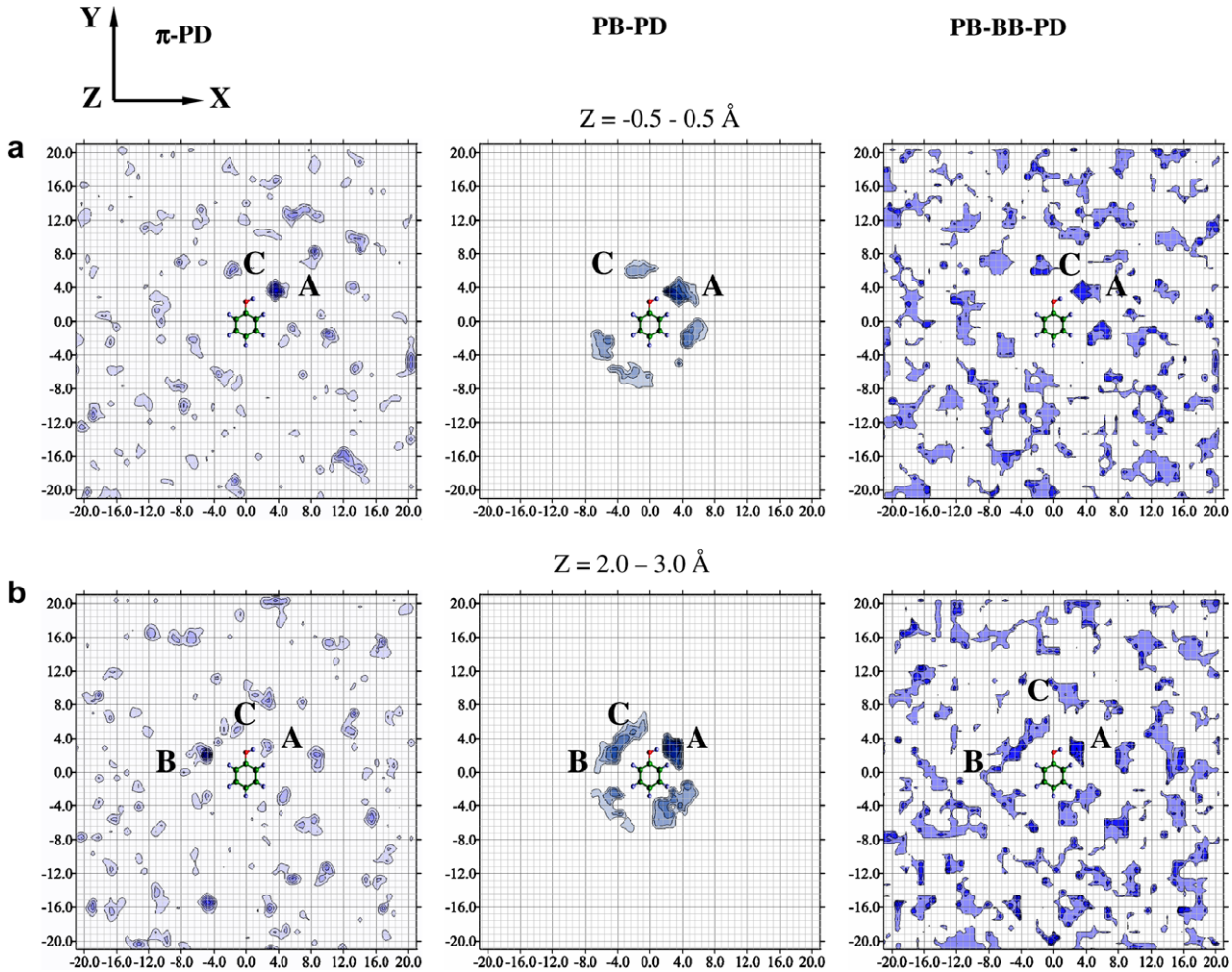

Fig. 3. Structural and energetic results obtained from MD-$[PhOH]^{frozen}_{Benz}$. *X*-, *Y*- and *Z*-axes are in Å, energies in kJ/mol. (a) and (b) The π-PD, PB-PD and PB-BB-PD maps. (c) and (d) Average potential energy landscapes and the cross section plots computed from longitudinal and transverse profile lines. (——) PB-BB-PD cross section plot. (– – – –) PB-PD cross section plot. (– – – –) BB-PD cross section plot. Note: π-PD contour: min = 0.0: max = 0.13: interval = 0.01. PB-PD contour: min = −18.0: max = −3.0: interval = 2.5. PB–BB–PD contour: min = −96.0: max = −75.0: interval = 7.0. (For interpretation of the references in colour in this figure legend, the reader is referred to the web version of this article.)

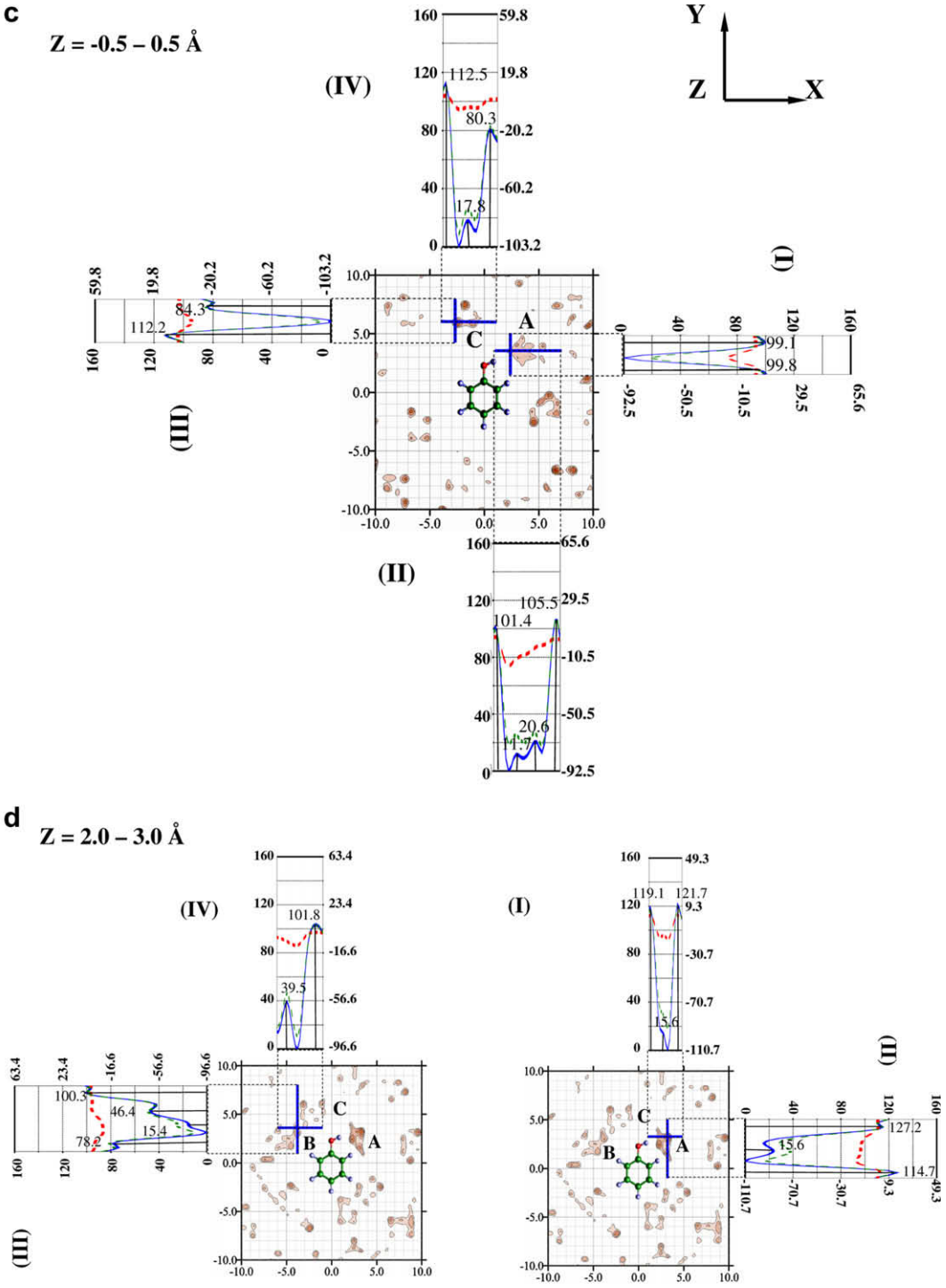

Fig. 3 *(continued)*

states", probed in the course of MD simulations. In other words, Benz molecules at the position with the highest $\langle P^{\pi\text{-PD}}\rangle_{\max}$ need not possess the lowest $\langle \Delta E_{\text{Benz}}^{\text{PB-BB-PD}}\rangle_{\min}$. Since the occupancies of the interaction energy states depend upon dynamics of individual solvent molecules, which could be described by structures of the average potential energy landscapes, it is necessary to include the cross section plots in the discussion of $[(\text{PhOH})_n]_{\text{Benz}}$ [52–54]. They show both the average potential energy barriers interconnecting interaction the energy states and the average potential energy wells, in which solvent molecules are confined. The latter could be related to the "average cage potentials" [26].

Fig. 3c and d shows the examples of the average potential energy landscapes and the cross section plots obtained from MD-$[\text{PhOH}]_{\text{Benz}}^{\text{frozen}}$. The cross section plots indicate that, the average potential energy barriers at **A**, **B** and **C** are quite high, in both longitudinal and transverse directions, *e.g.* about 120 kJ/mol at **A** in Fig. 3d (I) and (II). On the PB-PD and PB-BB-PD maps in Fig. 3b (Z = 2.0–3.0 Å), a possibility for the solvent exchange within the first solvation shell is evident from an interaction energy channel connecting **B** and **C**. All the cross section plots in Fig. 3c and d reveal that, the size and shape of the average potential energy wells are determined nearly exclusively by the average solvent-solvent

Table 2
The highest probabilities at the labeled contours on the π-PD maps ($\langle P^{\pi\text{-PD}}\rangle_{max}$) in Fig. 3, together with the corresponding lowest average interaction energies ($\langle \Delta E^{X}_{Benz}\rangle_{min}$) obtained from MD-$[PhOH]^{frozen}_{Benz}$. Energies are in kJ/mol and X = PB-PD, BB-PD or PB-BB-PD.

	$\langle P^{\pi\text{-PD}}\rangle_{max}$	$\langle \Delta E^{PB-PD}_{Benz}\rangle_{min}$	$\langle \Delta E^{BB-PD}_{Benz}\rangle_{min}$	$\langle \Delta E^{PB-BB-PD}_{Benz}\rangle_{min}$
Z = −0.5 to 0.5 Å				
A	0.104	−17.28	−74.23	−83.65
C	0.042	−7.29	−79.74	−81.41
Z = 0.0–1.0 Å				
A	0.080	−16.10	−78.33	−94.43
C	0.034	−7.53	−77.17	−82.12
Z = 1.0–2.0 Å				
A	0.033	−16.10	−72.97	−83.14
B	0.031	−10.84	−72.94	−82.91
C	0.024	−7.91	−76.35	−88.18
Z = 2.0–3.0 Å				
A	0.036	−9.48	−76.87	−91.47
B	0.114	−11.71	−75.00	−86.06
C	0.027	−9.78	−74.77	−82.46

interactions. These could restrict translational motion of Benz in the first solvation shell of PhOH, especially in the transverse direction. One could, therefore, conclude that, Benz molecules at **A**, **B** and **C** form a part of a quite well-defined local solvent cage at the O–H group of PhOH. Our qualitative interpretation of dynamics of individual solvent molecules in connection to the average potential energy landscapes is similar to Rabani et al. [63]; molecular translation in the liquid phase is characterized by average potential energy landscapes and occurs through jumps between basins separated by high-energy barriers, and the identity of the solvent cage should be more related to the multi-minimum basin itself, rather than to single actual configuration.

It appeared in general that, all structural information obtained from MD-$[PhOH]^{free}_{Benz}$ could be interpreted reasonably well based on the results of the PhOH–Benz 1:1 and 1:2 complexes in Figs. 1 and 2. $g(R_{O-H\cdots\pi})$ in Fig. 4a shows the main peak at $R_{O-H\cdots\pi}$=4.4 Å, with a small shoulder at $R_{O-H\cdots\pi}$ = 3.5 Å, and according to $n(R_{O-H\cdots\pi})$ at the first minimum ($R_{O-H\cdots\pi}$ = 5.5 Å), about five Benz molecules are in the first solvation shell of the O–H group. Since the main peak of $g(R_{C-H\cdots O_{ph}})$ in Fig. 4b is seen at $R_{C-H\cdots O_{ph}}$ = 3.3Å, one could conclude that, the main peak and small shoulder of $g(R_{O-H\cdots\pi})$ correspond to structures **b** and **a** in Fig. 1, respectively. The predominance of the C–H···O_{ph} H-bond in $[PhOH]_{Benz}$ was also suggested based on experiments in Ref. [4]. Additionally in Fig. 4a, $n(R_{O-H\cdots\pi})$ = 2.1 at the first maximum ($R_{O-H\cdots\pi}$ = 4.4 Å) indicates that, in $[PhOH]_{Benz}$, two Benz molecules are in close contact with the O–H group, with the H-bond structures similar to structures **b** and **a** in Fig. 2. These support the three-dimensional structures of solvent obtained from the π-PD maps and the preferential solvation order according to $\langle P^{\pi\text{-PD}}\rangle_{max}$.

Due to deep average potential energy wells, Benz molecules in the inner and outer shells of the O–H group seem not exchange as fast as water solvent [53,54,64]. The H-bond exchange diagram in Fig. 4c demonstrates the exchange of Benz 65 and Benz 423 in the course of MD-$[PhOH]^{free}_{Benz}$. At t_1 = 18.2 ps, Benz 423 entered and shared the first solvation shell with Benz 65, until Benz 65 left at t_2 = 28.3 ps. Therefore, the exchange process, taking place in panel **P1** in Fig. 4c, took about 10 ps. The residence time of Benz 423 could be approximated from the widths of panel **P1** and **P2** to be about 23 ps. The same exchange process repeated again in panel

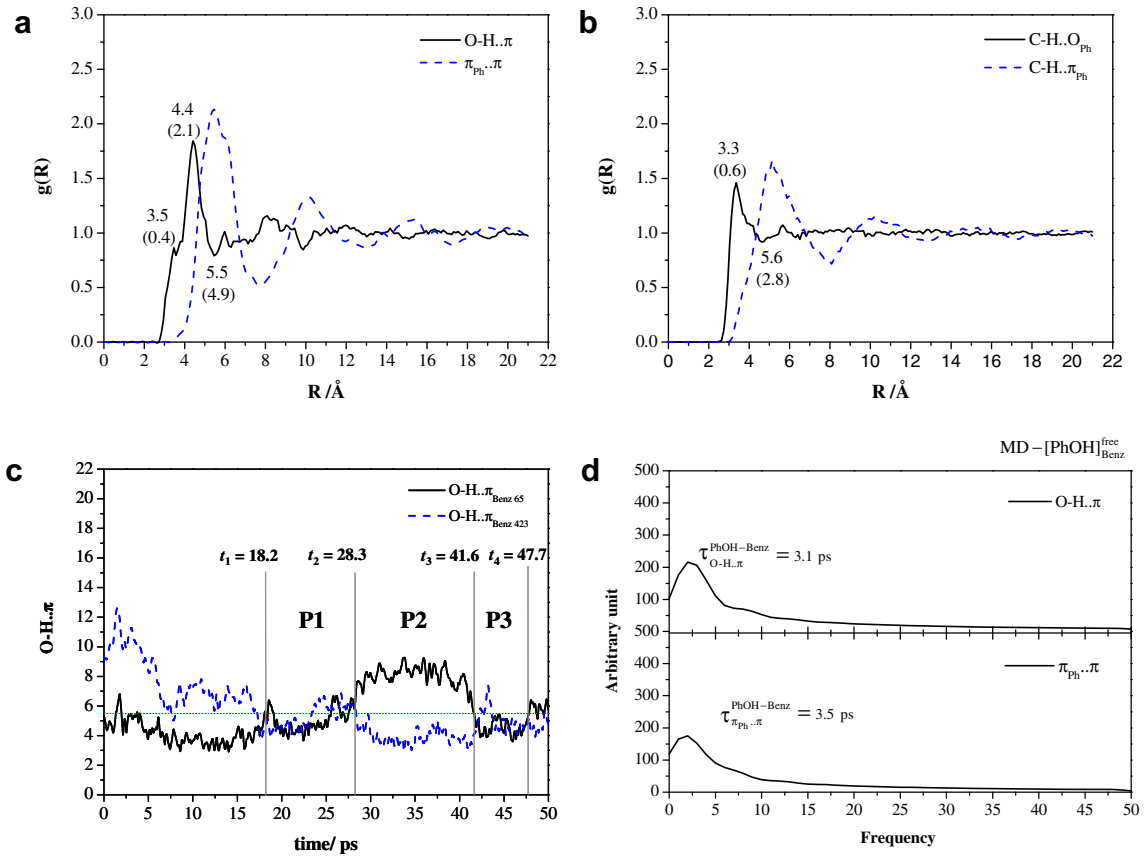

Fig. 4. Structural and dynamic results obtained from MD-$[PhOH]^{free}_{Benz}$. (a) and (b) $g(R)$; characteristic distances given with $n(R)$ in parentheses. (c) Example of H-bond exchange diagram. (d) Fourier transformations of the O–H···π H-bond and $\pi_{ph}\cdots\pi$ distances. Note: $\tau^{PhOH-Benz}_{O-H\cdots\pi}$ = the lifetime of the PhOH–Benz complex computed from FFT of the O–H···π H-bond distance. $\tau^{PhOH-Benz}_{\pi_{Ph}\cdots\pi}$ = the lifetime of the PhOH–Benz complex computed from FFT of the $\pi_{ph}\cdots\pi$ distance.

P3; at t_3 = 41.6 ps, Benz 65 reentered and shared the first solvation shell with Benz 423, etc.

Although the solvent exchange rates and residence times are extremely sensitive to the methods employed, some comparisons could be made using the results on liquid water. Based on MD simulations with the T-model potentials [52], the longest H-bond lifetime at the H atom of water was predicted to be 8.7 ps, whereas that at the O atom was 3.2 ps. These are compared well with the H-bond residence times of water obtained from NMR experiment of about 8 ps [65] and MD simulations of 4.5 ps [66]. Literature survey showed that the mean residence times of water within the first hydration shell of a single water molecule are ranging from 2.5 to 10 ps [67]. Therefore, the residence time of Benz in the first solvation shell of PhOH obtained in the present work is in reasonable agreement with the previous investigations.

Investigations of the H-bond exchange diagrams in details revealed that, Benz molecules at the O–H group of PhOH exchange through large-amplitude intermolecular vibrational motions, which involve periodic displacement of the O–H···π H-bond as discussed in Ref. [27]. According to the five-exchange mechanisms proposed by Langford and Gray [68], the exchanges seem to favor the associative-interchange (I_a) scheme, in which a solvent molecule enters and spends sometime in the first solvation shell before the other leaves.

Analyses of the time evolutions of the cage structures in $[Benz]_{liquid}$ [69,70] showed two relaxation components, which could affect the exchange of Benz molecules constituting the solvent cage; the slow relaxing component is associated with the cage lifetime, whereas the fast relaxing component with the structural rearrangements due to molecular vibrations. Since the average cage potentials or the average potential energy wells are quite low in $[PhOH]_{Benz}$, it was reasonable and possible to investigate the fast component. Based on the assumption that, at short time, the dynamic equilibrium between the associated and dissociated forms could be studied from characteristic intermolecular vibrational frequency [41], the lifetime of the PhOH–Benz 1:1 complex could be approximated. FFT [62] was performed on the O–H···π H-bond distance curve, from which the lifetime of the PhOH–Benz 1:1 complex ($\tau^{PhOH-Benz}_{O-H\cdots\pi}$) was approximated from the characteristic intermolecular vibrational frequency, as half of the association–dissociation dynamic equilibrium cycle time. Examples of FFT obtained from MD-$[PhOH]^{free}_{Benz}$ are shown in Fig. 4d, together with $\tau^{PhOH-Benz}_{O-H\cdots\pi}$. Due to lower degree of freedom, MD-$[PhOH]^{frozen}_{Benz}$ yielded the upper limit of $\tau^{PhOH-Benz}_{O-H\cdots\pi}$ to be 9.2 ps (not shown here), whereas MD-$[PhOH]^{free}_{Benz}$ predicted the lower limit to be 3.1 ps. The values are in reasonable agreement with the 2D-IR vibrational echo spectroscopy of 8 ps [43].

It should be noted that, the present MD simulations estimated $\tau^{PhOH-Benz}_{O-H\cdots\pi}$ directly from the intermolecular vibrational frequencies, whereas the 2D-IR vibrational echo experiment [43] compared the O–H stretching frequencies in the free PhOH with those in the PhOH–Benz 1:1 complex. Although efficient coupling of the O–H stretching with the low-frequency O–H···π H-bond vibrations could be presumed, the excited O–H stretching could live longer than 4 ps [21]. It should be augmented that, MD-$[PhOH]^{free}_{Benz}$ was based on pair-wise additive intermolecular potentials, in which many-body contributions were not taken into account. One could, however, expect that the inclusion of the cooperative effects will lead to slightly more associated PhOH–Benz 1:1 complex and longer $\tau^{PhOH-Benz}_{O-H\cdots\pi}$. In order to obtain a rough estimate of the cooperative effects, *ab initio* geometry optimizations were performed on the PhOH–Benz 1:1 complexes. For this weak O–H···π H-bond, MP2/6-311G(d,p) predicted the upper limit of the cooperative effects to be only about 0.6 kJ/mol, corresponding to the red shift of about 50 cm^{-1}. Therefore, the discrepancy between MD-$[PhOH]^{free}_{Benz}$ and the 2D-IR vibrational echo experiment is reasonable and explainable.

3.2.2. $[(PhOH)_2]_{Benz}$

In order to distinguish H-bonds in $[(PhOH)_2]_{Benz}$, the oxygen atoms were numbered as follow:

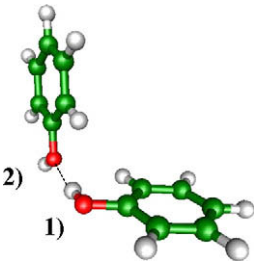

Since the O1–H···O2 H-bond was fixed in MD-$[(PhOH)_2]^{frozen}_{Benz}$, only the O2–H group could act as proton donor towards the π-electron cloud of Benz. Structural and energetic results obtained from MD-$[(PhOH)_2]^{frozen}_{Benz}$ demonstrated that, the solvent cages in $[(PhOH)_2]_{Benz}$ are stronger and more complicated than in $[PhOH]_{Benz}$. The π-PD maps in Fig. 5a–c, show well-defined solvent structures in the vicinities of $(PhOH)_2$; the preferential solvation positions are labeled with **A** to **E**. It is obvious that, Benz molecules prefer to stay at the O2–H group, with the highest probability at **A** (Z = −2.0–1.0 Å) in Fig. 5c and $\langle \Delta E^{PB-BB-PD}_{Benz}\rangle_{min}$ in Table 3 of −86.5 kJ/mol. It appeared that, the C–H···π H-bonds between PhOH and Benz become stronger upon dimer formation. They are labeled with **B**, **C** and **D** on the π-PD maps. The PB-PD and PB-BB-PD maps in Fig. 5b show a larger and more well-defined energy channel in $[(PhOH)_2]_{Benz}$, compared to $[PhOH]_{Benz}$. Therefore, a possibility for the solvent exchange within the first solvation shell of frozen $(PhOH)_2$ could be anticipated at **E**, **D** and **C**.

In $[(PhOH)_2]_{Benz}$, the preferential solvation order according to $\langle P^{\pi\text{-}PD}\rangle_{max}$ and the average interaction energy orders based on the absolute values of $\langle \Delta E^{PB-PD}_{Benz}\rangle_{min}$, $\langle \Delta E^{BB-PD}_{Benz}\rangle_{min}$ and $\langle \Delta E^{PB-BB-PD}_{Benz}\rangle_{min}$ in Table 3 can be written as

$$\langle P^{\pi\text{-}PD}\rangle_{max}: \quad \mathbf{A} > \mathbf{C} > \mathbf{D} > \mathbf{E} > \mathbf{B}$$
$$\langle \Delta E^{PB-PD}_{Benz}\rangle_{min}: \quad \mathbf{D} > \mathbf{E} \geqslant \mathbf{B} > \mathbf{A} > \mathbf{C}$$
$$\langle \Delta E^{BB-PD}_{Benz}\rangle_{min}: \quad \mathbf{C} > \mathbf{E} > \mathbf{A} > \mathbf{B} > \mathbf{D}$$
$$\langle \Delta E^{PB-BB-PD}_{Benz}\rangle_{min}: \quad \mathbf{A} > \mathbf{E} > \mathbf{B} > \mathbf{D} > \mathbf{C}$$

The cross section plots in Fig. 5d and e show high average potential energy barriers for solvent exchanges between the first solvation shell and the outside, up to about 138 kJ/mol at **A** in Fig. 5d (IV). Since the π-PD, PB-PD and PB-BB-PD maps show high-density contours in the vicinity of the O1–H···O2 H-bond, one could anticipate its easy access by Benz molecules, and due to additional entropic effects when $(PhOH)_2$ are free to move, the H-bond dissociation could be expected, as in the cases of $(BA)_2$ [51] and the guanidinium–formate (Gdm^+–FmO^-) complexes in aqueous solutions [52].

Structures and dynamics in $[(PhOH)_2]_{Benz}$ were further examined in MD-$[(PhOH)_2]^{free}_{Benz}$, in which both PhOH and all Benz molecules were free to move. As expected, due to weak solute–solute interaction and the thermal energy fluctuation at 298 K, the O1–H···O2 H-bond was dissociated in MD-$[(PhOH)_2]^{free}_{Benz}$. $g(R_{O1-O2})$ in Fig. 6a shows three well-defined peaks at R_{O1-O2} = 5.7, 8.1 and 9.4 Å, and for $g(R_{\pi_{Ph1}\cdots\pi_{Ph2}})$, two main peaks are seen at $R_{\pi_{Ph1}\cdots\pi_{Ph2}}$ = 6.5 and 9.2 Å. Since the latter is more structured, with two well-defined shoulders at $R_{\pi_{Ph1}\cdots\pi_{Ph2}}$ = 8.1 and 9.8 Å, one could conclude that, the majority of $(PhOH)_2$ in MD-$[(PhOH)_2]^{free}_{Benz}$ took solvent-separated structures. Comparison of $g(R_{O-H\cdots\pi})$ and $g(R_{\pi_{Ph}\cdots\pi})$ in Fig. 6b and c with those obtained

from MD-$[PhOH]^{free}_{Benz}$ in Fig. 4a confirms the dissociation of the O1–H···O2 H-bond and the existence of solvent-separated structures in MD-$[(PhOH)_2]^{free}_{Benz}$. Investigation of structures of $(PhOH)_2$ in the course of MD-$[(PhOH)_2]^{free}_{Benz}$ revealed four examples of close-contact and solvent-separated structures, with $R_{\pi_{Ph1}\cdots\pi_{Ph2}}$ comparable to the positions of the main peaks and shoulders of $g(R_{\pi_{Ph1}\cdots\pi_{Ph2}})$. They are shown in Fig. 6d, and will be used in the discussion of the exchange diagrams in Fig. 6e and f. In structure (**I**), both PhOH molecules are in close contact, with $R_{\pi_{Ph1}\cdots\pi_{Ph2}} = 6.7$ Å. In structures (**II**), (**III**) and (**IV**), Benz 496 separates both PhOH molecules, with $R_{\pi_{Ph1}\cdots\pi_{Ph2}}$ of 8.1, 9.0 and 9.7 Å, respectively.

Fig. 6e and f shows examples of solvent exchange diagrams. In Fig. 6e, the distances between the center of mass of Benz 496 ($\pi_{Benz\ 496}$) and those of PhOH molecules ($R_{\pi_{Ph1}\cdots\pi_{Benz\ 496}}$ and $R_{\pi_{Ph2}\cdots\pi_{Benz\ 496}}$) were plotted as functions of MD simulation time.

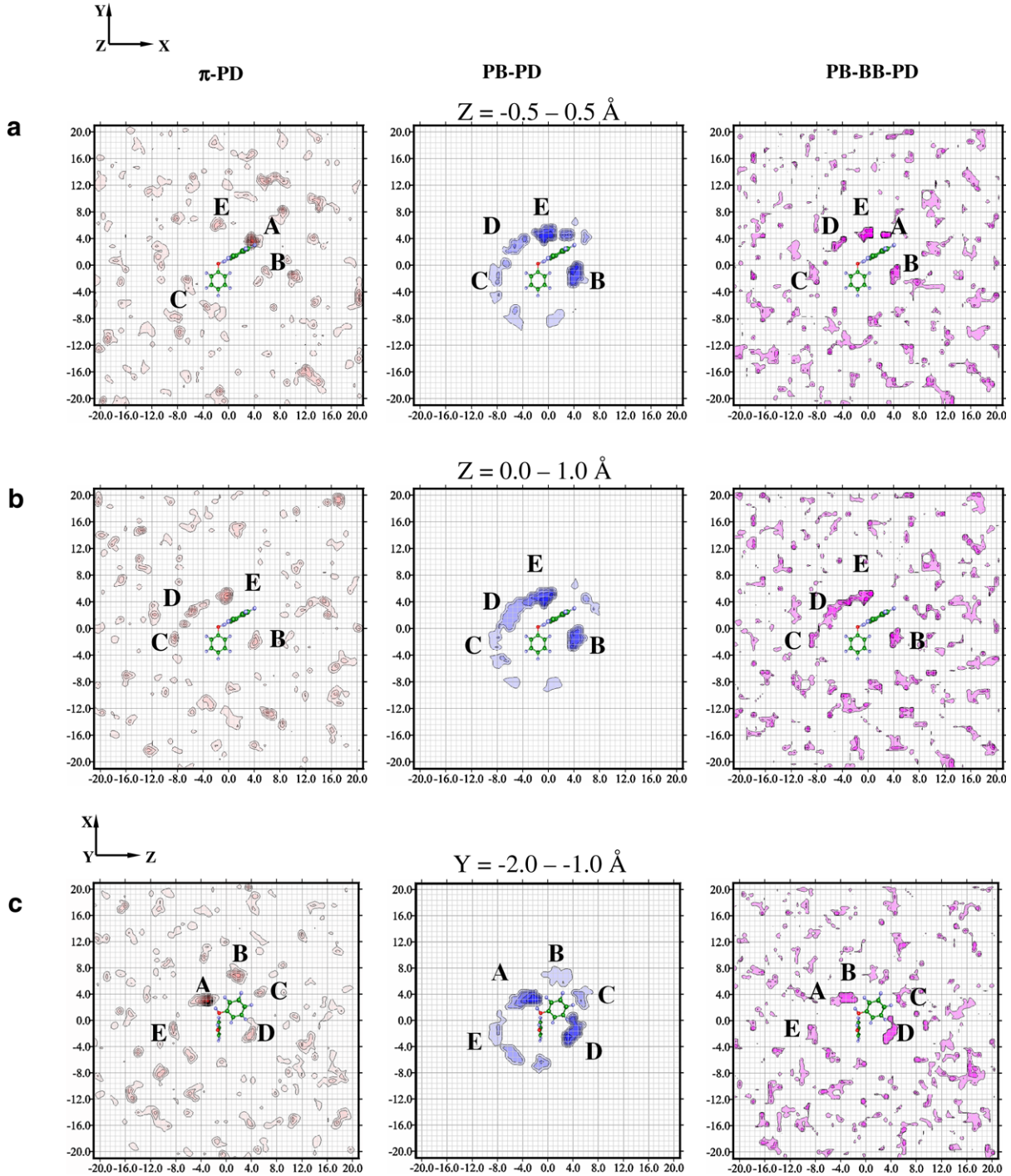

Fig. 5. Structural and energetic results obtained from MD-$[(PhOH)_2]^{frozen}_{Benz}$. *X*-, *Y*- and *Z*-axes are in Å, energies in kJ/mol. (a)–(c) The π-PD, PB-PD and PB-BB-PD maps. (d, e) Average potential energy landscapes and the cross section plots computed from longitudinal and transverse profile lines. (——) PB-BB-PD cross section plot. (- - - - -) PB-PD cross section plot. (- - - - -) BB-PD cross section plot. Note: π-PD contour: min = 0.0: max = 0.13: interval = 0.01. PB-PD contour: min = −30.0: max = −1.0: interval = 4.5. PB–BB–PD contour: min = −99.0: max = −70.0: interval = 7.2. (For interpretation of the references in colour in this figure legend, the reader is referred to the web version of this article.)

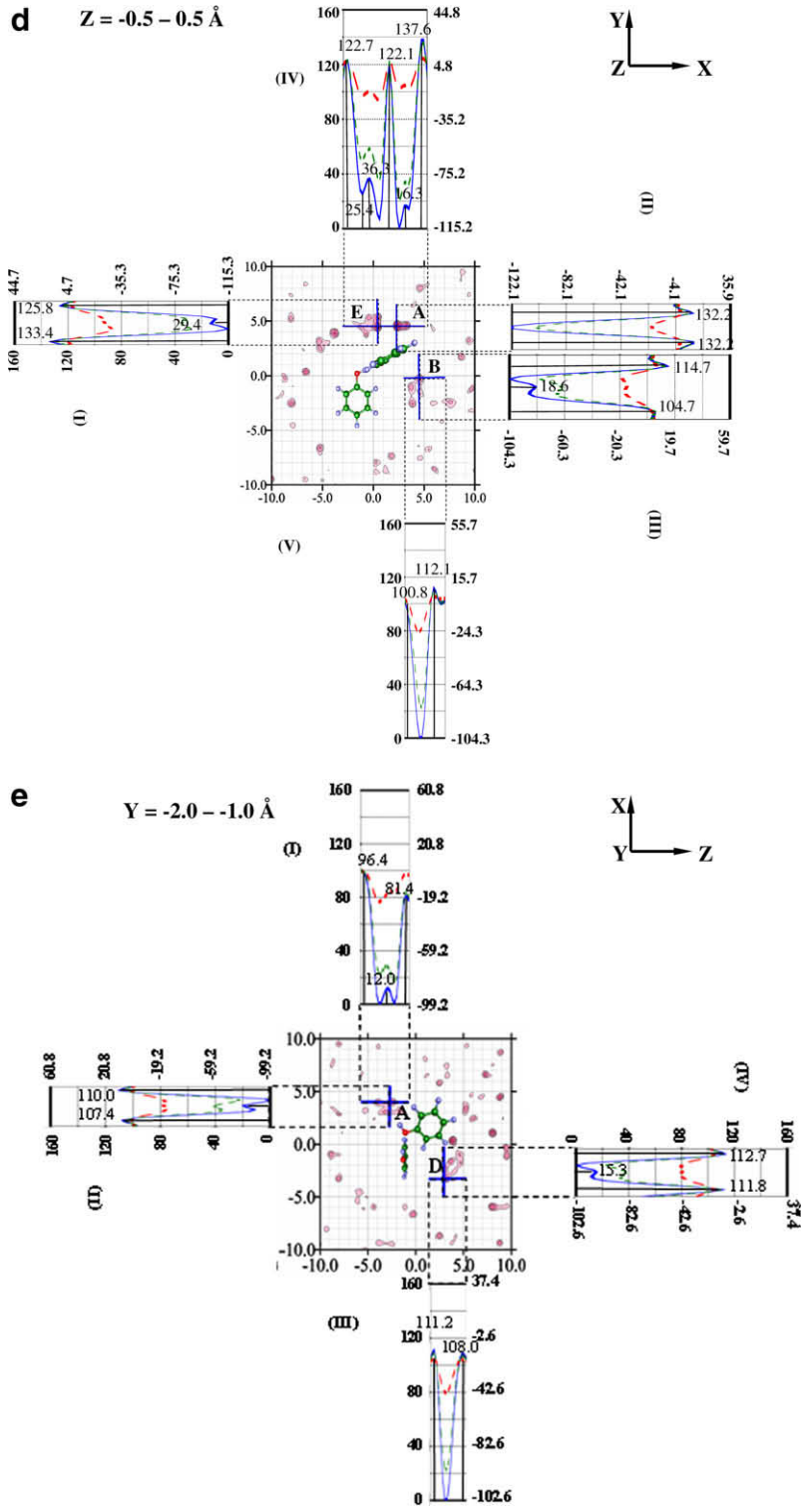

Fig. 5 *(continued)*

Instantaneous solvent-separated structures could be recognized in panels **P1** and $\mathbf{P_3}$, in which Benz 496 stayed between both PhOH molecules, with comparable $R_{\pi_{Ph1}\cdots\pi_{Benz\ 496}}$ and $R_{\pi_{Ph2}\cdots\pi_{Benz\ 496}}$. PhOH2 and PhOH1 could be temporarily separated from Benz 496 in panel $\mathbf{P_2}$ and $\mathbf{P_4}$, respectively. Finally, at $t_5 = 43.6$ ps, Benz 496 moved away from PhOH1, resulting in close-contact structures similar to structure (**I**) in Fig. 6d. Fig. 6f reveals further that, Benz 502 stayed closer to PhOH2 from $t = 15$–33 ps. A similar solvent separated structure was proposed from experiment, in which the association of $(PhOH)_2$ in water saturated CCl_4 was studied [5]; spectroscopic evidence revealed that, the hydrogen atoms of water are not involved in H-bond. It was presumed that, the dimer owes its stability to weak interaction between the hydrogen atoms of the O–H groups of both PhOH molecules and the oxygen atom of water. The so called "hemihydrate dimer" was used to describe this dimer.

Table 3
The highest probabilities at the labeled contours on the π-PD maps ($\langle P^{\pi\text{-PD}}\rangle_{max}$) in Fig. 5, together with the corresponding lowest average interaction energies ($\langle \Delta E^{X}_{Benz}\rangle_{min}$) obtained from MD-$[(PhOH)_2]^{frozen}_{Benz}$ Energies are in kJ/mol and X = PB-PD, BB-PD or PB-BB-PD.

	$\langle P^{\pi\text{-PD}}\rangle_{max}$	$\langle \Delta E^{PB-PD}_{Benz}\rangle_{min}$	$\langle \Delta E^{BB-PD}_{Benz}\rangle_{min}$	$\langle \Delta E^{PB-BB-PD}_{Benz}\rangle_{min}$
Z = −0.5 to 0.5 Å				
A	0.083	−15.11	−79.86	−94.14
B	0.048	−23.67	−65.44	−79.34
C	0.054	−11.66	−76.19	−79.58
E	0.023	−23.89	−71.31	−93.26
Z = 0.0 to 1.0 Å				
B	0.038	−20.32	−70.17	−89.78
C	0.047	−9.06	−79.95	−82.23
D	0.053	−11.79	−73.16	−84.73
E	0.062	−23.91	−71.35	−91.18
Y = −2.0 to −1.0 Å				
A	0.133	−22.14	−73.05	−86.50
B	0.056	−7.10	−74.90	−80.76
C	0.035	−10.94	−81.60	−81.30
D	0.037	−20.85	−70.79	−86.51
E	0.039	−8.33	−80.29	−84.28
X = −1.0 to 0.0 Å				
A	0.047	−13.68	−74.05	−85.53
B	0.043	−18.03	−74.05	−92.08
C	0.106	−9.08	−75.12	−79.62
D	0.091	−26.68	−67.89	−87.73
E	0.040	−15.16	−78.05	−91.64

3.2.3. $[(PhOH)_3]_{Benz}$

Structures and dynamics of $(PhOH)_3$ in Benz solution are discussed based on MD-$[(PhOH)_3]^{free}_{Benz}$. It appeared that, the cyclic O–H···O H-bonds, similar to the water trimer, could be partially opened in the course of MD-$[(PhOH)_3]^{free}_{Benz}$, as follow:

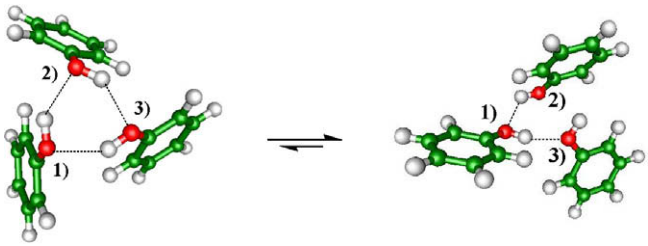

This is evident from $g(R_{O-O})$ in Fig. 7a; $g(R_{O_1-O_2})$ and $g(R_{O_1-O_3})$ are quite similar, with the main peak positions at the average O–H···O H-bond distance of 2.8 Å [50], whereas $g(R_{O_2-O_3})$ possesses different structure, a broad peak with maximum at 4 Å. In Fig. 7b and c, similar trends were observed for $g(R_{O_1\cdots\pi_{Ph2}})$, $g(R_{O_1\cdots\pi_{Ph3}})$ and $g(R_{O_2\cdots\pi_{Ph3}})$, as well as for $g(R_{\pi_{Ph1}\cdots\pi_{Ph2}})$, $g(R_{\pi_{Ph1}\cdots\pi_{Ph3}})$ and $g(R_{\pi_{Ph2}\cdots\pi_{Ph3}})$, respectively. Although the average structure is not as compact as

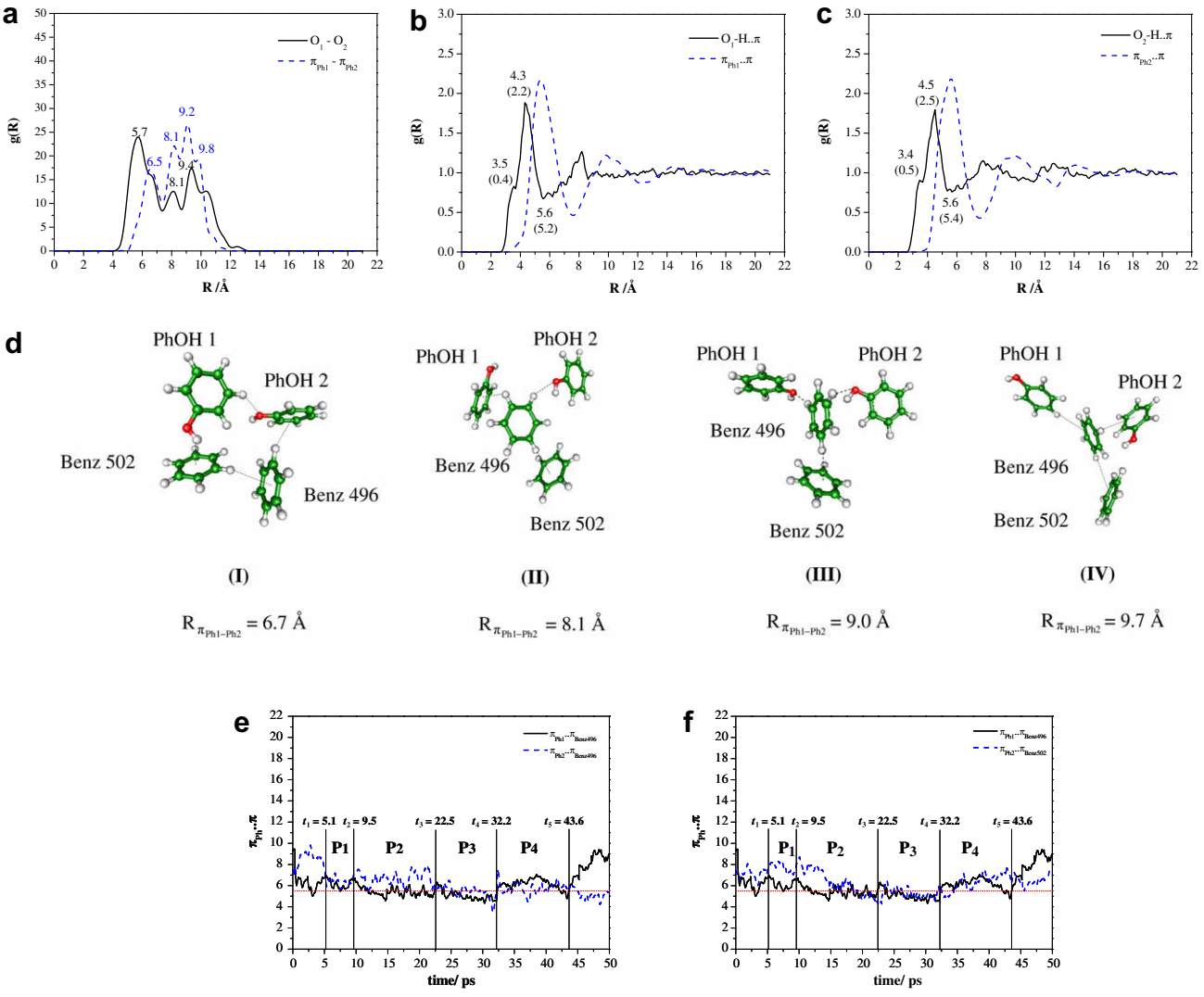

Fig. 6. Structural and dynamic results obtained from MD-$[(PhOH)_2]^{free}_{Benz}$. (a)–(c) $g(R)$; characteristic distances given with $n(R)$ in parentheses. (d) Snapshots of the PhOH–Benz clusters in $[(PhOH)_2]_{Benz}$. (e, f) Example of H-bond exchange diagram.

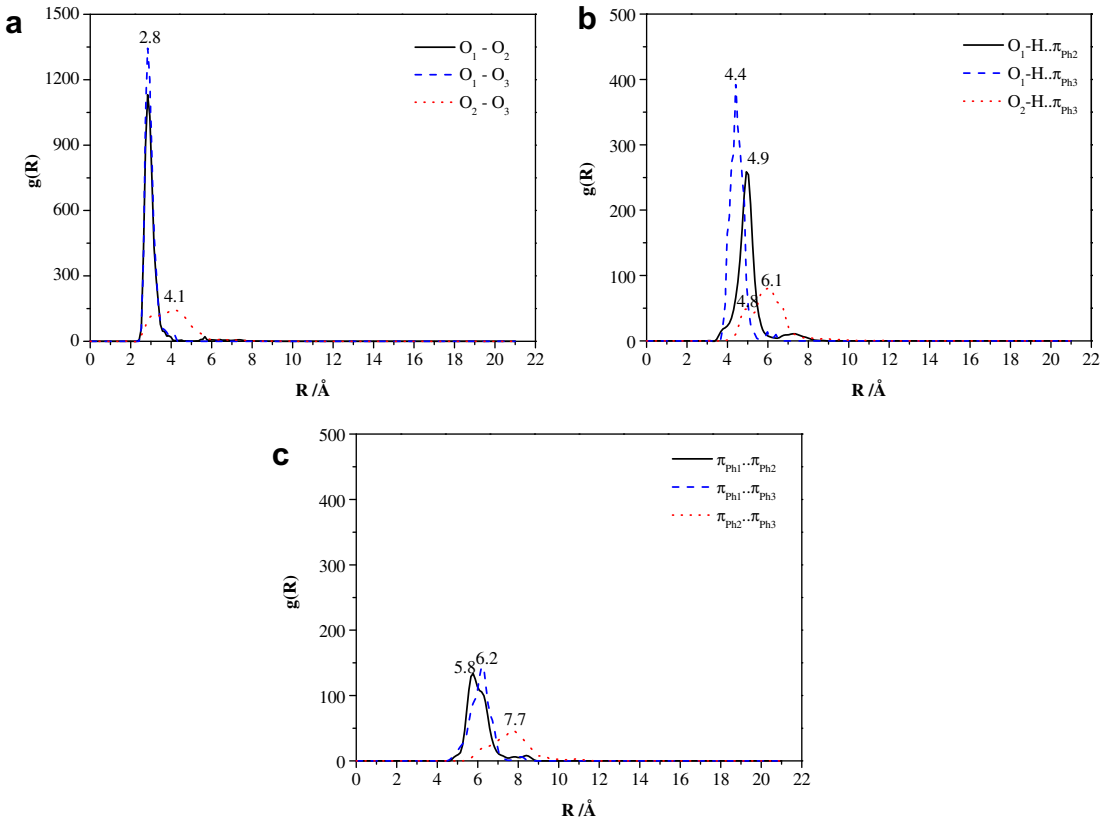

Fig. 7. $g(R)$ obtained from MD-$[(PhOH)_3]^{free}_{Benz}$, together with characteristic distances.

in the gas phase, one could conclude that, $(PhOH)_3$ forms H-bond clusters in $[(PhOH)_3]_{Benz}$. Comparison of the solute structures in the course of MD-$[(PhOH)_2]^{free}_{Benz}$ and MD-$[(PhOH)_3]^{free}_{Benz}$ revealed that, the O–H···O H-bonds in $(PhOH)_3$ are more sterically hindered by the three PhOH molecules, therefore not easily accessible by Benz molecules. Similar steric effects were observed in our previous MD-$[(BA)_2]^{free}_{Benz}$ in Ref. [33], in which cyclic H-bonds in $(BA)_2$ were sterically hindered from Benz molecules, but could be partially opened by small polar molecule such as water.

As mentioned earlier that, molecular associations of aromatic compounds in non-aqueous solvents, such as Benz and CCl_4, represent classical problems in the area of molecular associations, in which partition experiments and various spectroscopic methods have been generally employed in the investigations. For some H-bonded solutes, the associated forms are sufficiently stable to be detected in experiments. However, for PhOH, there have been disagreements as to the most important species in solutions. The majority of the partition experiments seem to point to the existence of the PhOH–$(PhOH)_3$ equilibrium in CCl_4, whereas several spectroscopic results were interpreted in terms of the PhOH–$(PhOH)_2$ equilibrium. At infinite dilution and within ps time scale, the present MD simulations seem to favor instantaneous solvent-separated structures in $[(PhOH)_2]_{Benz}$ and H-bond clusters in $[(PhOH)_3]_{Benz}$. Since it is well accepted that, different experiments could lead to different results, and the advancement of femtosecond laser technology has allowed experiments to probe instantaneous molecular structures and dynamics in weakly associated systems in smaller time scales, it seems unrealistic to rule out possibilities of finding various forms of dimers and trimers, as well as larger clusters in Benz or CCl_4 solutions. Therefore, we anticipate that, no single associated form could be representative in solutions, except in very restricted experimental conditions, such as temperature, concentration and time scale.

4. Conclusions

Structures and dynamics of aromatic clusters have been frequently and extensively studied to demonstrate that, cluster non-rigidity is a general phenomenon in weakly bound systems. In the present study, the effects of weak C–H···π, O–H···π H-bond and π···π interactions on structures and dynamics of H-bond clusters in non-aqueous environment, were studied using $[(PhOH)_n]_{Benz}$, n = 1–3, as model systems. In order to acquire some basic information on equilibrium structures and interaction energies in the gas phase, the PhOH–Benz m:n complexes, m and n = 1–2, were investigated using the T-model potentials. It appeared that, the H-bond structure, in which the O–H group of PhOH acts as proton donor towards the π-electrons of Benz, represents the absolute minimum energy geometry of the PhOH–Benz 1:1 complex. Although the C–H group is not an effective proton donor, various possibilities for the C–H···O and C–H···π H-bond formations were observed from the T-model results on larger PhOH–Benz complexes.

Based on the T-model potentials, a series of NVE-MD simulations was performed on $[(PhOH)_n]_{Benz}$, n = 1–3, at 298 K. Insights on the solvent cage structures and energetic were obtained from $[PhOH]_{Benz}$ and $[(PhOH)_2]_{Benz}$. It was observed from the average three-dimensional structures in $[PhOH]_{Benz}$ that, at least three Benz molecules solvate at the O–H group, and PhOH could act both as proton donor and acceptor towards Benz molecules. The average potential energy landscapes and cross section plots obtained from MD simulations indicated that, the size and shape of the average potential energy wells are determined nearly exclusively by the average solvent–solvent interactions, and the average potential energy barriers to solvent exchanges at the O–H group are quite high. Therefore, Benz molecules at the O–H group could from part of a quite strong local solvent cage. Our interpretation of dynamics of

solvent molecules in connection to the average potential energy landscapes is similar to Rabani et al., by which molecular translation in liquid was proposed to occur through jumps between potential energy wells, separated by high-energy barriers. Investigation on the H-bond exchange diagrams revealed that, Benz molecules at the O–H group could exchange through large-amplitude intermolecular vibrational motions, which involve the periodic displacement of the O–H$\cdots\pi$ H-bond, and the solvent exchanges seem to favor the associative-interchange scheme, in which a solvent molecule enters and spends sometime in the first solvation shell before the other leaves. From the characteristic intermolecular vibrational frequencies of the O–H$\cdots\pi$ H-bond, the lifetimes of the PhOH–Benz 1:1 complex were approximated and in reasonable agreement with 2D-IR vibrational echo experiment.

Due to weak interaction and the thermal energy fluctuation at 298 K, the O–H$\cdots$O H-bond in $(PhOH)_2$ was disrupted in MD simulations. Instantaneous solvent-separated structures, in which a Benz molecule separates both PhOH molecules, were observed in $[(PhOH)_2]_{Benz}$, whereas the cyclic H-bonds in $(PhOH)_3$ were partially opened in $[(PhOH)_3]_{Benz}$. A similar water separated dimer was suggested from experiment, in which spectroscopic evidence revealed that the hemihydrate $(PhOH)_2$ owes its stability to weak interaction between the hydrogen atoms of the O–H groups of both PhOH molecules and the oxygen atom of water. Comparisons of the π-PD maps and the dimer and trimer structures in the course of MD simulations revealed that, the O–H$\cdots$O H-bonds in $(PhOH)_3$ were quite well protected by the three PhOH molecules, therefore not easily accessible by Benz molecules as in the case of $(PhOH)_2$. This suggests that, the competition between solute–solute and solute-solvent interactions could be studied only when explicit solvent molecules are taken into account in the model calculations.

It should be noted finally that, the MD results reported here were based on pair-wise additive scheme, in which many-body effects were not taken into account. Since the interactions among aromatic compounds are not particularly strong, the inclusion of the cooperative effects in our model calculations should not lead to significant change in structures and stability of the complexes considered here; only slightly more associated complexes with longer association times could be anticipated. For organic and biological systems, weak intermolecular interactions could produce complexes that are short-lived. Although short-lived and cannot be detected easily by conventional experimental techniques, the dissociation and association of such complexes can influence chemical processes, especially reactivity and mechanisms in biochemical reactions. Therefore, progress is being made in our laboratory to apply similar theoretical approaches to investigate short-lived phenomena in some biological systems.

Acknowledgements

The authors would like to acknowledge the financial supports from the Thailand Research Fund (TRF): the Royal Golden Jubilee (RGJ) Ph.D. Program, Grant No. PHD/0071/2547 to Sermsiri Chaiwongwattana and Prof. Kritsana Sagarik: the Advanced Research Scholarship, Grant No. BRG51-80022 to Prof. Kritsana Sagarik. Linux clusters provided by the following organizations are also gratefully acknowledged: School of Mathematics and School of Chemistry, SUT; National Electronics and Computer Technology Center (NECTEC) and National Nanotechnology Center (NANOTEC), National Science and Technology Development Agency (NSTDA); the Thai National Grid Center (THAIGRID), Ministry of Information and Communication Technology.

References

[1] E.M. Woolley, L.G. Hepler, J. Phys. Chem. 76 (1972) 3058.
[2] S.H. Weidman, L.E. Swearingen, J. Am. Chem. Soc. 35 (1931) 836.
[3] J.N. Spencer, J.C. Andrefsky, A. Grushow, J. Naghdi, L.M. Patti, J.F. Trader, J. Phys. Chem. 91 (1987) 1673.
[4] F.A. Philbrick, J. Am. Chem. Soc. 56 (1934) 2581.
[5] R.M. Badger, R.C. Greenough, J. Phys. Chem. 65 (1961) 2088.
[6] F.T. Wall, J. Am. Chem. Soc. 64 (1942) 472.
[7] F.T. Wall, P.E. Rouse Jr., J. Am. Chem. Soc. 63 (1941) 3002.
[8] A.K.M. Shamsul Huq, S.A.K. Lodhi, J. Phys. Chem. 70 (1966) 1354.
[9] R. Van Duyne, S.A. Taylor, S.D. Christian, H.E. Affsprung, J. Phys. Chem. 71 (1967) 3427.
[10] K.E. Van Holde, W.C. Johnson, P.S. Ho, Principles of Physical Biochemistry, Prentice-Hall, New Jersey, 1998.
[11] B. Brutschy, Chem. Rev. 100 (2000) 3891.
[12] J.L. Knee, L.R. Khundkar, A.H. Zewail, J. Chem. Phys. 87 (1987) 115.
[13] M.F. Perutz, Philos. Trans. Roy. Soc. London Ser. A 345 (1993) 105.
[14] E.A. Meyer, R.K. Castellano, F. Diederich, Angew. Chem., Int. Ed. Engl. 42 (2003) 1210.
[15] W. Roth, M. Schmitt, C. Jacoby, D. Spangenberg, C. Janzen, K. Kleinerman, Chem. Phys. 239 (1998) 1.
[16] N. Mikami, Bull. Chem. Soc. Jpn. 68 (1995) 683.
[17] R.J. Lipert, S.D. Colson, J. Chem. Phys. 89 (1988) 4579.
[18] Ch. Jacoby, W. Roth, M. Schmitt, Ch. Janzen, D. Spangenberg, K. Kleinermanns, J. Phys. Chem. A 102 (1998) 4471.
[19] T. Sawamura, A. Fujii, S. Sato, T. Ebata, N. Mikami, J. Phys. Chem. 100 (1996) 8131.
[20] K. Ohashi, Y. Inokuchi, N. Nishi, Chem. Phys. Lett. 257 (1996) 137.
[21] G.V. Hartland, B.F. Henson, V.A. Venturo, P.M. Felker, J. Phys. Chem. 96 (1992) 1164.
[22] D.C. Young, Computational Chemistry: A Practical Guide for Applying Techniques to Real-World Problems, Wiley Interscience, New York, 2001.
[23] M.O. Sinnokrot, C.D. Sherrill, J. Am. Chem. Soc. 126 (2004) 7690.
[24] B.M. Rode, C.F. Schwenk, T.S. Hofer, B.R. Randolf, Coord. Chem. Rev. 249 (2005) 2993.
[25] M. Ricci, P. Bartolini, R. Chelli, G. Cardini, S. Califano, R. Righini, Phys. Chem. Chem. Phys. 3 (2001) 2795.
[26] A. Magro, D. Frezzato, A. Polimeno, G.J. Moro, R. Chelli, R. Righini, J. Chem. Phys. 123 (2005) 124511.
[27] S. Sun, E.R. Bernstein, J. Phys. Chem. 100 (1996) 13348.
[28] G.J. Kearley, M.R. Johnson, J. Tomkinson, J. Chem. Phys. 124 (2006) 044514.
[29] R. Chelli, G. Cardini, P. Procacci, R. Righini, S. Califano, A. Albrecht, J. Chem. Phys. 113 (2000) 6851.
[30] L.S. Bartell, F.J. Dulles, J. Phys. Chem. 99 (1995) 17107.
[31] J.R. Grover, E.A. Walters, E.T. Hui, J. Phys. Chem. 91 (1987) 3233.
[32] M.O. Sinnokrot, E.F. Valeev, C.D. Sherrill, J. Am. Chem. Soc. 124 (2002) 10887.
[33] K. Sagarik, S. Chaiwongwattana, P. Sisot, Chem. Phys. 306 (2004) 1.
[34] C.A. Hunter, J. Singh, J.M. Thornton, J. Mol. Biol. 218 (1991) 837.
[35] R. Parthasarathi, V. Subramanian, N. Sathyamurthy, J. Phys. Chem. A 109 (2005) 843.
[36] A. Olkawa, H. Abe, N. Mikami, M. Ito, J. Phys. Chem. 87 (1983) 5083.
[37] R.C. Guedes, K. Coutinho, B.J. Costa Cabral, S. Canuto, C.F. Correia, R.M. Borges dos Santos, J.A. Martinho Simões, J. Phys. Chem. A 107 (2003) 9197.
[38] S. Tsuzuki, K. Honda, T. Uchimaru, M. Mikami, K. Tanabe, J. Am. Chem. Soc. 124 (2002) 104.
[39] K. Kwac, C. Lee, Y. Jung, J. Han, K. Kwak, J. Zheng, M.D. Fayer, M. Cho, J. Chem. Phys. 125 (2006) 244508.
[40] K. Endo, Bull. Chem. Soc. Jpn. 1 (1926) 25.
[41] M. Saunders, J.B. Hyne, J. Chem. Phys. 29 (1958) 1319.
[42] E.N. Lassettre, R.G. Dickinson, J. Am. Chem. Soc. 61 (1939) 54.
[43] J. Zheng, K. Kwak, J. Asbury, X. Chen, I.R. Piletic, M.D. Fayer, Science 309 (2005) 1338.
[44] J. Zheng, K. Kwak, M.D. Fayer, Acc. Chem. Res. 40 (2007) 75.
[45] K. Kwak, J. Zheng, H. Cang, M.D. Fayer, J. Phys. Chem. B 110 (2006) 19998.
[46] J. Zheng, K. Kwak, X. Chen, J.B. Asbury, M.D. Fayer, J. Am. Chem. Soc. 128 (2006) 2977.
[47] I.J. Finkelstein, J. Zheng, H. Ishikawa, S. Kim, K. Kwak, M.D. Fayer, Phys. Chem. Chem. Phys. 9 (2007) 1533.
[48] Y.S. Kim, R.M. Hochstrasser, Proc. Natl. Acad. Sci. 102 (2005) 11185.
[49] R.M. Hochstrasser, Proc. Natl. Acad. Sci. 104 (2007) 14190.
[50] K. Sagarik, P. Asawakun, Chem. Phys. 219 (1997) 173.
[51] K. Sagarik, B.M. Rode, Chem. Phys. 260 (2000) 159.
[52] K. Sagarik, S. Chaiyapongs, Biophys. Chem. 117 (2005) 18.
[53] K. Sagarik, S. Dokmaisrijan, J. Mol. Struct. (Theochem) 718 (2005) 31.
[54] N. Deeying, K. Sagarik, Biophys. Chem. 125 (2006) 14.
[55] M. Orozco, F.J. Luque, Chem. Rev. 100 (2000) 4187.
[56] B.J. Costa Cabral, R.G. Bakker Fonseca, J.A. Martinho Simões, Chem. Phys. Lett. 258 (1996) 436.
[57] H.J. Böhm, R.J. Ahlrichs, J. Chem. Phys. 77 (1982) 2028.
[58] J.H. Dymond, E.B. Smith, The Virial Coefficients of Pure Gases and Mixtures, Clarendon Press, Oxford, 1980.
[59] H.B. Schlegel, J. Comput. Chem. 3 (1982) 214.

[60] Selected Values of Physical and Thermodynamics Properties of Hydrocarbons and Related Compounds, American Petroleum Institute Research Project, vol. 44, Carnegie Press, Pittsburg, 1953.
[61] SURFER for Window, V. 6.04, Golden Software Inc., USA, 1997.
[62] G.J. Borse, Numerical Methods with MATLAB: A Resources for Scientists and Engineers, PWS Publishing, Boston, 1997.
[63] J.D. Gezelter, E. Rabani, B.J. Berne, J. Chem. Phys. 107 (1997) 4618.
[64] S. Chaiwongwattana, K. Sagarik, in preparation.
[65] H.G. Hertz, in: F. Franks (Ed.), Water, A Comprehensive Treatise, vol. 3, Plenum Press, New York, 1973.
[66] R.W. Impey, P.A. Madden, I.R. McDonald, J. Phys. Chem. 87 (1983) 5071.
[67] F. Brugé, E. Parisi, S.L. Fornili, Chem. Phys. Lett. 250 (1996) 443.
[68] C.H. Langford, H.B. Gray, Ligand Substitution Processes, W.A. Benjain, New York, 1966.
[69] E. Rabani, J.D. Gezelter, B.J. Berne, J. Chem. Phys. 107 (1997) 6867.
[70] J.D. Gezelter, E. Rabani, B.J. Berne, J. Chem. Phys. 110 (1999) 3444.